JAERI-M
91-122

CONCEPTUAL DESIGN OF SC MAGNET SYSTEM FOR ITER (III)

— AC LOSS —

August 1991

Mitsuru HASEGAWA, Kiyoshi OKUNO, Yoshikazu TAKAHASHI
Satoshi NISHIO and Kiyoshi YOSHIDA

日本原子力研究所
Japan Atomic Energy Research Institute

JAERI-Mレポートは，日本原子力研究所が不定期に公刊している研究報告書です。
入手の問合わせは，日本原子力研究所技術情報部情報資料課（〒319-11茨城県那珂郡東海村）あて，お申しこしください。なお，このほかに財団法人原子力弘済会資料センター（〒319-11 茨城県那珂郡東海村日本原子力研究所内）で複写による実費頒布をおこなっております。

JAERI-M reports are issued irregularly.
Inquiries about availability of the reports should be addressed to Information Division, Department of Technical Information, Japan Atomic Energy Research Institute, Tokai-mura, Naka-gun, Ibaraki-ken 319-11, Japan.

編集兼発行　日本原子力研究所
印　　刷　㈱原子力資料サービス

JAERI-M 91-122

Conceptual Design of SC Magnet System for ITER (Ⅲ)
- AC Loss -

Mitsuru HASEGAWA+, Kiyoshi OKUNO, Yoshikazu TAKAHASHI
Satoshi NISHIO+ and Kiyoshi YOSHIDA

Department of Fusion Engineering Research
Naka Fusion Research Establishment
Japan Atomic Energy Research Institute
Naka-machi, Naka-gun, Ibaraki-ken

(Received July 8, 1991)

The International Thermonuclear Experimental Reactor (ITER) is an experimental thermonuclear tokamak reactor testing the basic physics performance and technologies. The joint work of the conceptual design activity of ITER was carried out at the Max Planck Institute for Plasma Physics in Garching Germany from 1988 to 1990. The Japanese proposals for the superconducting (SC) coil system were summarized by the Fusion Experimental Reactor (FER) Team and the Superconducting Magnet Laboratory of the Japan Atomic Energy Research Institute (JAERI). This report is one of the series reports of "CONCEPTUAL DESIGN OF SC MAGNET SYSTEM FOR ITER", and treats the AC losses of the superconducting coil.

The AC loss means the heat production in the winding packs and the supporting structure due to magnetic field change. Since the AC losses occupy about 50 % of the total heat loads during the normal operation, the estimation of AC loss is important. On the other hand, the estimation of the AC loss during the disruption is also required to consider the stability of the superconducting coil.

From these reasons, AC losses in the TF and PF coil winding packs and the supporting structures were computed for the normal operation and for the disruption. In addition the AC losses due to the separatrix

---

+ Fusion Experimental Reactor Team

sweep were also estimated. In these computations not only the time dependencies of the AC loss power, but also the spatial power distributions were obtained.

Keywords: ITER, Superconducting Coil, AC Loss, Fusion

JAERI－M 91－122

ITER用超電導マグネット・システム概念設計（Ⅲ）
－交流損失－

日本原子力研究所那珂研究所核融合工学部
長谷川 満[+]・奥野 清・高橋 良和
西尾 敏[+]・吉田 清

（1991年7月8日受理）

21世紀初頭に完成が予定されている国際熱核融合実験炉（ITER）の概念設計活動の超電導マグネット・システムに対する日本の提案を示す。

1988年から90年まで西ドイツのミュンヘン郊外のガルヒンにおけるマックスプランク・プラズマ物理学研究所で，ITERの概念設計活動は行われた。超電導コイルに関しては，原研那珂研究所の核融合実験炉特別チームと超電導磁石研究室が日本の設計案のまとめを行った。本レポートはこれらの作業をまとめた「ITER用超電導コイル・システム概念設計」の一連のレポートの1分冊であり，超電導コイルの交流損失を扱ったものである。

超電導コイルの交流損失とは，超電導導体及び支持構造物の変動磁場による発熱の総称である。交流損失は，巻線部のヒステリシス損失，カップリング損失，渦電流損失及び，コイル支持構造物の渦電流損失に分類される。

通常運転時においては全熱負荷の50％を交流損失が占めるため，通常運転時の交流損失の評価は冷凍系の設計のため非常に重要である。他方，ディスラプション時の交流損失の評価は超電導コイルの安定性を考えるうえで必要となる。

このような理由で，TF，PFコイルの巻線部及び支持構造物の交流損失が通常運転時及びディスラプション時に対して計算された。この他，セパラトリックス・スィープを行うことによる冷凍設備の増設を評価するため，セパラトリックス・スィープ時の交流損失も計算された。これらの計算においては，交流損失パワーの時間変化だけではなく，交流損失パワーの空間分布も求められている。

那珂研究所：〒311－01 茨城県那珂郡那珂町大字向山801－1
＋ 核融合実験炉特別チーム

Contents

目　　次

PREFACE

All of technical design reports from Japanese contributors to ITER magnet design are listed below:

JAERI-M 91-120
CONCEPTUAL DESIGN OF SC MAGNET SYSTEM FOR ITER (I)
- OVERVIEW -

(1) Design Basis
(2) Toroidal Field Coils
(3) Central Solenoid Coils
(4) Outer Ring Coils
(5) Mechanical Design Guideline

JAERI-M 91-121
CONCEPTUAL DESIGN OF SC MAGNET SYSTEM FOR ITER (II)
- STRESS ANALYSIS -

(1) Toroidal Field Coils at End of Burn
(2) Toroidal Field Coils at Fault Conditions
(3) Center Solenoid Coils
(4) PF Coil Support Structure and Outer Ring Coil
(5) Winding Rigidity Analysis

JAERI-M 91-122
CONCEPTUAL DESIGN OF SC MAGNET SYSTEM FOR ITER (III)
- AC LOSS -

(1) Analysis and Measurement of AC Losses in Large Superconducting Coil
(2) AC Loss Analysis
(3) AC Loss in Cryogenic Structure

JAERI-M 91-123
CONCEPTUAL DESIGN OF SC MAGNET SYSTEM FOR ITER (IV)
- POWER SUPPLY AND CRYOGENIC SYSTEM -

(1) Power Supply System for Magnet System
(2) Fault Analysis of TF Power Supply System
(3) Cryogenic System

JAERI-M 91-124

CONCEPTUAL DESIGN OF SC MAGNET SYSTEM FOR ITER (V)

- MATERIAL -

(1) Superconducting Material

(2) Steels

(3) Insulator

JAERI-M 91-125

CONCEPTUAL DESIGN OF SC MAGNET SYSTEM FOR ITER (VI)

- R&D PROPOSALS -

(1) Requirements of Scalable Model Coil Test

(2) TF Scalable Model Coil

1. Introduction

There are several heat loads in the superconducting coil system, such as thermal radiation from the 80 K shield, heat conduction from the coil leg and surrounding facilities, joule loss at current lead, nuclear heating, AC losses in the winding pack and the supporting structure. The AC loss means the heat production in the winding packs and the supporting structure due to magnetic field change. Since the AC losses occupy large part of the total heat loads during the normal operation, the estimation of AC loss is important to design the whole coil system, especially, cryogenic system.

On the other hand, there is a possibility of the coil quench by the heat pulse that are produced by AC losses at the plasma disruption. Hence, the estimation of the AC loss during the disruption is also required to consider the stability of the superconducting coil.

From these reasons, AC losses in the TF and PF coil winding packs and the supporting structures were computed for the normal operation and for the disruption. In addition the AC losses due to the separatrix sweep are also considered. In these computations not only the time dependencies of the AC loss power, but also the spatial power distributions were obtained.

This report consists of the following sections. In section 2, the principle of the analysis of AC loss in the winding pack is explained and the comparison of the analysis with the experimental results are discussed. In section 3, the procedure and the results of AC losses in the winding packs are described. In section 4, the AC loss in the supporting structure is treated using the eddy current analysis code.

2. Analysis and Measurement of AC Losses in Large Superconducting Coils

2.1 Introduction

In the ITER coil system, a heat load due to AC losses of the winding is about 20% of total heat load of the system. Therefore, it is very important to estimate the AC losses, in order to design the suitable system.

High performance conductors, developed recently, have complex structure. However, there is no AC loss expression which can be applied to such complex conductor. At the same time that AC losses of a conductor are analyzed, therefore, the measurements of the AC losses on the conductor have to be performed. These results have to be checked and reviewed each other. JAERI always has been carrying out the short sample test at each conductor level, strands, sub-size cables and full-size cables.

The comparison between analysis and measurement is described in this report.

2.2 Analysis

The following components of AC losses are analyzed:

a) Hysteresis loss in superconductor
b) Coupling loss between superconducting filaments
c) Eddy current loss in normal metal

These expressions are shown in Fig. 2.1.[1] The formulae of the coupling time constants (τ_c) of the two kinds of strands are shown in Fig. 2.2. (a), (b) [2]. Because the geometries of the coils and the generated field are complex, the analysis is carried out by the computer program, "MOMOKO". The basic structure of this program is shown in Fig. 2.3. The formula of the coupling time constant of the monolithic conductor is listed in Fig. 2.4.[1]

In the analysis of the cable-in-conduit type conductor, the coupling losses in and between the strands have to be calculated. If strands are insulated perfectly, it is not necessary to count the coupling loss between the strands. If not, it is necessary. However, it is difficult to calculate the coupling loss between the strands, because the resistance between the strands depends on the surface condition, the construction of the conductors and procedure of a twist, etc.. Therefore, the coupling loss between the strands should be measured to calculate the losses of the coils.

The effect of the transport current on the coupling losses is ignored, because it is generally very small in the operating condition of the large coils.[3]

2.3 Comparison between analysis and measurement

1) Short sample

The measurements of AC losses on strands and sub-size cables were always performed by using the electromagnetic method. The electromagnetic method is more suitable than the thermal one for the small sample test, because the loss value is very small. The measured results of three kinds of the strands, which were developed for the Proto-type Toroidal coils[4] in JAERI, are shown in Fig. 2.5. The calculated results are listed in Table 2.1, compared with the measured results. In a case of the A strand, a good agreement between the measured and calculated results is obtained, because the A strand has a simple structure as shown in Fig. 2.5. In the case of other two strands, the good agreement can not be obtained due to their complex structure. The calculated values are larger than the measured values. In the calculation, the resistance of the interface between two kinds of metals is assumed to be zero. According to the analysis, the resistance, however, has to be a finite value. This value depends on the structure and the fabricating process of the strands. It can be considered that

this is one of the reason of the disagreement. The resistance of the interface can not be obtained theoretically, because it depends on the fabrication process, the structure of strands and materials. Therefore, every strand has to be measured the AC losses before the construction of the coils.

2) Large coils

JAERI has constructed many large coils, for example the Japanese LCT coil, the Test Module Coil(TMC) and the Cluster Back-up Coil(CBC) in the Cluster Program and the Demo Poloidal Coils(DPC-U1,U2 and -EX). AC losses of these coils were measured by using the thermal method. In the case of the former three pool-cooled coils, AC losses are estimated by measuring the value of the evaporated liquid helium. In the case of the later three forced-cooled coils, the AC losses are evaluated by summing up the enthalpy change of the helium at the outlet. Because the value of AC losses is large in the large coil, the thermal method is suitable. However, the electromagnetic method is not suitable, because it is difficult to eliminate the influence of a large metallic structures on the measurement of magnetization.

The former three pool-cooled coils, developed for the toroidal coil, were operated in DC mode. AC losses of these coils were measured during the manual dump, whose time constants were 4-20 s. The measured and the calculated results are shown in Fig. 2.6 and 2.7.[5,6] The conductors of the coils are a monolithic type. A good agreements between the measurement and the calculation are obtained. AC losses of the later three forced-cooled coils, developed for the poloidal coils, were measured during a pulsed operation. Figure 2.8 shows these results.[7,8] The conductors of these coils are a cable-in-conduit type. In the case of the DPC-U, the calculated results agree with the measured those. Figure 2.9 shows the measured and the calculated hysteresis losses of the DPC-EX strand. The measured hysteresis losses are much larger than the calculated those.[9] [10] According to the microscopic observation on the cross section

of the strand, some Nb_3Sn filaments contact each other. This is the reason of the increase of the hysteresis losses.

2.4 Concluding remarks

(a) The computer program "MOMOKO" can estimate AC losses of the large coils, and the results agree with the measurements.

(b) Measurements of AC losses of the conductor have to be conducted before the design work and the construction of the coils.

(c) The measurements should be performed at each level of the conductor, i.e., strand, sub-size and full-size.

References

[1] H. Tsuji, et al.,"Pulsed Field Loss Characteristics of the Japanese Test coil", IEEE Trans. MAG-17, 42, (1981).

[2] B. Turck,"Coupling losses in various outer normal layers surrounding the filament bundle of a superconducting composite", J. Appl. Phys., 50, 5397, (1979).

[3] T. Ogasawara. et al.,"Alternating field losses in superconducting wires carrying dc transport currents. Part 2: multifilamentary composite conductors", Cryogenics, 21, 97, (1981).

[4] M. F. Nishi, et al.,"Development of the Proto-type Conductors and Design of the Test Coil for the Fusion Experimental Reactor", Proceeding of 13th Symposium on Fusion Engineering, (1989).

[5] T. Ando, et al.,"Experiment of 10-T, 60-cm-bore Nb3Sn Test Module Coil (TMC-1) for the Cluster Test Program", IEEE Trans., MAG-19, 312, (1983).

[6] S. Shimamoto, et al.,"Domestic Test Result of the Japanese LCT Coil", IEEE Trans., MAG-19, 851, (1983).

[7] K. Okuno, et al.,"Experiments of the 1-m-bore, 30-kA Superconducting Demo Poloidal Coils", Proceeding of 13th Symposium on Fusion Engineering, (1989).

[8] S. Shimamoto, et al.,"Development of Superconducting Pulsed Poloidal Coil in JAERI", Proceeding of ICEC-13, (1990).

[9] T. Ando, et al.,"DPC-EX Test Results", to be published at SOFT.

[10] Y. Takahashi, et al., "Experimental Results of the Nb3Sn Demo poloidal coil (DPC-EX)", Proceeding of Symposium on Superconductor Stability '90, to be published.

Table 2.1 Measured and calculated coupling time constants of the strands for the Proto-type Toroidal coils

	A	B	C
Measured	0.5	28	8
Calculated	0.5	110	16

(unit: ms)

ANALYSIS CODE OF AC LOSSES FOR SUPERCONDUCTOR

1. Hysteresis loss in Superconductor Q_h
2. Eddy current loss in normal metal Q_e
3. Coupling loss between S.C. Q_c

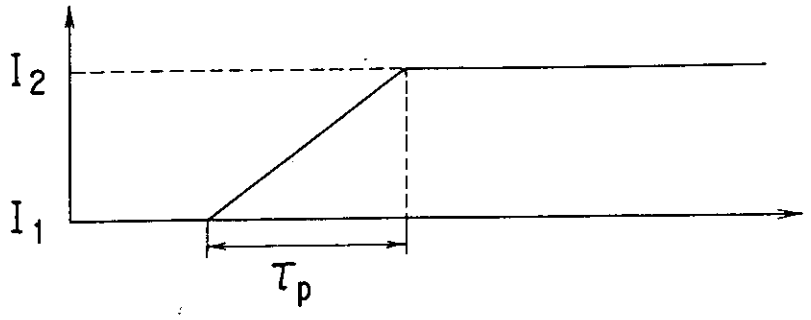

$$Q_h = \frac{2}{3\pi} J_c D_f \left(1+\left(\frac{I_t}{I_c}\right)^2\right) V_h \Delta B$$

$$Q_e = V_e \frac{\Delta B^2}{\mu_o} \frac{\tau_{ce}}{\tau_p} \left(1-\frac{\tau_{ce}}{\tau_p}\left(1-\exp\left(-\frac{\tau_p}{\tau_{ce}}\right)\right)\right)$$

$$Q_c = V_c \frac{\Delta B^2}{\mu_o} \frac{\tau_{cc}}{\tau_p} \left(1-\frac{\tau_{cc}}{\tau_p}\left(1-\exp\left(-\frac{\tau_p}{\tau_{cc}}\right)\right)\right)$$

Fig.2.1 AC Loss Expression.

$$\tau_{cc} = \mu_0 \left(\frac{\ell_p}{2\pi}\right)^2 \left(\frac{R_f}{R_3}\right)^2 \left(\frac{1}{\rho_\perp} + \frac{m}{\rho_1} + \frac{n}{\rho_2} + \frac{q}{\rho_3}\right) \quad (\text{sec})$$

$$m = \frac{R_1^2 - R_f^2}{R_f^2}\left(R_f^2 + \delta^2 R_1^2\right) a_1^2,$$

$$n = \frac{R_2^2 - R_1^2}{R_1^2}\left(R_1^2 + \gamma^2 R_2^2\right) a_2^2,$$

$$q = \frac{R_3^2 - R_2^2}{R_2^2}\left(R_2^2 + R_3^2\right) a_3^2,$$

$$\gamma = \frac{\rho_3(R_2^2 + R_3^2) + \rho_2(R_3^2 - R_2^2)}{\rho_3(R_2^2 + R_3^2) - \rho_2(R_3^2 - R_2^2)}$$

$$\delta = \frac{\rho_2(R_1^2 + \gamma R_2^2) + \rho_1(\gamma R_2^2 - R_1^2)}{\rho_2(R_1^2 + \gamma R_2^2) - \rho_1(\gamma R_2^2 - R_1^2)}$$

$$a_1 = \frac{R_f}{R_f^2 + \delta R_1^2}$$

$$a_2 = \frac{a_1 R_1^2 (\delta + 1)}{R_1^2 + \gamma R_2^2}$$

$$a_3 = \frac{a_2 R_2^2 (\gamma + 1)}{R_3^2 + R_2^2}$$

ℓ_p : twist pitch (m)

ρ : resistivity (Ω-m)

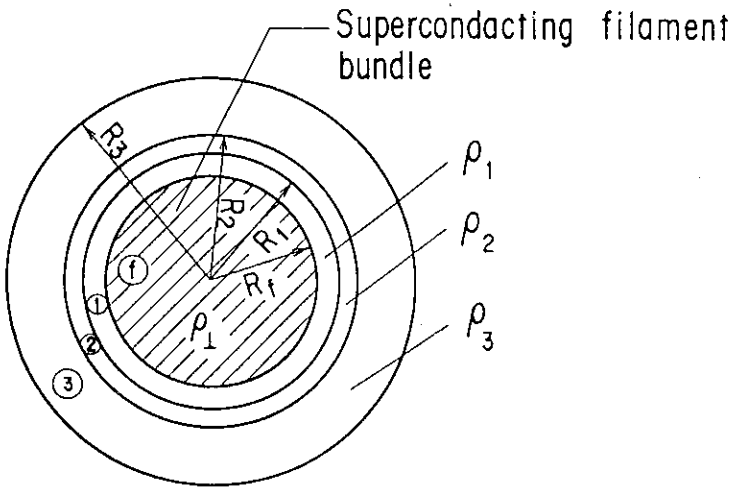

Fig.2.2 (a)Formula of the coupling time constant. (No Cu core)

$$\tau_{cc} = \mu_0 \left(\frac{\ell_p}{2\pi}\right)^2 \left(\frac{R_f}{R_0}\right)^2 \left(\frac{k}{\rho_\perp} + \frac{\ell}{\rho_C} + \frac{m}{\rho_B} + \frac{n}{\rho_0}\right)$$

$$k = \frac{R_f^2 - R_c^2}{R_f^2} = 1 - \ell$$

$$\ell = \left(\frac{R_c}{R_f}\right)^2$$

$$m = \frac{R_B^2 - R_f^2}{R_f^2} \left(R_f^2 + s^2 R_B^2\right) a_1^2$$

$$n = \frac{R_0^2 - R_B^2}{R_B^2} \left(R_B^2 + R_0^2\right) a_2^2$$

$$a_1 = \frac{R_f}{R_f^2 + sR_B^2} \qquad a_2 = \frac{a_1 (1+s) R_B^2}{R_B^2 + R_0^2}$$

$$s = \frac{\rho_0 (R_0^2 + R_B^2) + \rho_B (R_0^2 - R_B^2)}{\rho_0 (R_0^2 + R_B^2) - \rho_B (R_0^2 - R_B^2)}$$

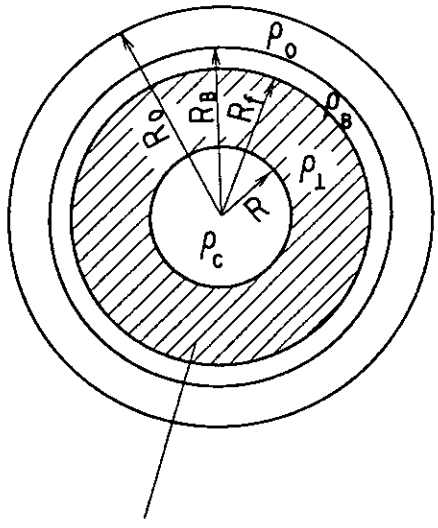

ℓ_p : Twist Pitch (m)

ρ : Resistivity (Ω－m)

Fig.2.2 (b)Formila of the coupling time constant. (With Cu core)

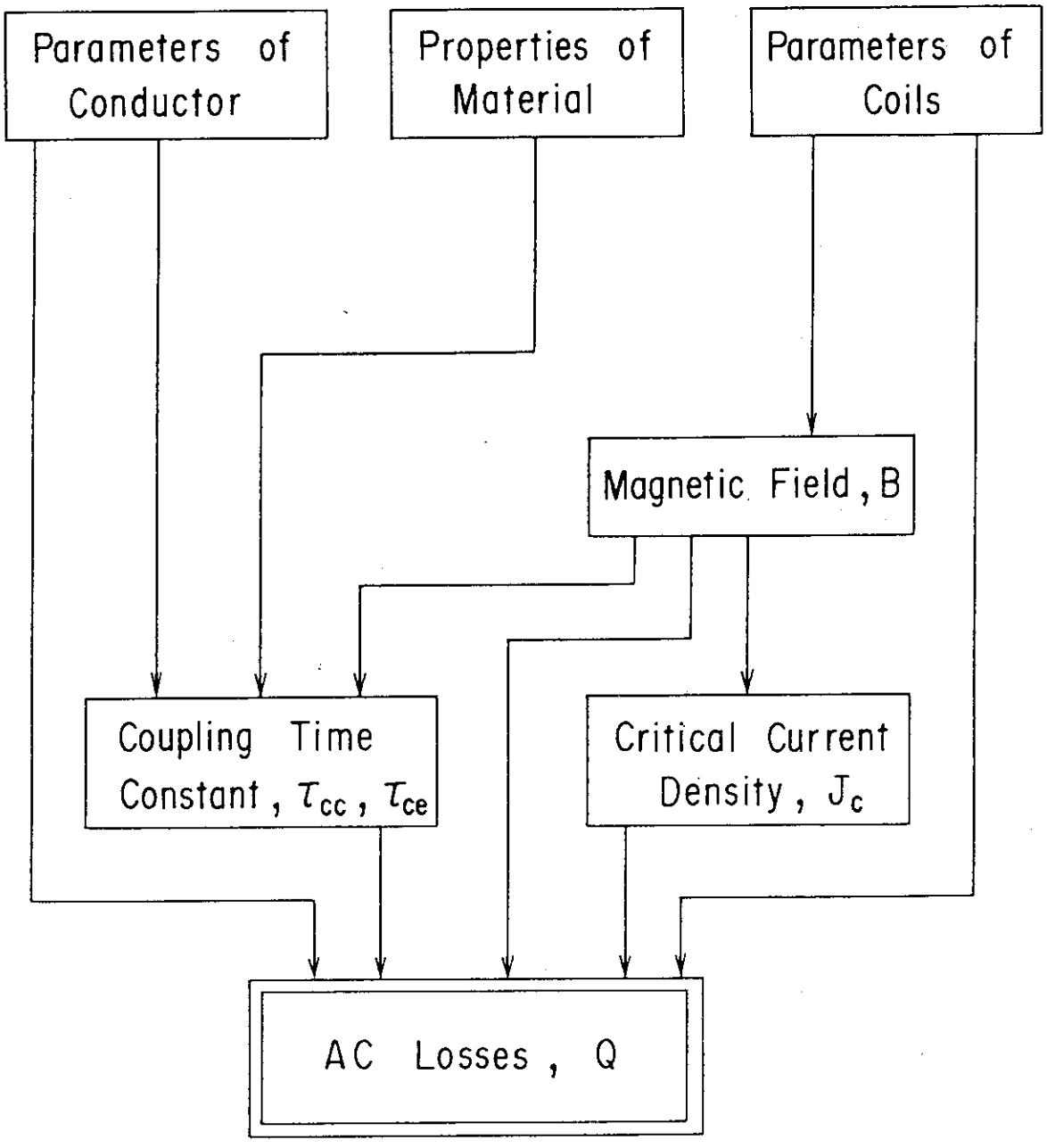

BLOCK DIAGRAM OF THE PROGRAM "MOMOKO"

Fig.2.3 Block diagram of the program "MOMOKO".

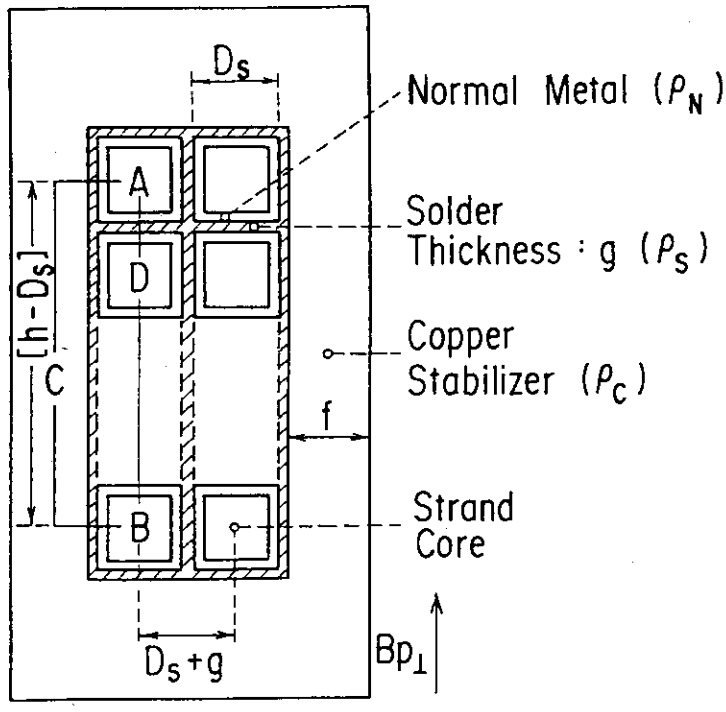

$$\tau_{cs} = \frac{\mu_0}{8}(D_s + g)\left(\frac{\ell_s}{h - D_s}\right)^2\left(\frac{f}{\rho_c} + \frac{D_s}{\rho_{eff}}\right)$$

$$Q_s = \frac{\tau_{cs}}{\tau_p}(h - D_s)(D_s + g)\left[1 - \frac{\tau_{cs}}{\tau_p}\left\{1 - \exp\left(-\frac{\tau_p}{\tau_{cs}}\right)\right\}\right]\frac{(\Delta Bp_\perp)}{\mu_0}$$

$$\rho_{eff} = \frac{1}{D_s + g}\left(D_s \cdot \frac{1+\lambda}{1-\lambda}\rho_N + g\rho_s\right)$$

λ : Fraction of S.C. in Strands.

Fig.2.4 Formula of the coupling time constant for the monolithic conductor.

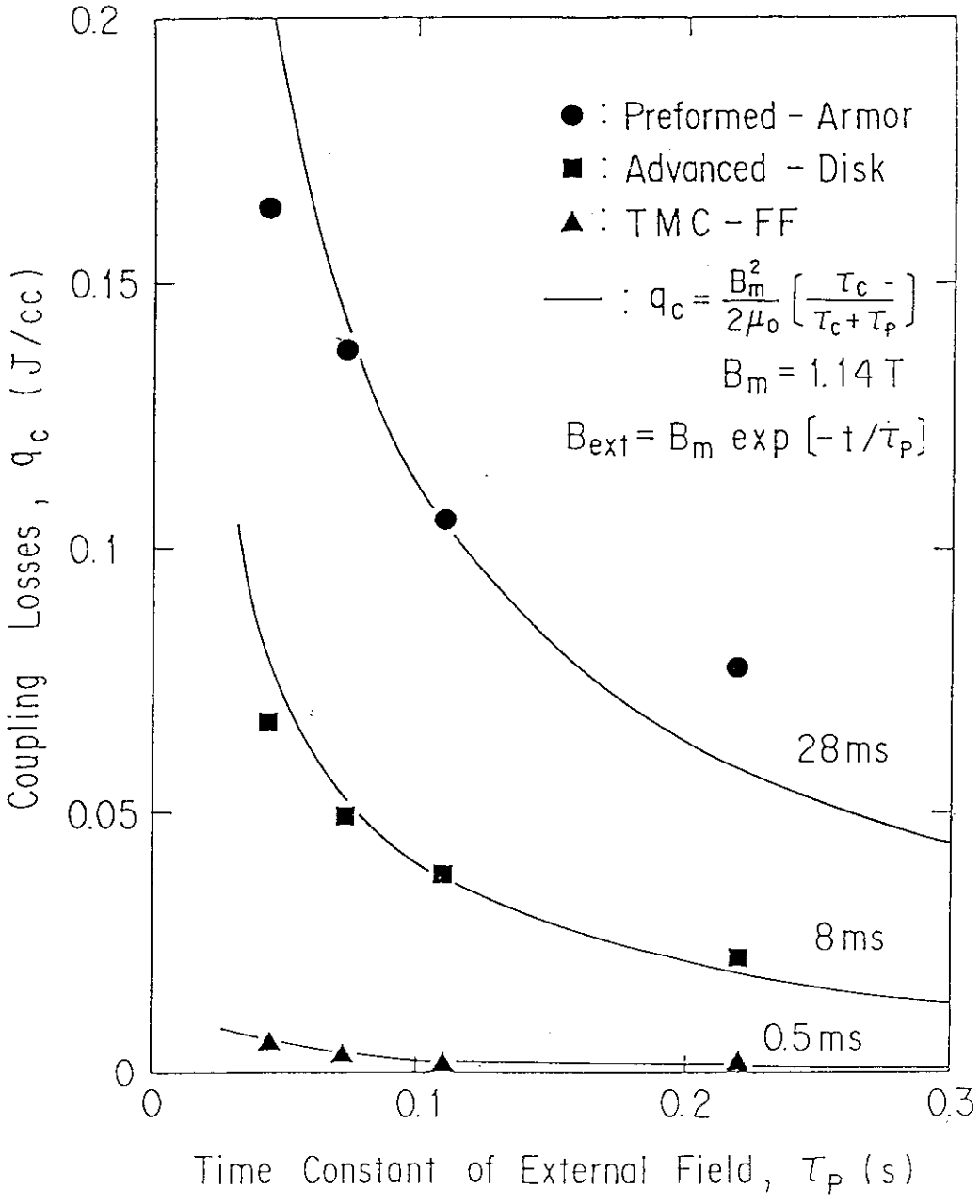

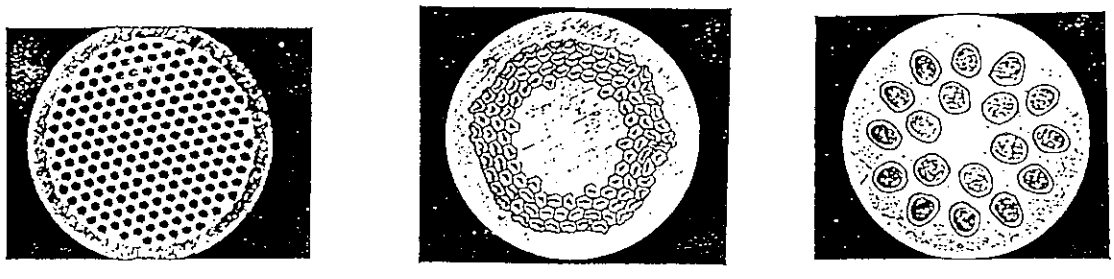

A; TMC-FF　　B; Preformed-Armor　　C; Advanced-Disk

Fig.2.5 Measured coupling losses of Nb_3Sn strands.

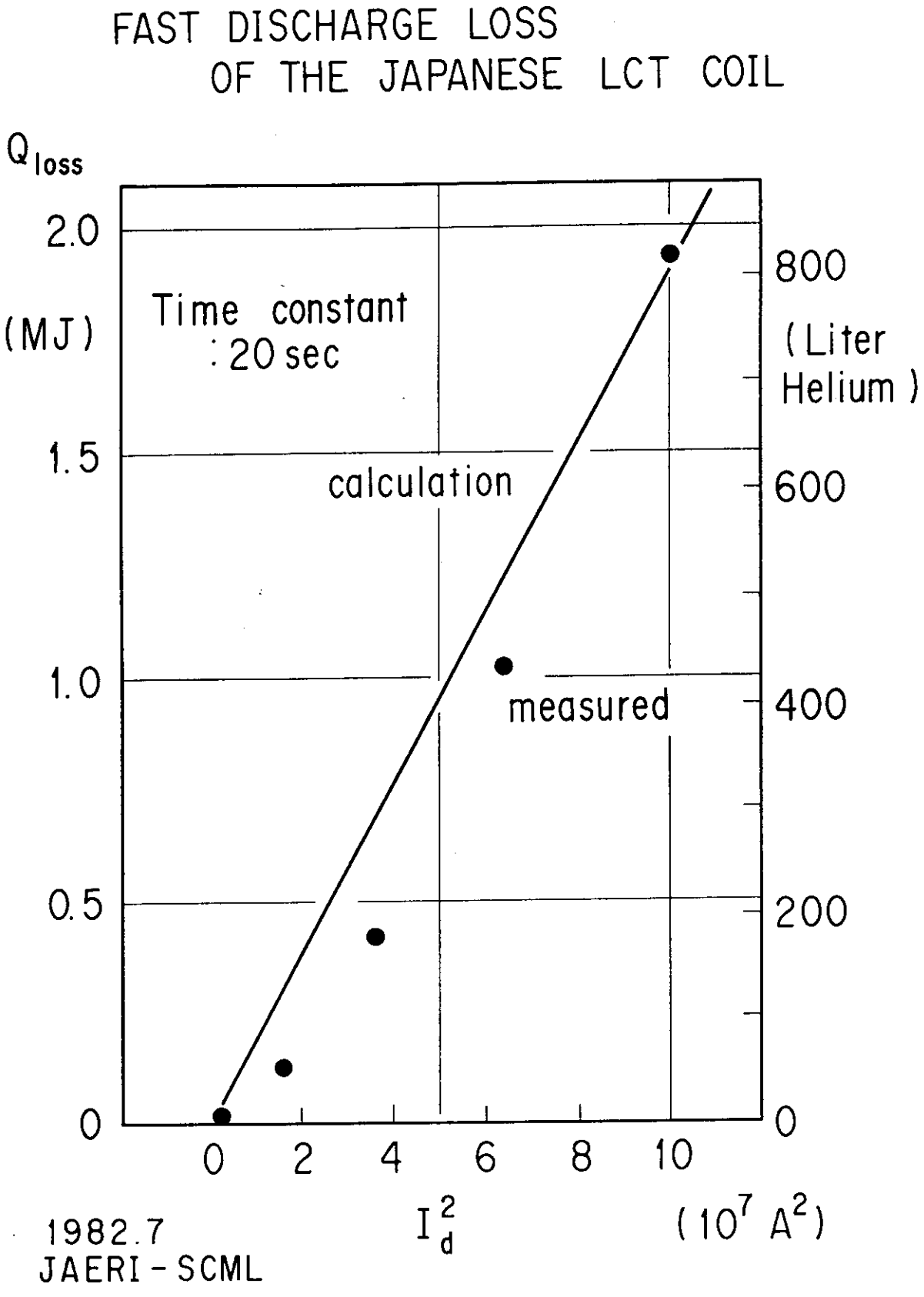

Fig.2.6 Measured and calculated AC losses of LCT coil.

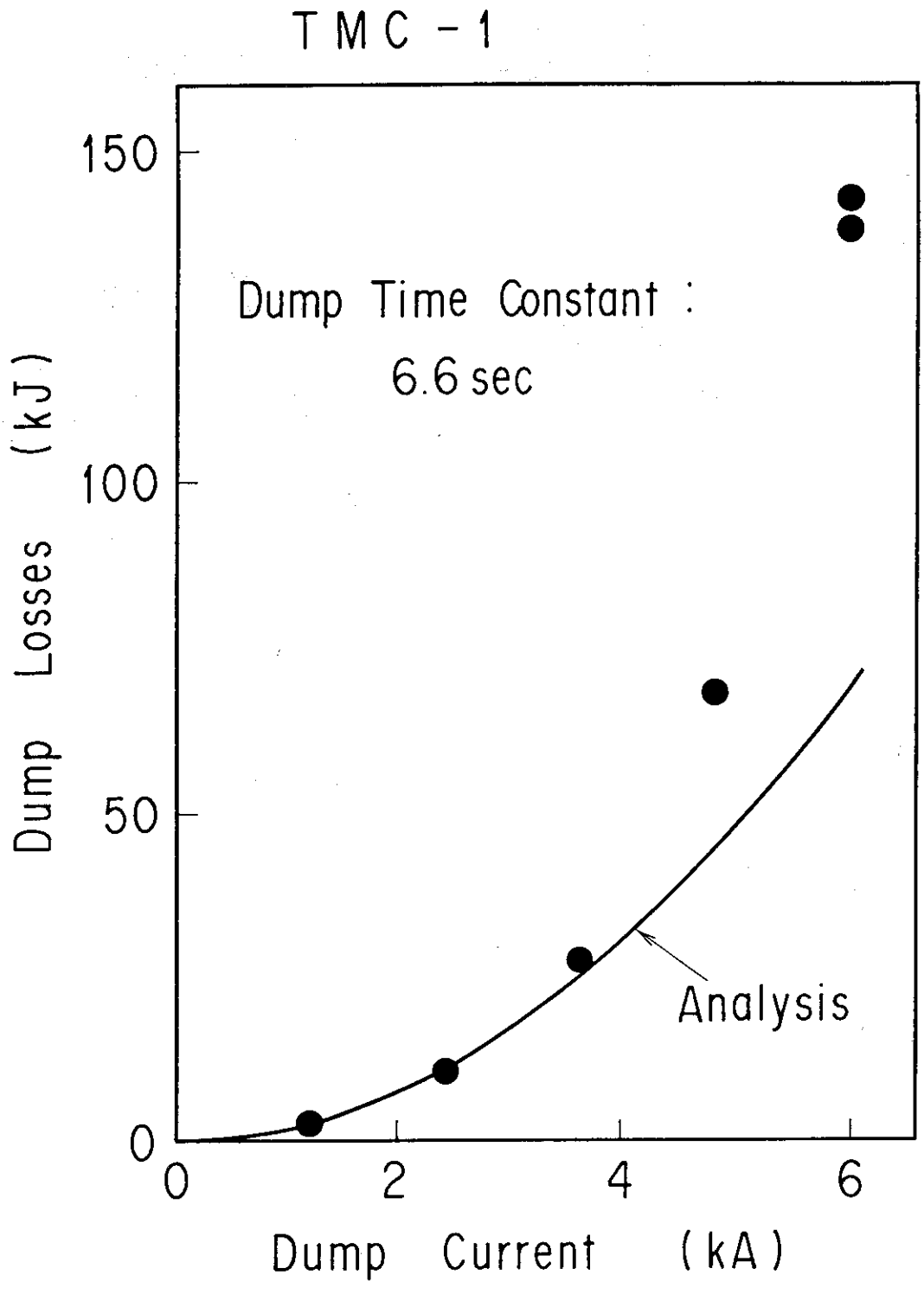

Fig.2.7 Measured and calculated AC losses of TMC.

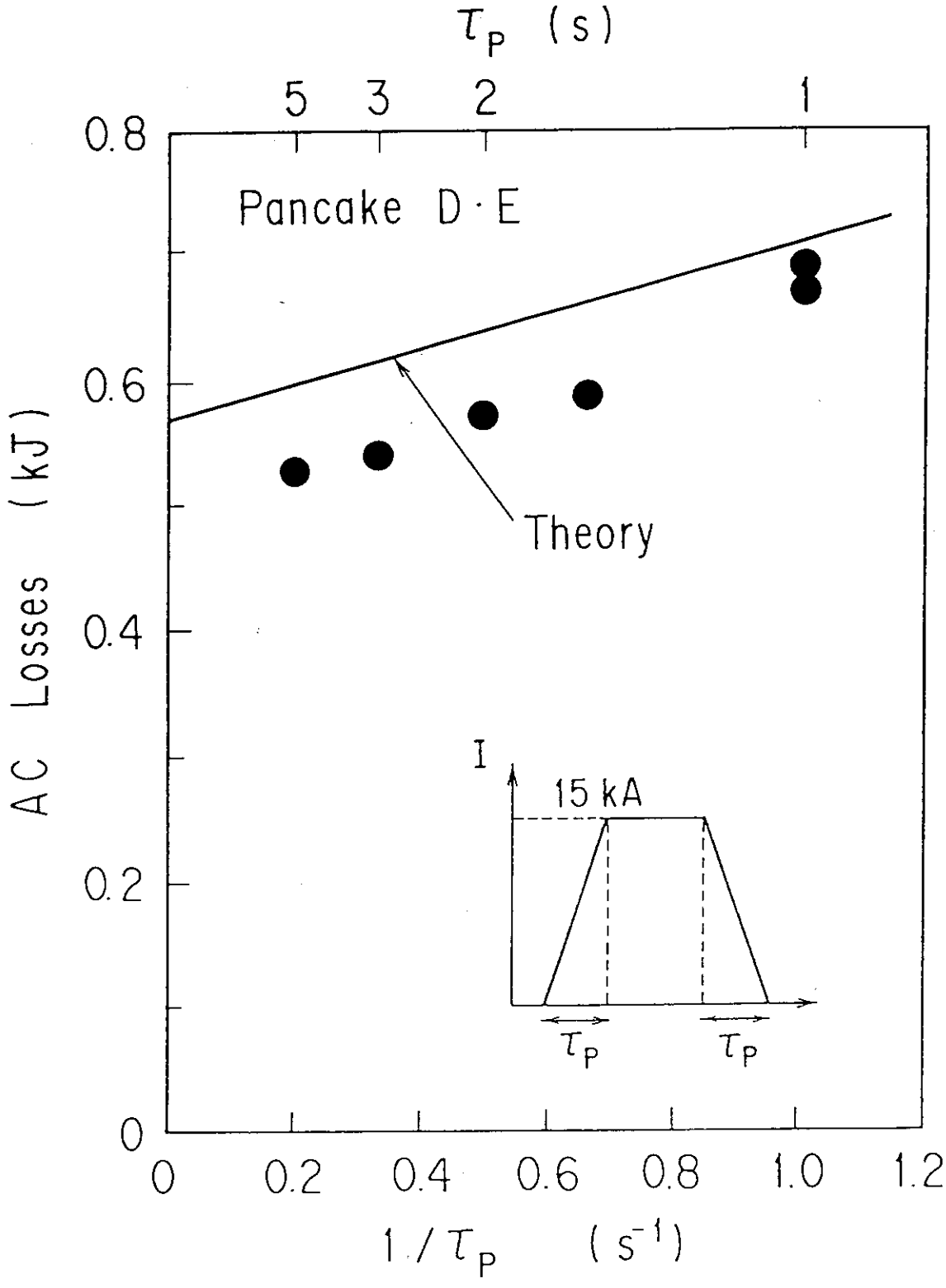

Fig.2.8 Measured and calculated AC losses of DPC-U1, U2.

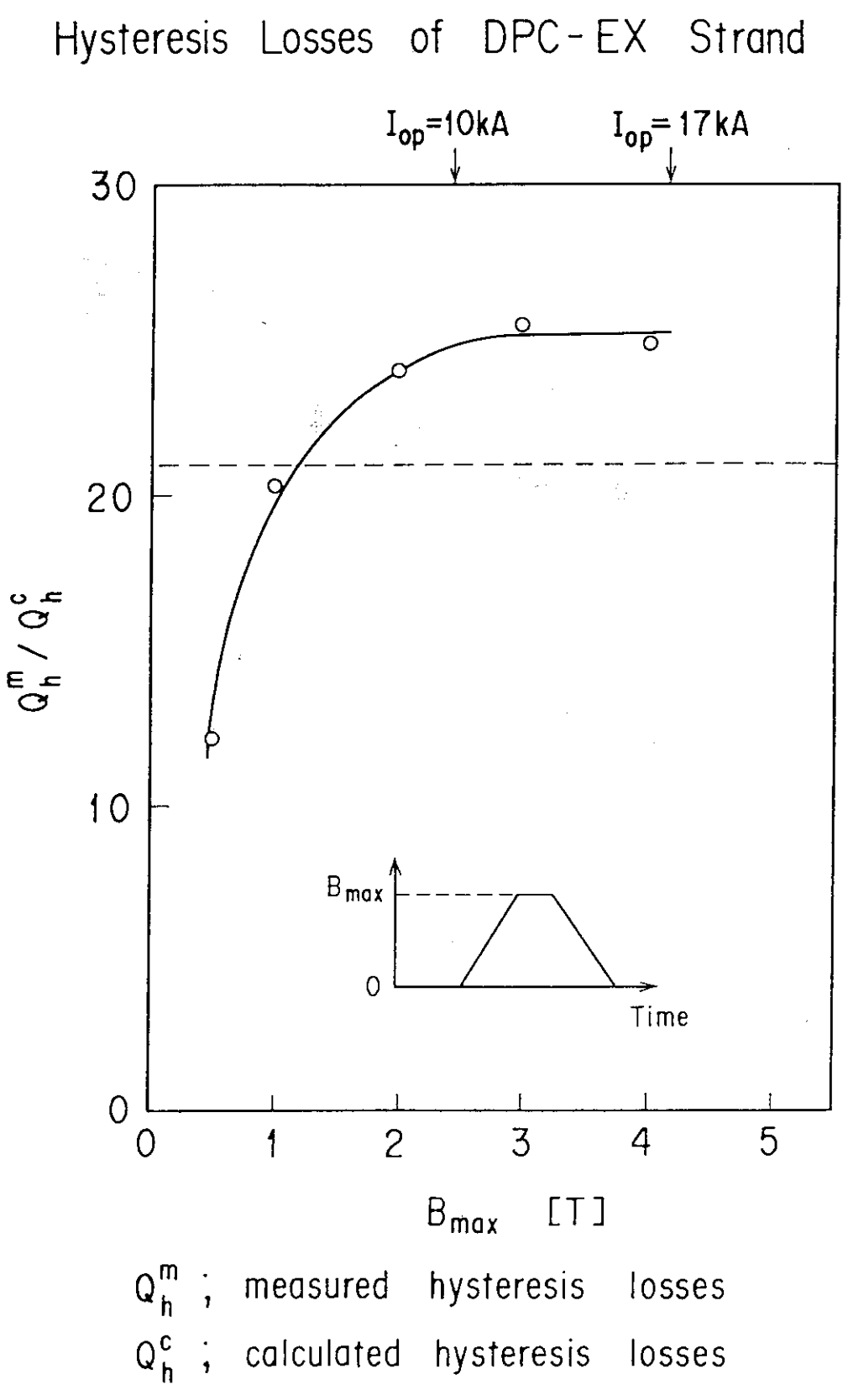

Fig.2.9 Measured and calculated hysterisis losses of DPC-EX strand.

3. AC Loss in winding

3.1 Introduction

AC losses of TF and PF coils were calculated for the reference operation and for the disruption. In this calculation not only the time dependence of the AC loss power, but also the spatial power distribution was obtained.

From the results of the time dependence of the AC loss power during the reference operation, the required cryogenic power was estimated.

On the other hand, from the spatial distribution of the AC loss power during the disruption, the maximum heat production per unit volume was estimated and was used to discuss the stability.

3.2 Procedure

The procedure of AC loss analysis is described as follows.

1) Make the grid point for TF and PF coils.

TF coil : 10 (R) x 10 (θ) x 50 (circumferential)

PF coil : 10 (R) x 10 (Z)

2) Calculate the magnetic field on the grid point at the given times.

3) Calculate AC loss on each grid point interpolating the magnetic field temporally.

The method of AC loss calculation is explained in previous section. The required parameters and the explanations of the parameters are shown in Table 3.1, 2.

The 'Coupling loss Area' in Table 3.1 includes all the area that produces the AC loss power which is proportional to $(dB/dt)^2$ except the conduit area. In the same way 'Coupling

time constant' means the averaged coupling time constant in this area. For example, as for the toroidal coil conductor, there are several time constants as

(1) Strand eddy current time constant. (τ_{eSt})
(2) Filament coupling time constant. (τ_{cF})
(3) Strand coupling time constant. (τ_{cSt})
(4) Copper eddy current time constant (τ_{eCu})

The averaged coupling time constant is

$$\tau_{Ave.} = [(\tau_{eSt}+\tau_{cSt})A_{St} + \tau_{cF}A_{sc} + \tau_{eCu}A_{Cu}] / A_{coup.}$$

where,

A_{St} : Area of Strand.
A_{sc} : Area of super conductor. (In TMC-FF conductor $A_{sc} \sim A_{St}$)
A_{Cu} : Area of stabilizing copper.
$A_{coup.}$: Area of global coupling loss. ($A_{coup.} = A_{St} + A_{Cu}$)

The formulas of filament coupling time constant for PF coils are shown in the previous section. The calculated time constants are shown in Fig.3.1.

The formulas of the critical current density for Nb_3Sn and NbTi are Miller's formula [1] as shown in Fig.3.2. The value at 12 T for Nb_3Sn formula is about 850 A/mm^2.

3.3 Interpretation of the results

3.3.1 AC loss during the reference operation

The current variations of the each coil and plasma for the reference operation are shown in Fig.3.3. This operation is a 500 sec. scenario.

The time dependencies of AC loss power of each component (E.L. : Eddy loss of the conduits, C.L. : Coupling loss of the filament and the strand, H.L. : Hysteresis loss of the super conductor) for each coil are shown in Fig.3.4(a) ~ Fig.3.11(a). The spatial distributions of the power per unit volume at the maximum power production time are shown in Fig.3.4 (b),(c),

Fig.3.5 (b) ~ Fig.3.11 (b).

The averaged power and total avelage power of each component for each coils during 500 s operation dulation are shown in Table 3.3 and 3.4, respectively. The time dependencies of total powers of TF and PF coils are shown in Fig.3.12. The total averaged powers for TF, CS, PF-5(U,L) and PF-6(U,L), 7(U,L) coils are shown in Table 3.5. The averaged powers for the period except the burning time are also shown in this Table.3.5. The maximum values of the spatially averaged power per unit volume for each coil are shown in Table 3.6. These values arise during 0 - 0.6 s. In the same table the local peak values and the values at the maximum field points are shown for the purpose of obtaining the peaking factor. The peaking factor is 10 for TF coil, 2 ~ 3 for PF coils.

It should be noted that this peak value is for one conductor including the He space, the insulator and S.S. conduits. Hence the values for the winding can be obtained by multiplying to this value $(W_{cnd}*T_{cnd})/A_{coup}$. in Table 3.2, since the loss in conduit is negligibly small and the main part of the .

The total averaged power for all coils is about 15.4 kW. In the case that the burn time is excluded, the averaged power is 25.7 kW.

3.3.2 AC loss during the plasma disruption

The current variations of the each coil, the vacuum vessel and the plasma are shown in Table 3.7. The detail of the calculation for these current variations are described in the next section.

The time dependencies of AC loss power for each coil are shown in Fig.3.14(a) ~ Fig.3.21(a). The spatial distributions of the power per unit volume at t=10-22 ms and t=22-50 ms are shown in Fig.3.14 (b),(c),(d),(e), Fig.3.15 (b),(c) ~ Fig.3.21 (b),(c). The time dependencies of total powers of TF and PF coils are shown in Fig.3.22.

The total losses of each component for each coil are shown in Table 3.8. The total loss for TF, CS, PF-5's and PF-6,7's coils are summarized in Table 3.9. The time dependencies of the power for all TF and PF coils are shown in Fig. 3.22. The

spatially local peak values of losses are listed in Table 3.10.

Total loss for all the coils is 673 kJ. The spatially local peak values are 13.7 mJ/cc and 26.6 mJ/cc for TF and CS coil, respectively. The positions of these values are located at low field region.

The maximum loss near the maximum field region are 3 mJ/cc (8 mJ/cc for Strand + stabilizing Cu) at 11 T for toroidal coil. The value for CS coil is also about 3 mJ/cc (15 mJ/cc for strand) at 12 T. The change in magnetic field in the high field region is suppressed by the coil current change due to the flux conservation. For example, the magnetic field change inside of PF-1 coil is reduced to 40 % of that without the flux conservation effect. These losses are also summarized in Table 10.

3.3.3 AC loss during the separatrix sweep

The coil current variations during the separatrix sweep at Start of Burn are shown in Table 3.10. The detail of this computation is shown in the next section. The sweep condition is as follows.

Frequency (f)	0.3	Hz
Amplitude (d)	+/-12	cm (on divertor plate)

The averaged powers of each component for each coil are shown in Table 3.11. The total averaged powers for TF, CS, PF-5(U,L) and PF-6(U,L),7(U,L) coils are shown in Table 3.12.

The corresponding tables for the separatrix sweep at End of Burn are shown in Tables 3.13 ~ 3.15.

Since the dominant part of the AC losses during the sepapratix sweep is due to Hysteresis loss, the AC losses are almost proportional to (f*d).

Reference

[1] Report of WORK by the Magnet Design Unit (Feb.- Mar. 1989) ITER-EL-MG-1-9-U-1

Table 3.1 Required Parameters for AC Loss Calculation

		TF	CS(PF-5)	EF
Conductor		TMC-FF	PA-CS40	CICC-EF40
SC Mat.		$(NbTi)_3Sn$	$(NbTi)_3Sn$	NbTi
Asc	mm^2	111.01	162.11	98.3
Acoup.	mm^2	343.51	421.5	528.7
WcndxTcnd	mm^2	849.3	2018(1564.2)	2171.6
Strand type			type1	type2
RF	mm		0.256	0.321
R1(Rc)	mm		0.262	0.045
R2(Rb)	mm		0.282	0.327
R3(R0)	mm		0.460	0.450
ρf	Ωm		1.2E-7	3.E-8
ρ1(ρc)	Ωm		4.E-8	4.E-8
ρ2(ρb)	Ωm		5.E-9	1.4E-7
ρ3(ρ0)	Ωm		4.2E-11 * B(T) + 1.5E-10	
Lp	mm		20.0 20.0	
τcc($\perp$)	s	5.22E-3	Above parameter's func.	
τcc(//)	s	1.59E-4	-	-
Deff	μm	10.0	10.0	10.0
Jc fom.	A/mm^2	Miller(Nb_3Sn)	Miller(Nb_3Sn)	Miller(NbTi)
TXX(TRR)	mm	21.5	41.0(41.6)	46.6
TZZ(Tθ θ)	mm	39.5	49.1(37.6)	46.6
DDX	mm	3.5	10.8(5.0)	6.1
DDZ	mm	3.5	4.7(5.0)	6.1
τce($\perp$)	s	6.13E-5	Above parameter's func.	
τce(//)	s	4.52E-5	-	-

Table 3.2 Explanations of Parameters for AC Loss Calculation

Conductor	Conductor Name.
SC Mat.	Material of super conductor.
Asc	SC Area in one conductor. (Asc*Jc = Ic)
Acoup.	Coupling loss Area. (Include area for Strand coupling.)
WcndxTcnd	Area of one conductor.(Include the counduits)
Strand type	Distinction of strand type.(See Fig.2.2(a),(b))
RF	See Fig.2.2 (a),(b).
R1(Rc)	See Fig.2.2 (a),(b).
R2(Rb)	See Fig.2.2 (a),(b).
R3(R0)	See Fig.2.2 (a),(b).
ρ f	See Fig.2.2 (a),(b).
ρ 1(ρ c)	See Fig.2.2 (a),(b).
ρ 2(ρ b)	See Fig.2.2 (a),(b).
ρ 3(ρ 0)	See Fig.2.2 (a),(b).
Lp	Twist pitch of filament.
τ cc($\perp$)	Coupling time constant for perpendicular field.
τ cc(//)	Coupling time constant for parallel field. (Include Strand Coupling.)
Deff	Effective Filament Diameter.
Jc fom.	Critical current density formula.

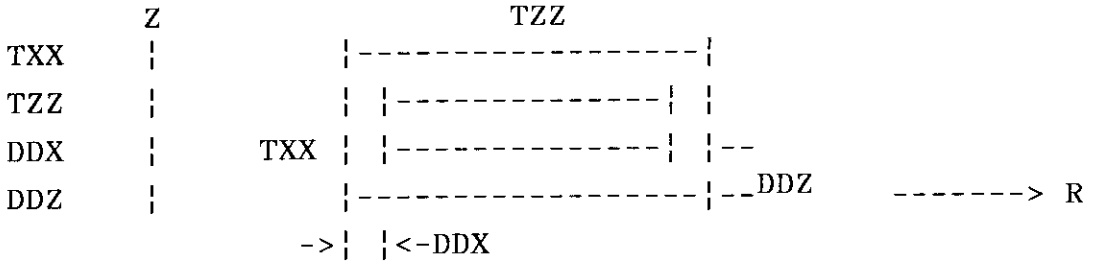

τ ce($\perp$)	Eddy current time const. of S.S. conduit for perpendicular field.
τ ce(//)	Eddy current time const. of S.S. conduit for parallel field.

Table 3.3 Averaged Power of Each Component
(Reference Operation)

	H.L. (W)	C.L. (W)	E.L. (W)	Total (W)
TF(1)(⊥)	9.46E1	1.92E0	1.85E-2	
(//)	9.11E1	6.50E-2	2.05E-2	1.87E2
PF-1	9.94E2	2.98E1	4.29E0	1.03E3
PF-2	1.03E3	2.92E1	4.94E0	1.06E3
PF-3	1.14E3	3.30E1	5.85E0	1.18E3
PF-4	1.16E3	3.68E1	6.36E0	1.20E3
PF-5	1.53E3	2.00E1	2.62E0	1.56E3
PF-6	1.15E2	3.97E0	8.74E-1	1.19E2
PF-7	6.42E1	1.94E0	4.26E-1	6.65E1

Table 3.4 Total Averaged Power of PF and TF coils
(Reference Operation)

	H.L. (kW)	C.L. (kW)	E.L. (kW)	Total (kW)	Burn (kW)
TF coils	2.97	0.03	6.25E-4	2.99	4.98
CS coils	8.65	0.26	4.29E-2	8.94	14.9
PF-5's	3.06	0.04	5.24E-3	3.12	5.2
PF-6,7's	0.36	0.01	2.60E-3	0.37	0.62
TOTAL	15.04	0.34	5.13E-2	15.4	25.7

Table 3.5 Maximum Power per Unit Volume in Each Coil.
(Reference scinario. 0 sec - 0.6 sec)

	Spatially Averaged Value (mW/cc)	Local peak value (mW/cc)	Local value at maximum field (mW/cc)
TF	0.16	1.6	0.01
PF-1	0.90	1.47	1.47
PF-2	0.90	1.47	1.47
PF-3	1.12	1.46	1.46
PF-4	1.07	3.53	~1.8
PF-5	0.85	1.29	1.29
PF-6	0.016	0.040	0.040
PF-7	0.023	0.059	0.059

Table 3.6 Current variations of each PF coil
(Disruption)

t(s)	0.0	0.01	0.022	0.05	0.075	0.1	0.2
PF1U	-22.30	-22.101	-21.100	-19.290	-18.720	-18.480	-18.250
PF2U	-22.30	-22.017	-21.270	-20.190	-19.770	-19.570	-19.360
PF3U	-9.14	-8.991	-8.590	-8.149	-7.890	-7.750	-7.570
PF4U	0.00	0.068	0.248	0.381	0.499	0.575	0.690
PF5U	6.25	6.319	9.498	6.578	6.667	6.731	6.842
PF6U	-6.49	-6.457	-6.340	-6.251	-6.189	-6.139	-6.007
PF7U	-5.25	-5.223	-5.071	-4.830	-4.723	-4.640	-4.397
PF7L	-5.25	-5.222	-5.102	-4.838	-4.728	-4.644	-4.402
PF6L	-6.49	-6.431	-6.403	-6.269	-6.198	-6.145	-6.012
PF5L	6.25	6.316	6.317	6.496	6.630	6.715	6.844
PF4L	0.00	0.0476	0.0556	0.323	0.485	0.577	0.698
PF3L	-9.14	-9.053	-8.857	-8.176	-7.880	-7.730	-7.550
PF2L	-22.30	-22.174	-21.524	-20.170	-19.730	-19.540	-19.340
PF1L	-22.30	-22.203	-21.230	-19.250	-18.690	-18.460	-18.240
PL	22.0	12.0	0.0	0.0	0.0	0.0	0.0
V.V.	0.0	8.8	16.92	9.8	6.96	5.47	3.25
PL+V.V.	22.0	20.8	16.92	9.8	6.96	5.47	3.25

Table 3.7 Total Loss of Each Component
(Disruption)

	H.L. (kJ)	C.L. (kJ)	E.L. (kJ)	Total (kJ)
TF(1) (⊥)		2.54	2.55	0.033
(//)		8.37	3.93	1.25	18.6
PF-1		24.6	46.3	6.82	77.7
PF-2		20.3	24.0	3.68	48.0
PF-3		13.1	8.07	1.28	22.4
PF-4		9.21	2.63	0.40	12.2
PF-5		9.86	2.48	0.33	12.7
PF-6		1.41	1.75	0.50	3.66
PF-7		2.19	6.94	1.56	10.7

Table 3.8 Total loss for PF and TF coils
(Disruption)

	H.L. (kJ)	C.L. (kJ)	E.L. (kJ)	Total (kJ)
TF coils	175	104	21	298
CS coils	134	162	24	321
PF-5's	20	5	1	25
PF-6,7's	7	17	1	29
TOTAL	336	288	47	673

Table 3.9 Maximum Loss per Unit Volume in Each Coil. (Disruption)

	Local peak value (mJ/cc)	Local value at maximum field (mJ/cc)
TF	13.7	2.98
PF-1	26.6	~3
PF-2	20.9	~2.
PF-3	12.3	~1.5
PF-4	3.1	~1.
PF-5	2.0	~1.
PF-6	0.24	0.24
PF-7	1.2	1.2

Table 3.10 Change in PF Coil Current
(0.3 Hz, ΔX = +/- 12 cm Separatrix Sweep Operation at SOB)

	+/-ΔI (kAT)	+I (MAT)	-I (MAT)
PF-1	84.0	-17.786	-17.954
PF-2	84.0	-17.786	-17.954
PF-3	-603.0	-3.013	-1.807
PF-4	-27.6	-0.0276	0.0276
PF-5	423.0	11.213	10.367
PF-6	13.2	-7.1268	-7.1532
PF-7	-31.2	-4.8212	-4.7588

Table 3.11 Averaged Power of Each Component
(0.3 Hz, ΔX = +/- 12 cm Separatrix Sweep Operation at SOB)

	H.L. (W)	C.L. (W)	E.L. (W)	Total (W)
TF(1)(⊥)	3.54E2	1.33E1	1.28E-1	
(//)	2.33E2	3.28E-1	1.04E-1	6.01E2
PF-1	2.86E2	2.23E0	3.55E-1	2.89E2
PF-2	9.89E2	2.76E1	4.89E0	1.02E3
PF-3	2.98E3	1.06E2	1.52E1	3.10E3
PF-4	2.98E3	3.58E1	5.31E0	3.02E3
PF-5	3.74E3	1.80E2	1.35E1	3.94E3
PF-6	7.96E1	7.09E-1	7.81E-2	8.04E1
PF-7	1.17E2	2.33E0	2.61E-1	1.20E2

Table 3.12 Total Averaged Power of PF and TF coils
(0.3 Hz, ΔX = +/- 12 cm Separatrix Sweep operation at SOB)

	H.L. (kW)	C.L. (kW)	E.L. (kW)	Total (kW)
TF coils	9.39	0.22	3.71E-3	9.62
CS coils	14.47	0.34	5.15E-2	14.86
PF-5's	7.48	0.36	2.70E-2	7.88
PF-6,7's	0.39	6.08E-3	6.78E-4	0.40
TOTAL	31.73	0.93	0.083	32.75

Table 3.13 Change in PF Coil Current
(0.3 Hz, ΔX = +/- 12 cm Separatrix Sweep Operation at EOB)

	+/-ΔI (kAT)	+I (MAT)	-I (MAT)
PF-1	84.0	-22.216	-22.384
PF-2	84.0	-22.216	-22.216
PF-3	-603.0	-9.743	-8.537
PF-4	-27.6	-0.0276	0.0276
PF-5	423.0	6.673	5.827
PF-6	13.2	-6.4768	-6.5032
PF-7	-31.2	-5.2812	-5.2188

Table 3.14 Averaged Power of Each Component
(0.3 Hz, ΔX = +/- 12 cm Separatrix Sweep Operation at EOB)

	H.L. (W)	C.L. (W)	E.L. (W)	Total (W)
TF(1)(⊥)	3.59E2	1.34E1	1.28E-1	
(//)	2.32E2	3.29E-1	1.04E-1	6.05E2
PF-1	3.21E2	2.44E0	4.24E-1	3.24E2
PF-2	8.81E2	2.50E1	4.54E0	9.10E2
PF-3	1.85E3	9.77E1	1.52E1	1.96E3
PF-4	2.21E3	3.50E1	5.49E0	2.25E3
PF-5	5.87E3	1.94E2	1.35E0	6.08E3
PF-6	8.18E1	7.27E-1	7.95E-2	8.26E1
PF-7	1.15E2	2.31E0	2.61E-1	1.18E2

Table 3.15 Total Averaged Power of PF and TF coils
(0.3 Hz, ΔX = +/- 12 cm Separatrix Sweep operation at EOB)

	H.L. (kW)	C.L. (kW)	E.L. (kW)	Total (kW)
TF coils	9.46	0.22	3.71E-3	9.68
CS coils	10.52	0.32	5.13E-2	10.89
PF-5's	11.74	0.39	2.70E-2	12.2
PF-6,7's	0.39	6.07E-3	6.81E-4	0.40
TOTAL	32.11	0.94	0.083	33.17

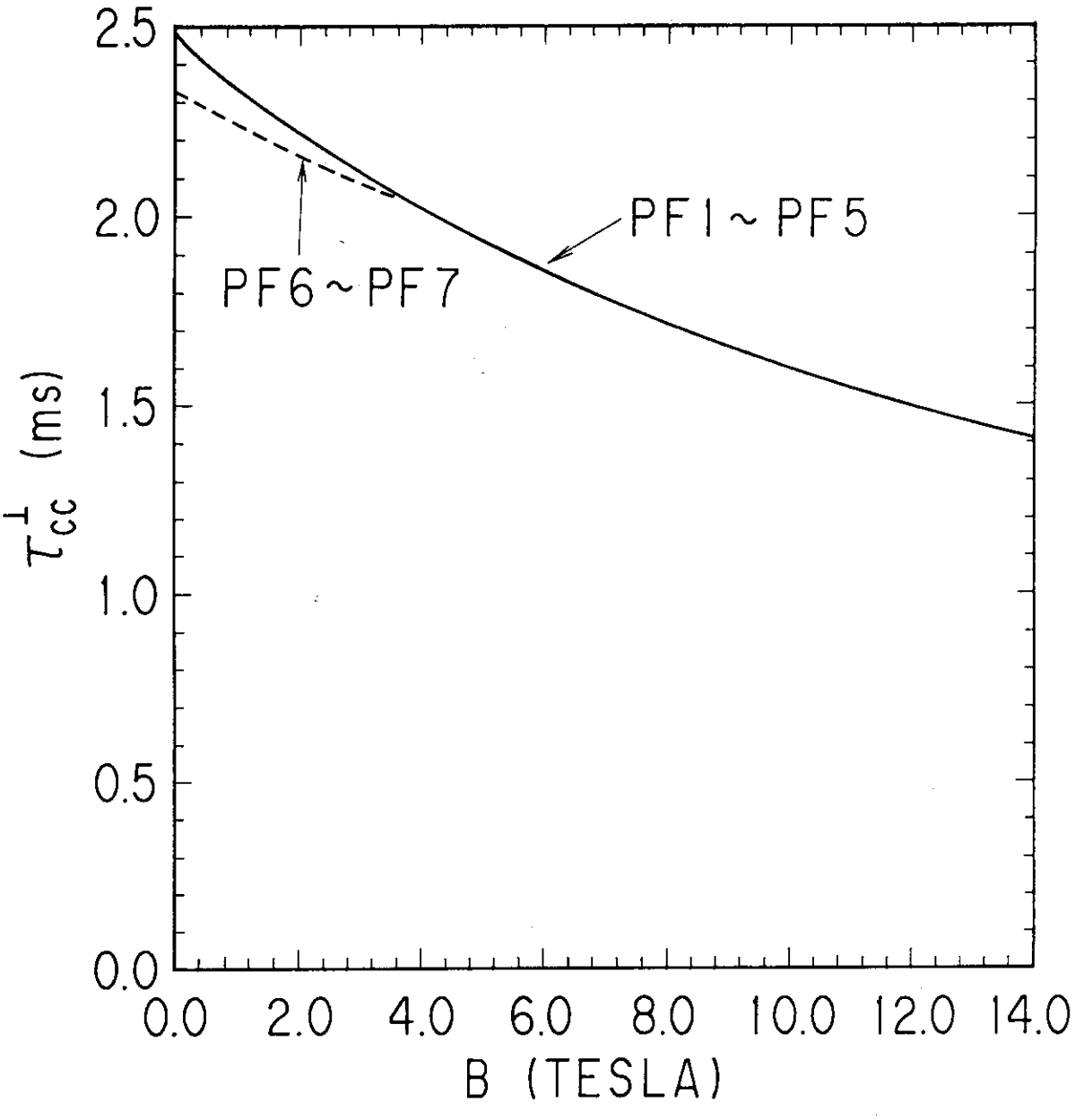

Fig.3.1 Dependence of the coupling time constant on the magnetic field.

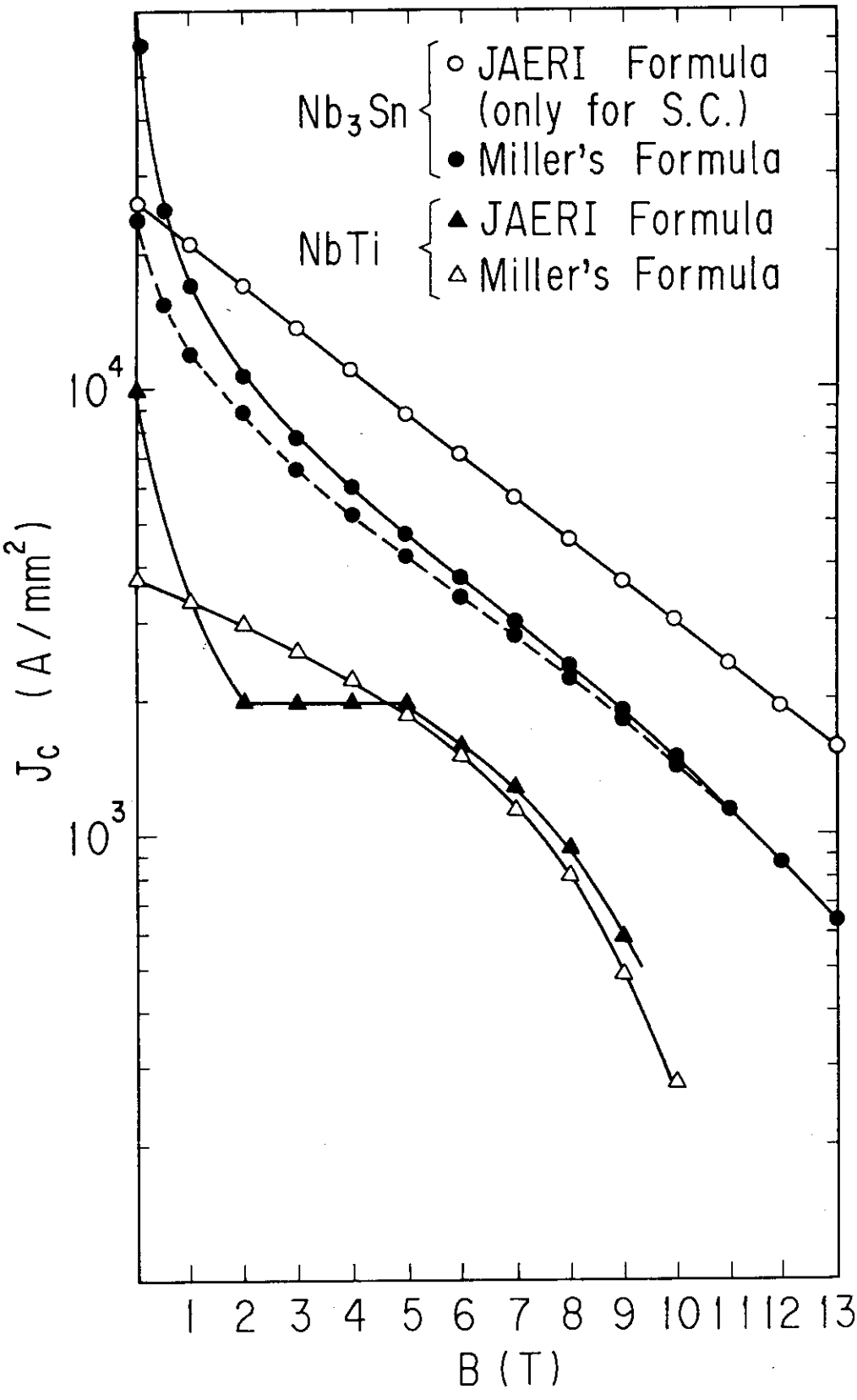

Fig.3.2 Dependence of Jc on perpendicular magnetic field.

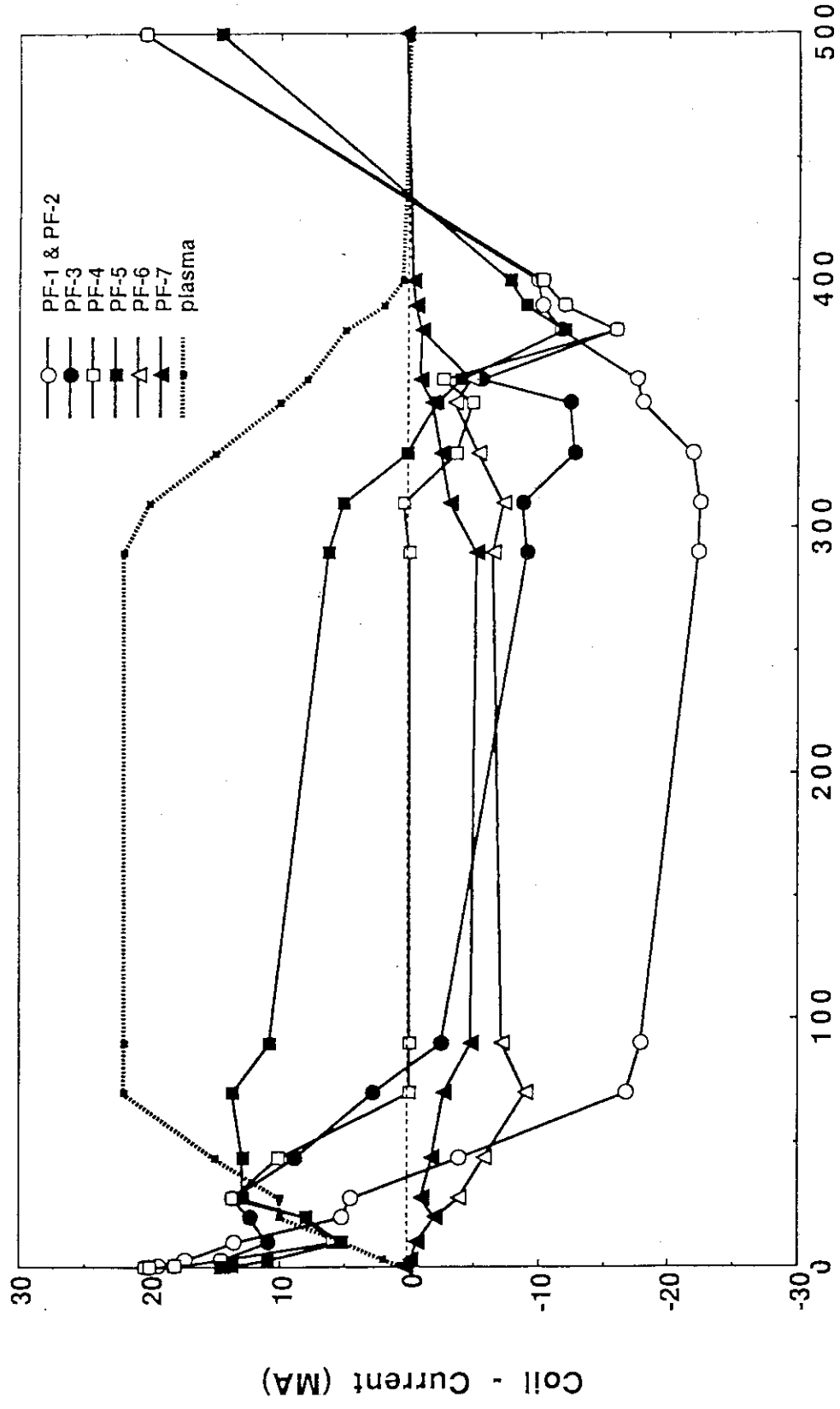

Fig.3.3 Current Variation of the Reference Operation.

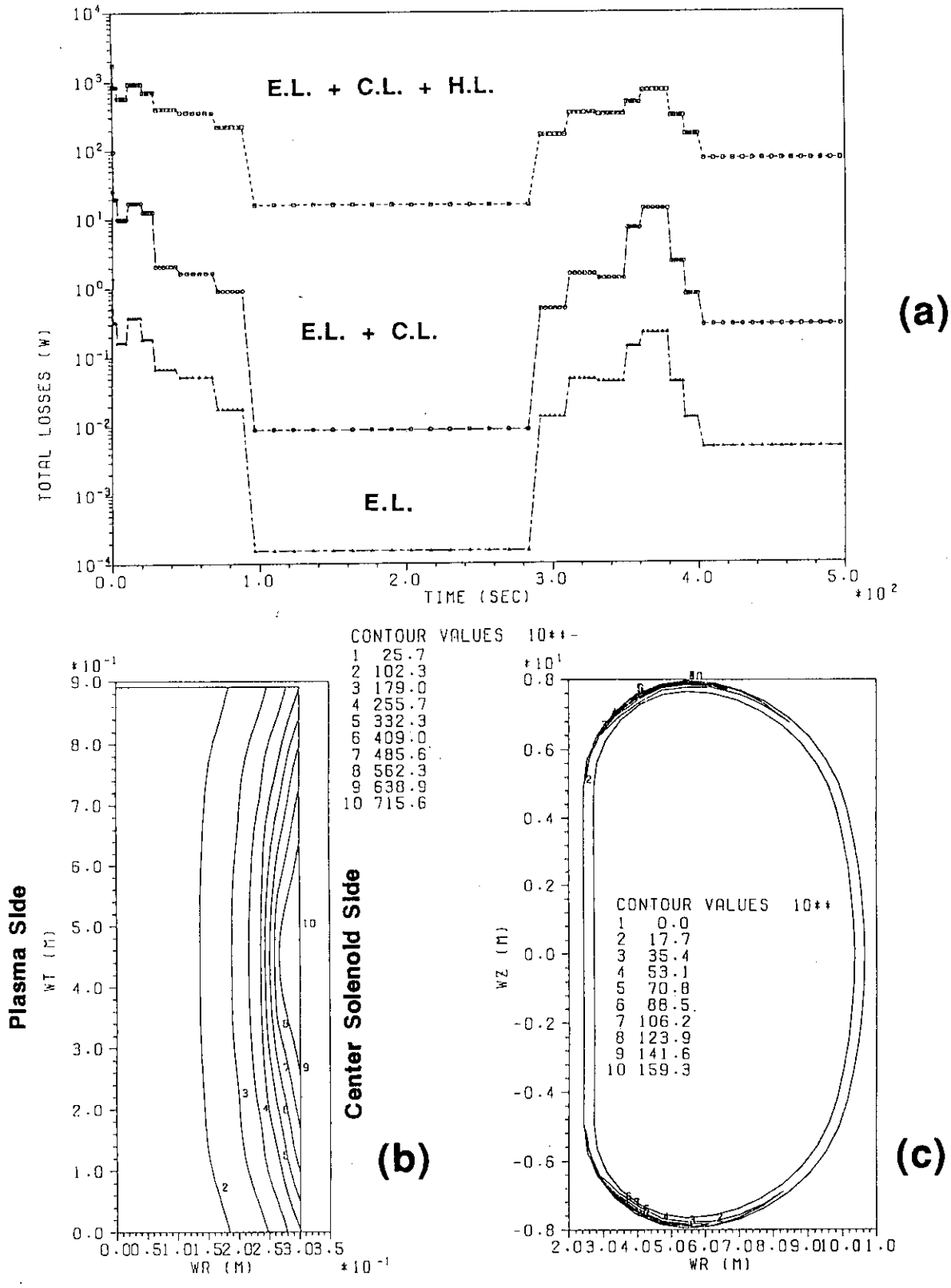

Fig.3.4 TF coil AC loss.(Reference scenario)
(a) Time dependencies of each component. (1 coil) (unit:W)
(b) Spatial distribution of the power per unit volume on the inner mid-plane at t=0.5s. (unit : W/m^3)
(c) Spatial distribution of the power per unit volume on the mid Vertical plane at t=0.5s. (unit : W/m^3)

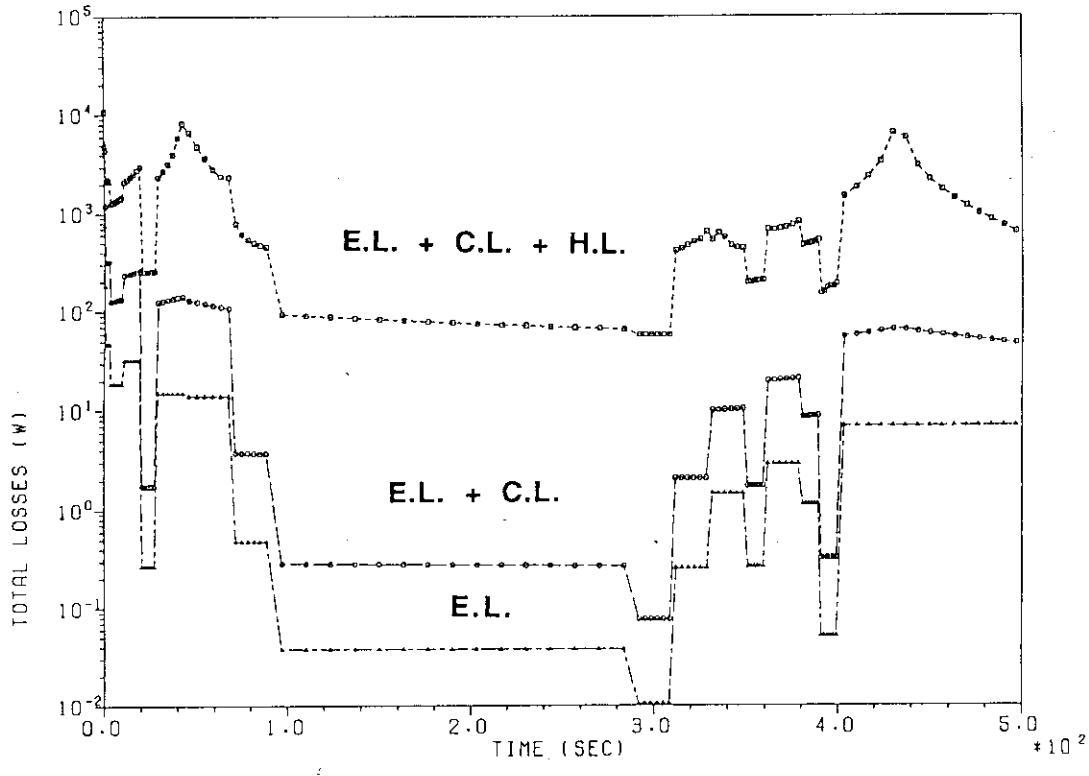

(a)

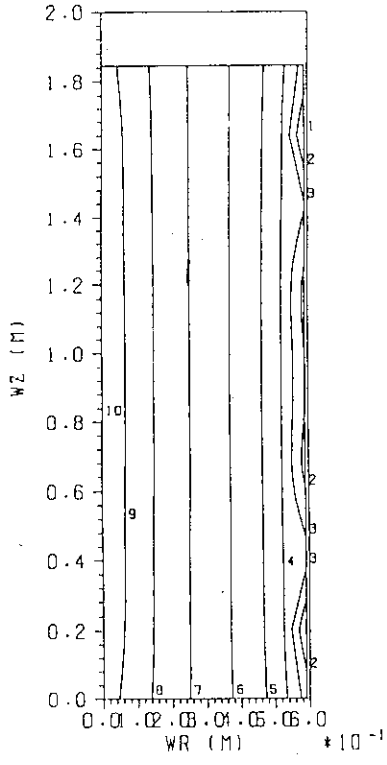

CONTOUR VALUES 10** 1

1	6.5
2	22.1
3	37.7
4	53.3
5	68.9
6	84.5
7	100.1
8	115.7
9	131.3
10	146.9

(b)

Fig.3.5 PF-1 coil AC loss.(Reference scenario)
(a) Time dependencies of each component. (1 coil) (unit:W)
(b) Spatial distribution of the power per unit volume in the cross-section at t=0.5s. (unit : W/m^3).

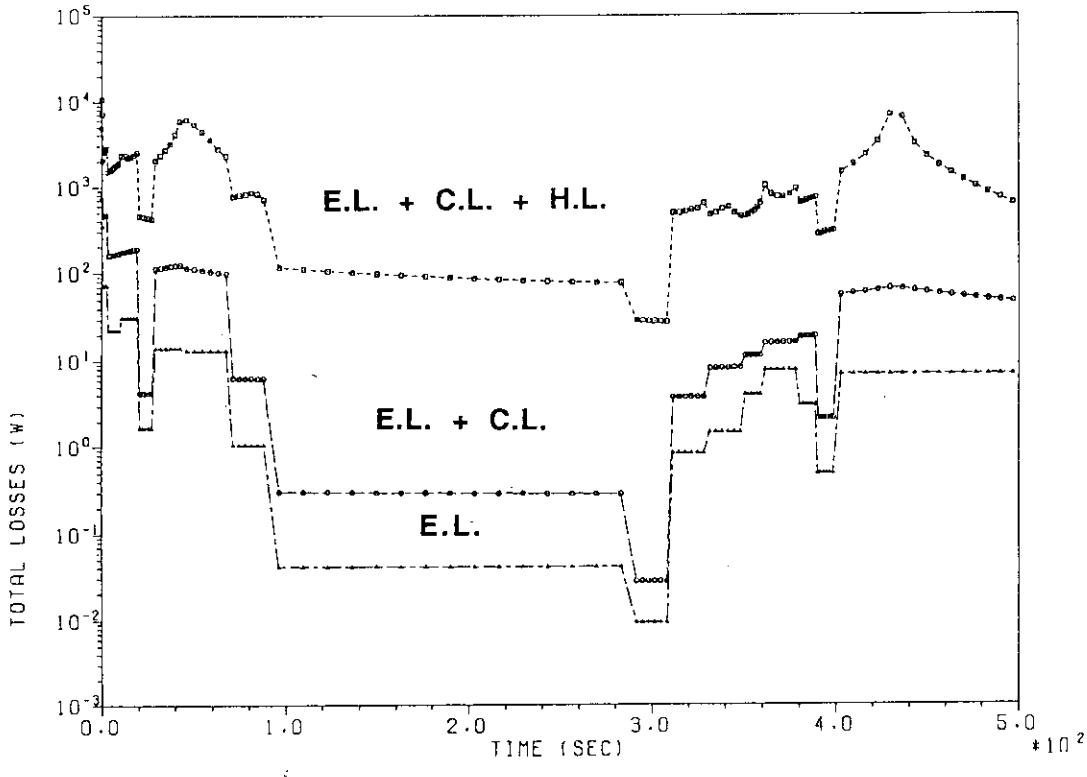

(a)

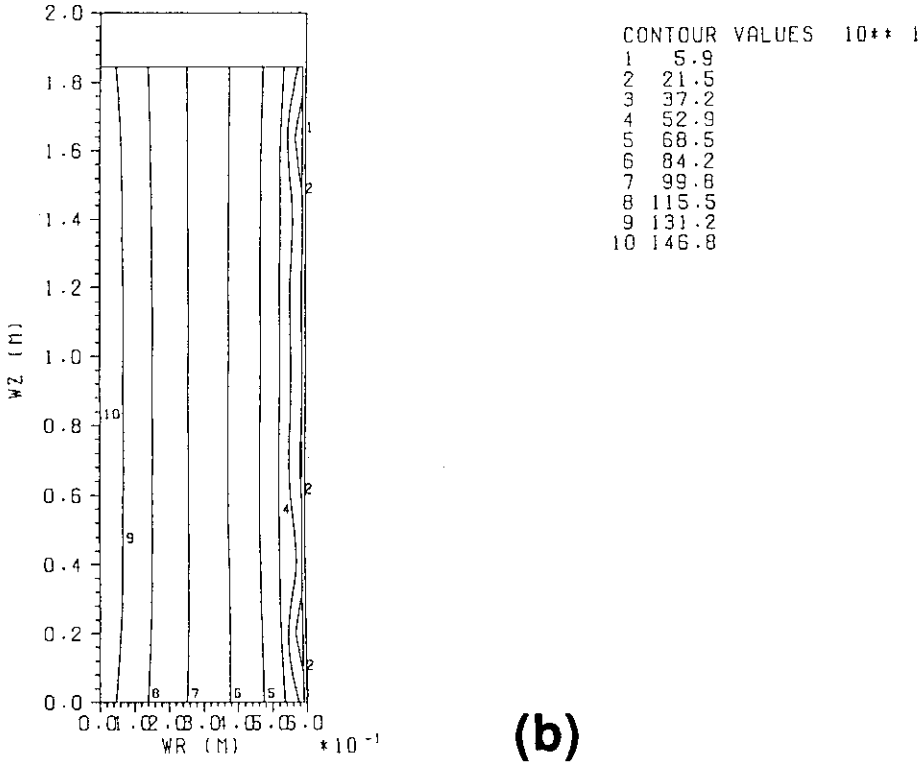

(b)

Fig.3.6 PF-2 coil AC loss.(Reference scenario)
(a) Time dependencies of each component. (1 coil) (unit:W)
(b) Spatial distribution of the power per unit volume in the cross-section at t=0.5s. (unit : W/m^3).

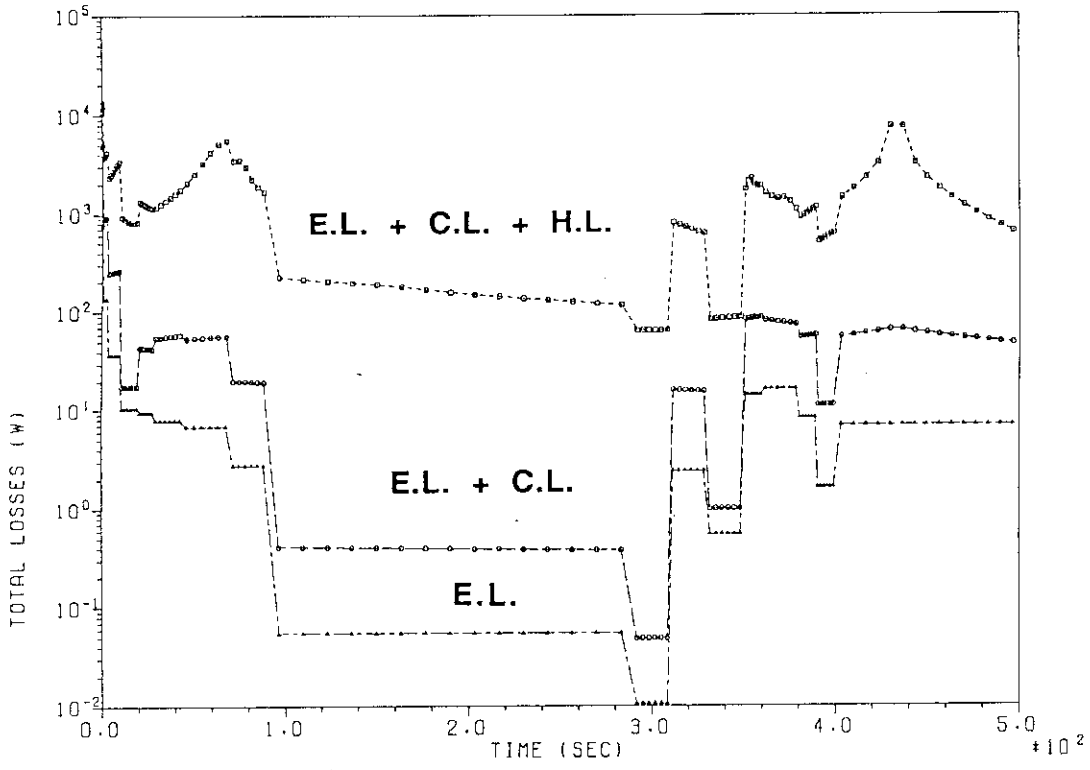

(a)

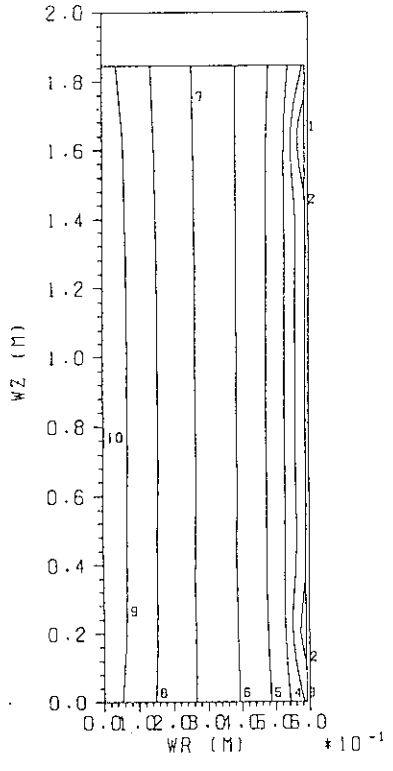

CONTOUR VALUES 10** 1

1	2.1
2	18.1
3	34.1
4	50.1
5	66.1
6	82.0
7	98.0
8	114.0
9	130.0
10	145.9

(b)

Fig.3.7 PF-3 coil AC loss.(Reference scenario)
(a) Time dependencies of each component. (1 coil) (unit:W)
(b) Spatial distribution of the power per unit volume in the cross-section at t=0.5s. (unit : W/m^3).

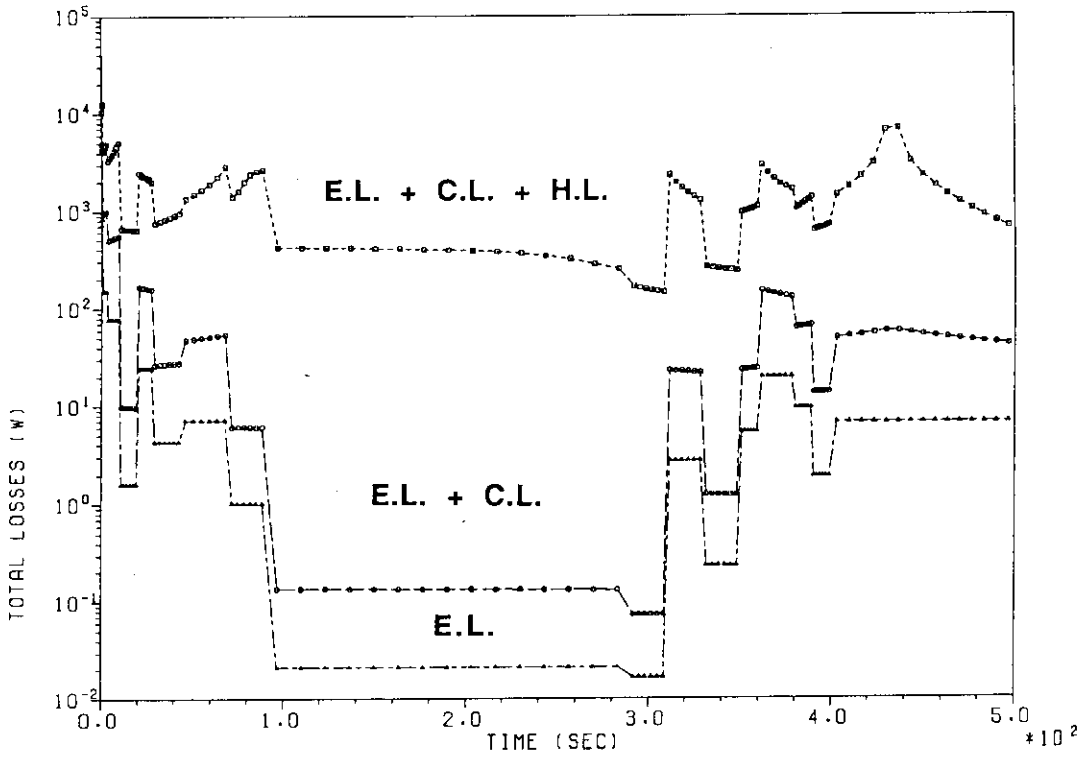

(a)

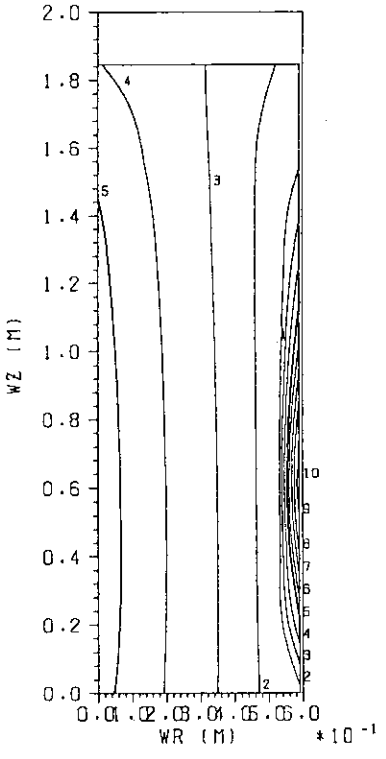

CONTOUR VALUES 10** 1
1 17.0
2 54.3
3 91.7
4 129.1
5 166.4
6 203.8
7 241.2
8 278.5
9 315.9
10 353.3

(b)

Fig.3.8 PF-4 coil AC loss.(Reference scenario)
(a) Time dependencies of each component. (1 coil) (unit:W)
(b) Spatial distribution of the power per unit volume in the cross-section at t=0.6s. (unit : W/m^3).

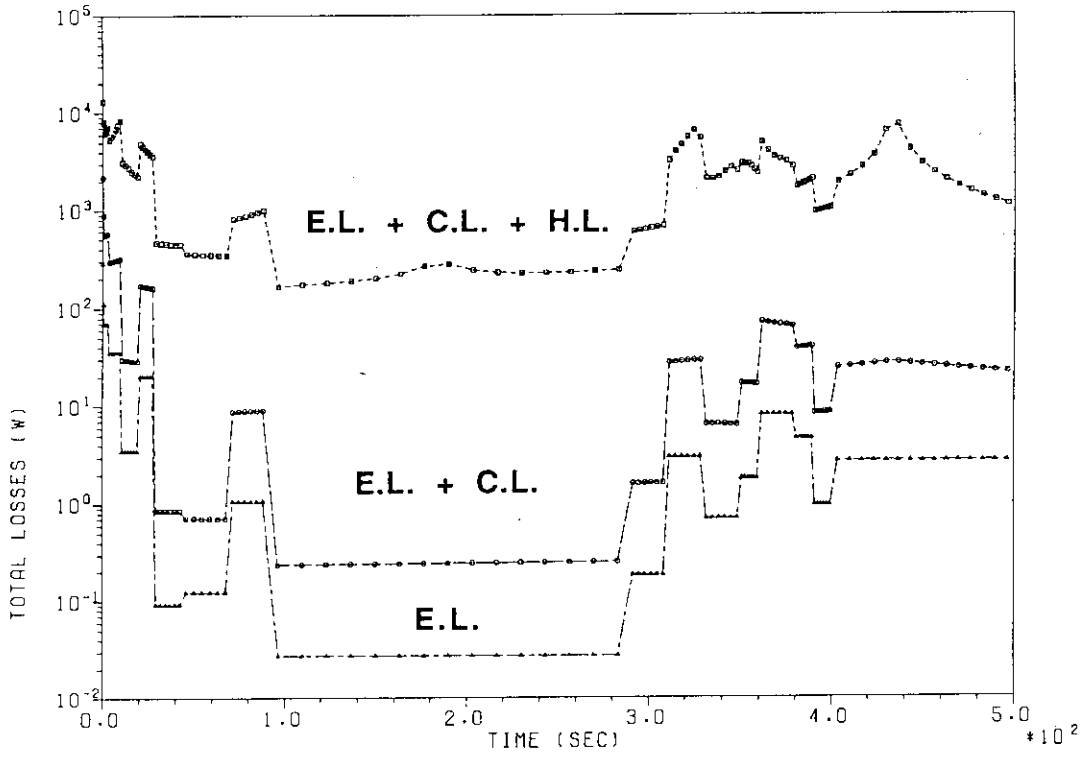

(a)

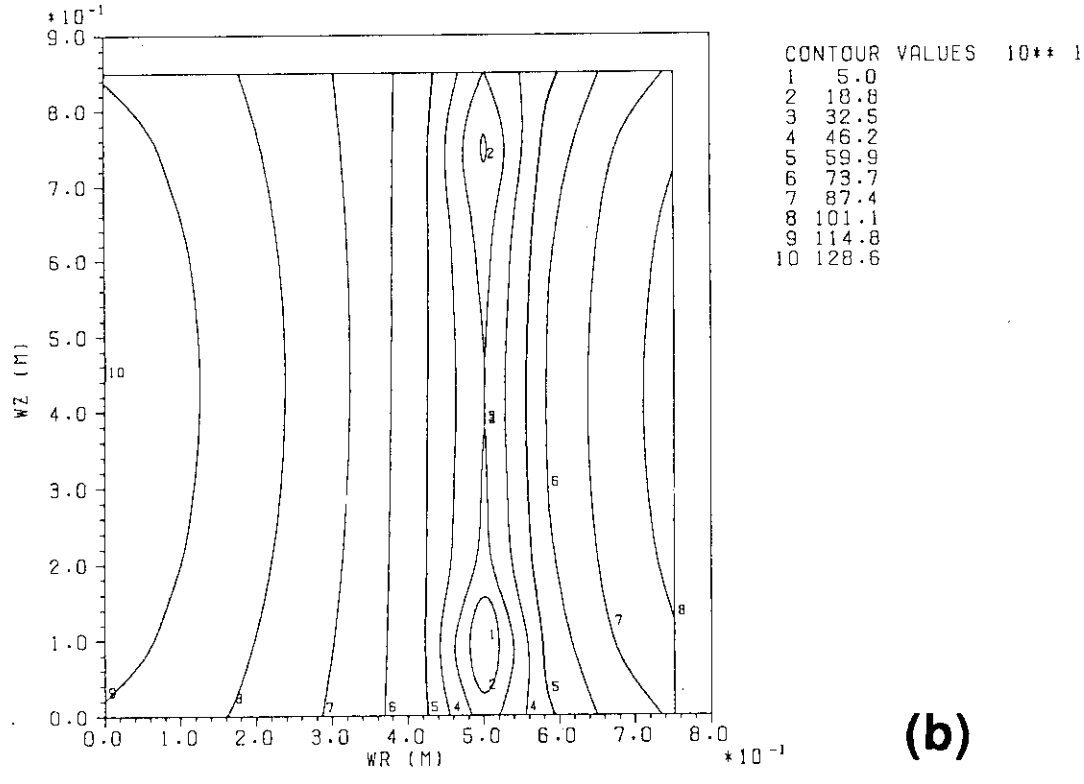

(b)

Fig.3.9 PF-5 coil AC loss.(Reference scenario)
(a) Time dependencies of each component. (1 coil) (unit:W)
(b) Spatial distribution of the power per unit volume in the cross-section at t=0.5s. (unit : W/m^3).

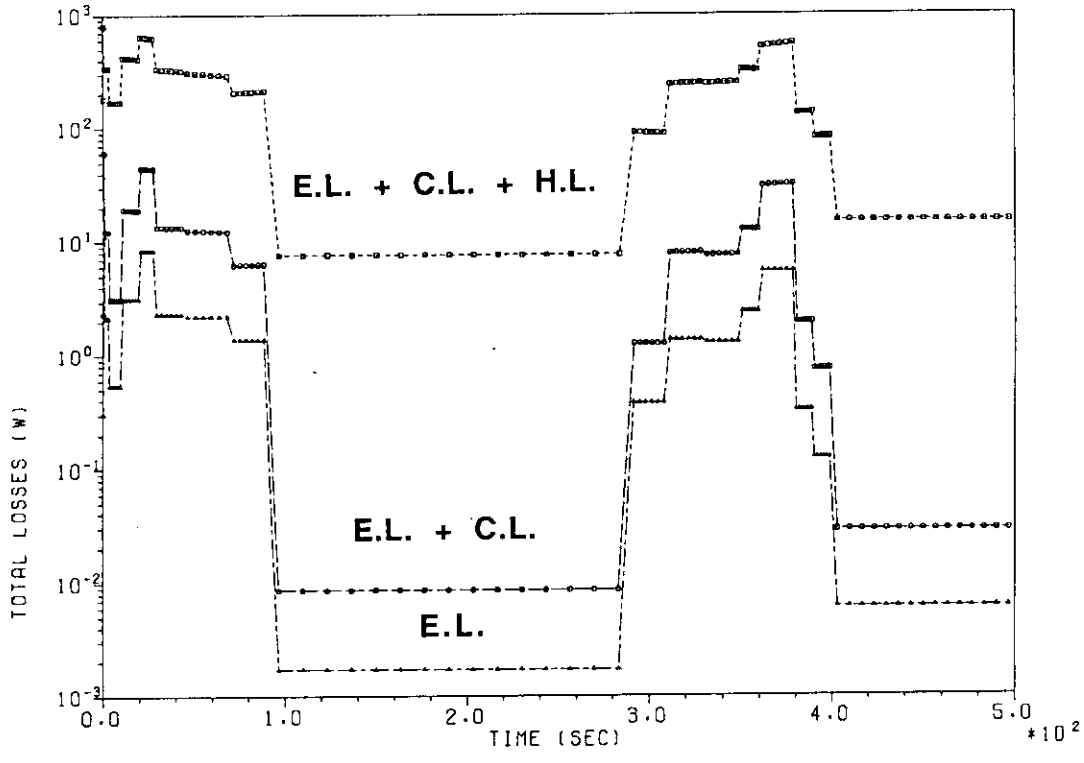

(a)

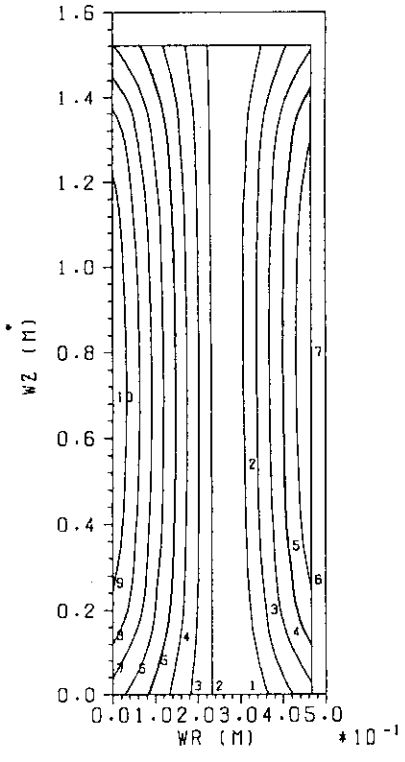

CONTOUR VALUES 10**-1

1	12.4
2	55.3
3	98.2
4	141.1
5	183.9
6	226.8
7	269.7
8	312.6
9	355.5
10	398.4

(b)

Fig.3.10 PF-6 coil AC loss.(Reference scenario)
(a) Time dependencies of each component.(1 coil) (unit:W)
(b) Spatial distribution of the power per unit volume in the cross-section at t=0.2s. (unit : W/m^3).

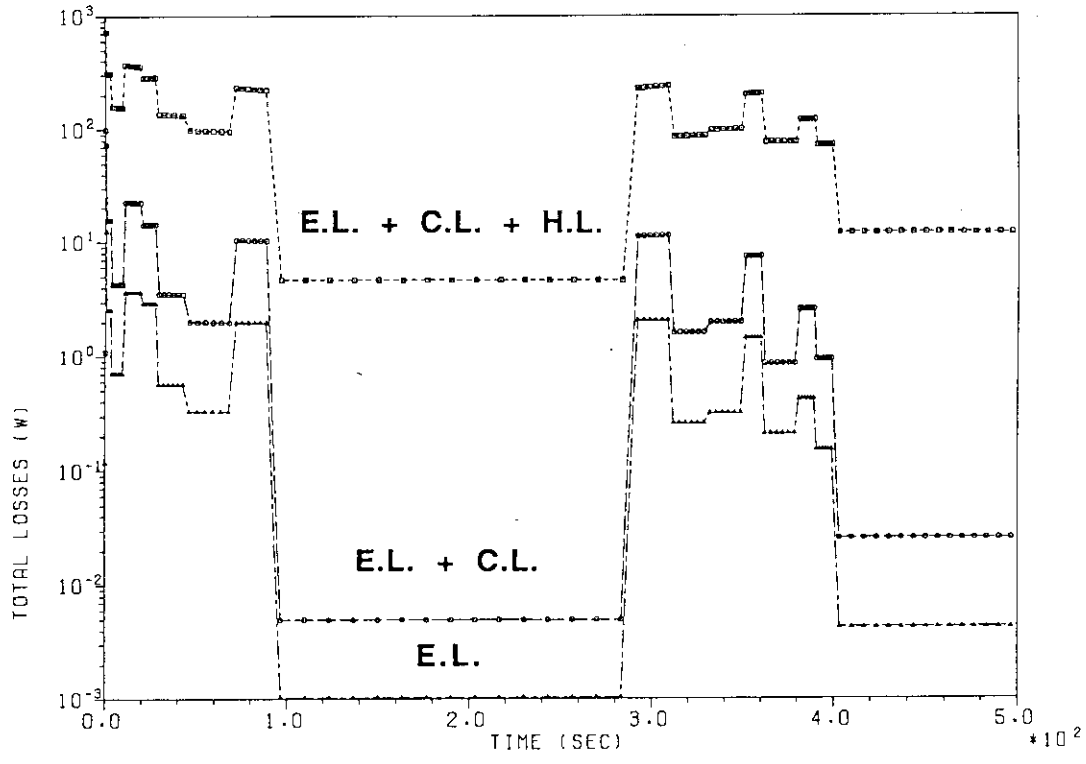

(a)

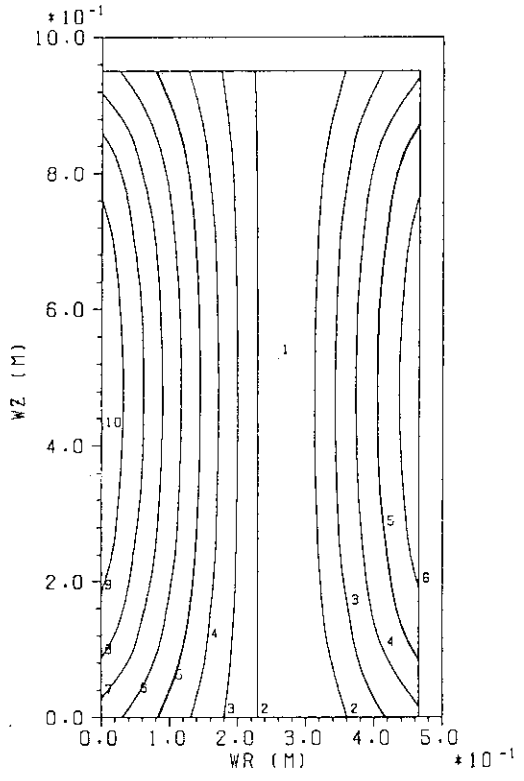

CONTOUR VALUES 10**-1

1	23.2
2	86.2
3	149.3
4	212.3
5	275.4
6	338.4
7	401.5
8	464.6
9	527.6
10	590.7

(b)

Fig.3.11 PF-7 coil AC loss.(Reference scenario)
(a) Time dependencies of each component.(1 coil) (unit: W)
(b) Spatial distribution of the power per unit volume in the cross-section at t=0.3s. (unit : W/m^3).

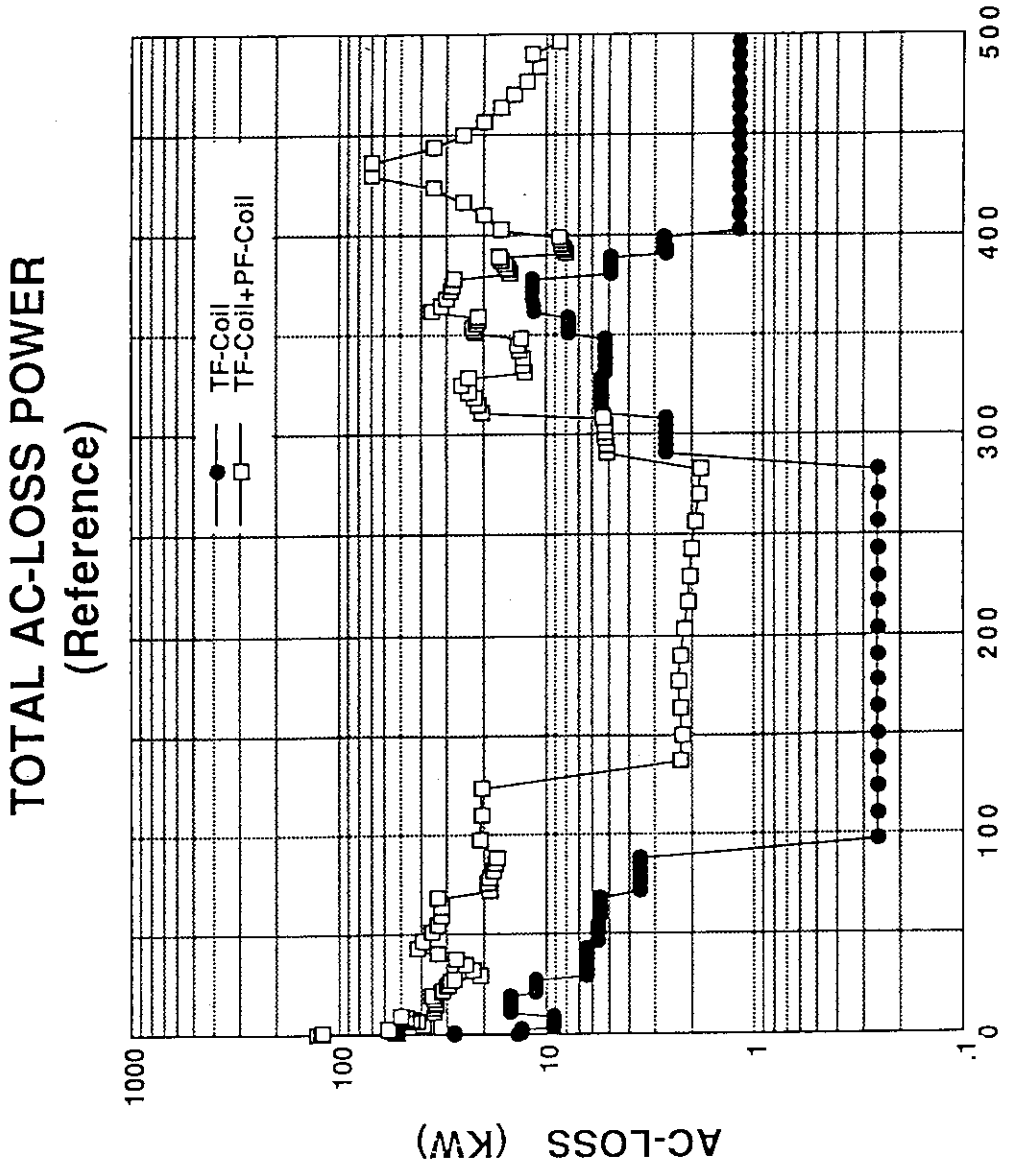

Fig.3.12 Total power of AC loss for all TF and PF coils.(unit :kW)
(Reference scenario)

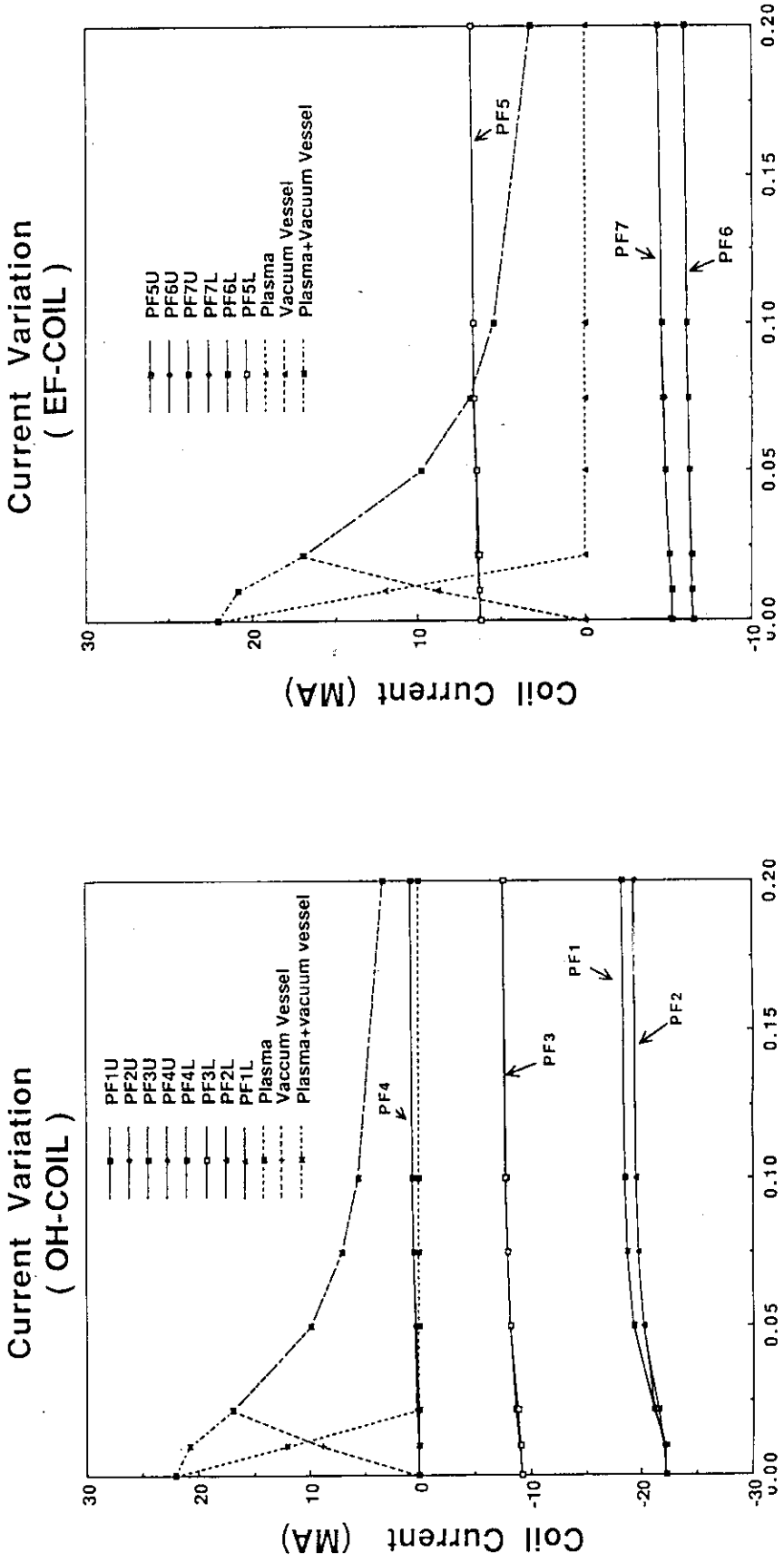

Fig.3.13 Current variations of each coil, plasma and the vacuum vessel at the disruption.
(a) Center solenoid coil.
(b) PF-5 and outer ring coils.

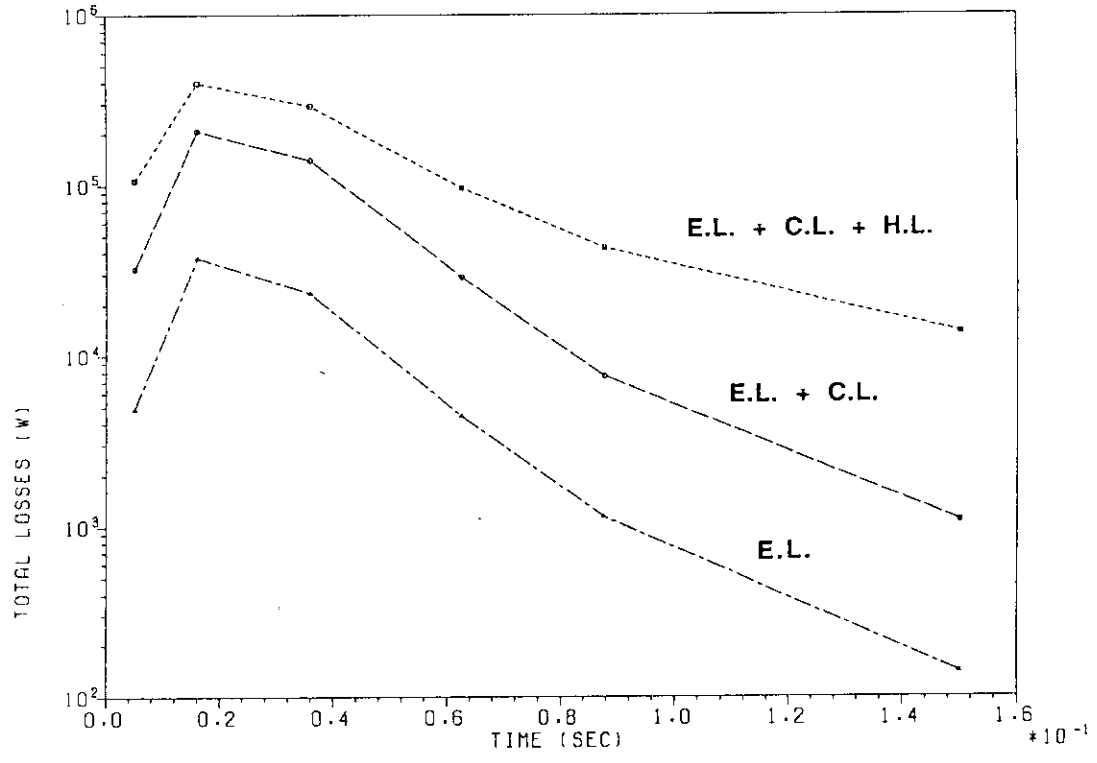

(a)

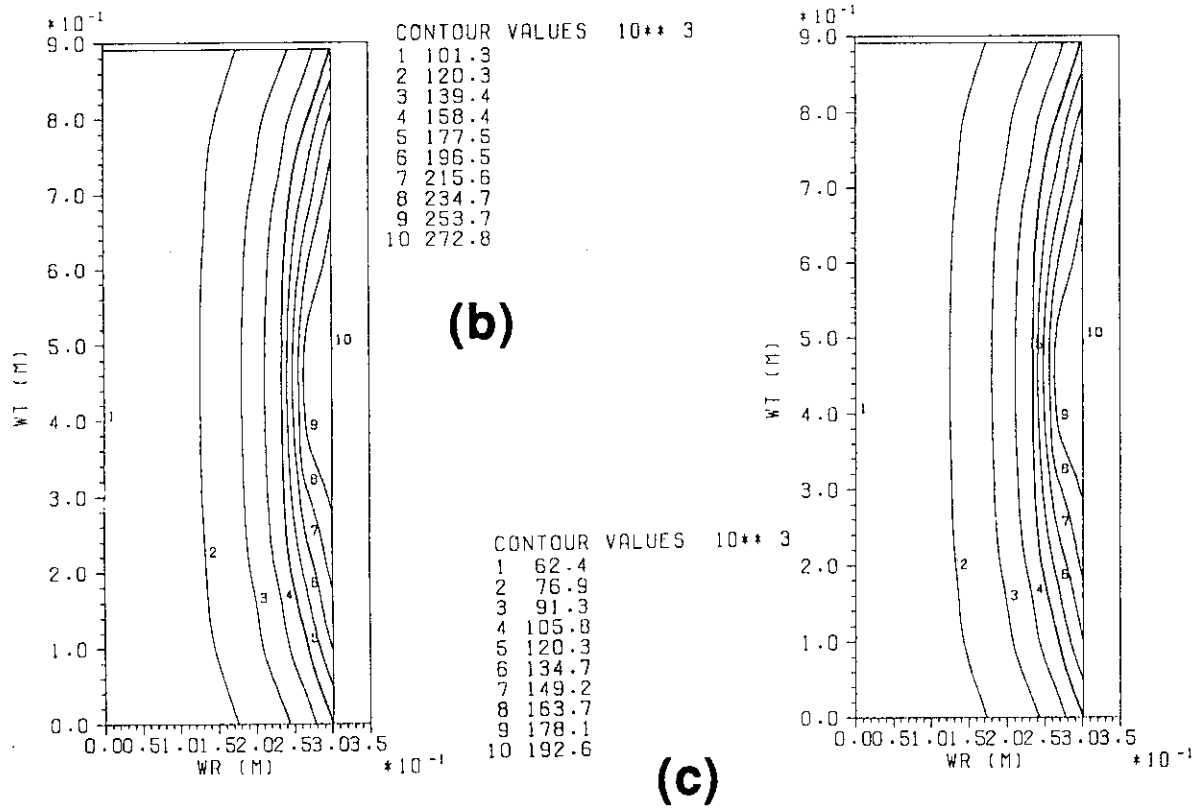

(b)

(c)

Fig.3.14 TF coil AC loss.(during Disruption)
(a) Time dependencies of each component.(1 coil) (unit:W)
(b),(c) Spatial distribution of the power per unit volume on the inner mid-plane at t= (b)15 ms,(c)35 ms. (unit : W/m^3)

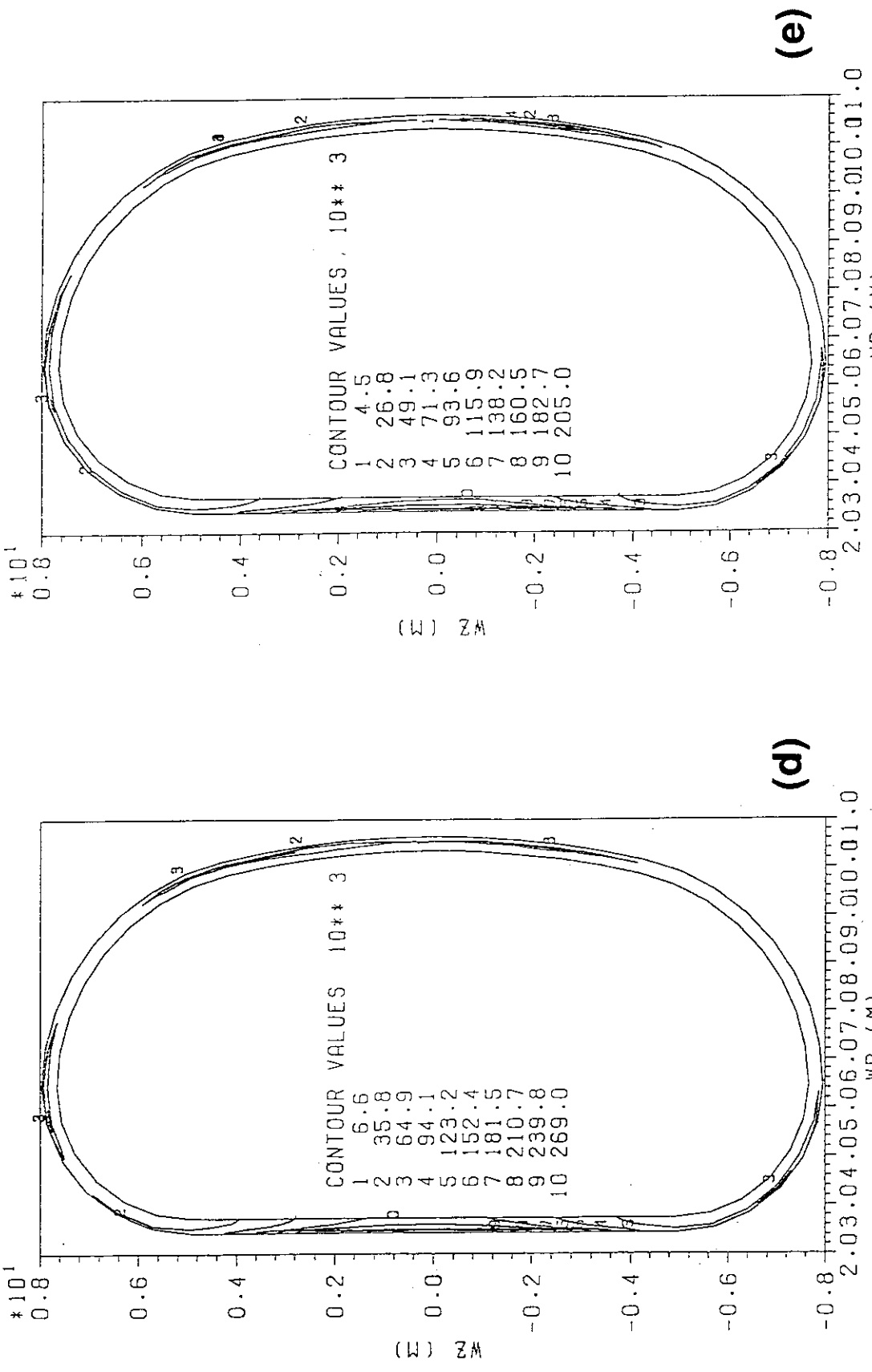

Fig.3.14 TF coil AC loss.(during Disruption)
(d),(e) Spatial distribution of the power per unit volume on the mid Vertical plane at t= (d)15 ms, (e)35 ms. (unit : W/m^3)

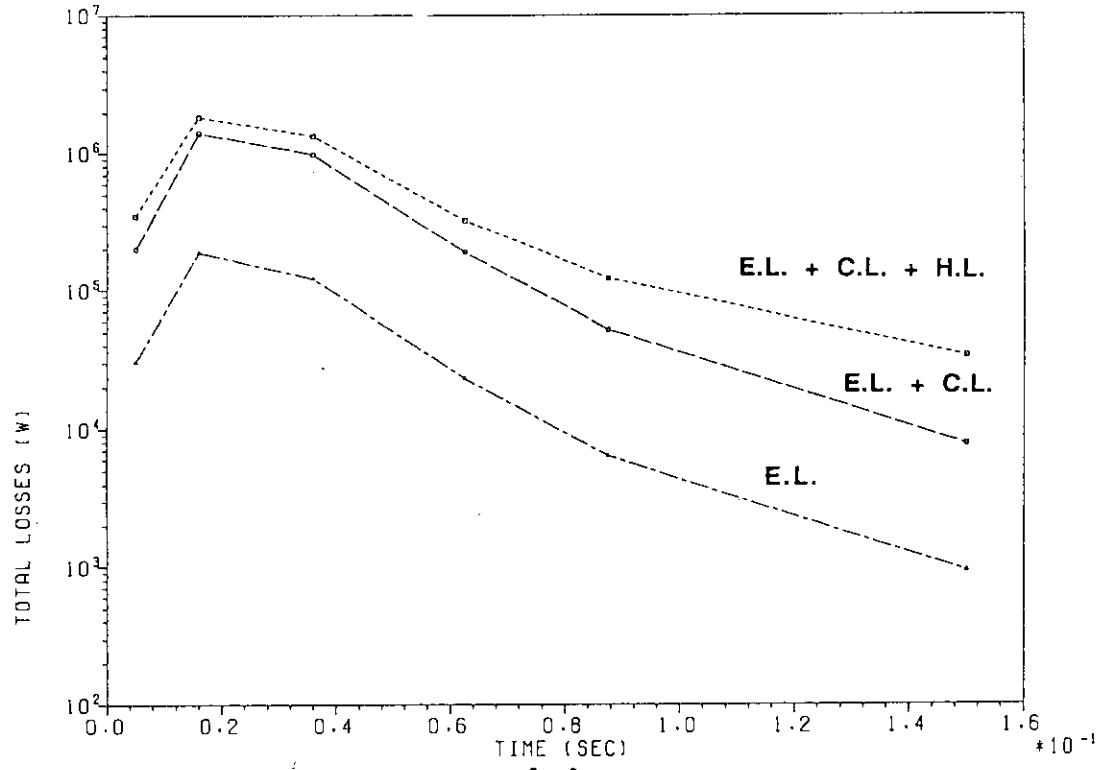

(a)

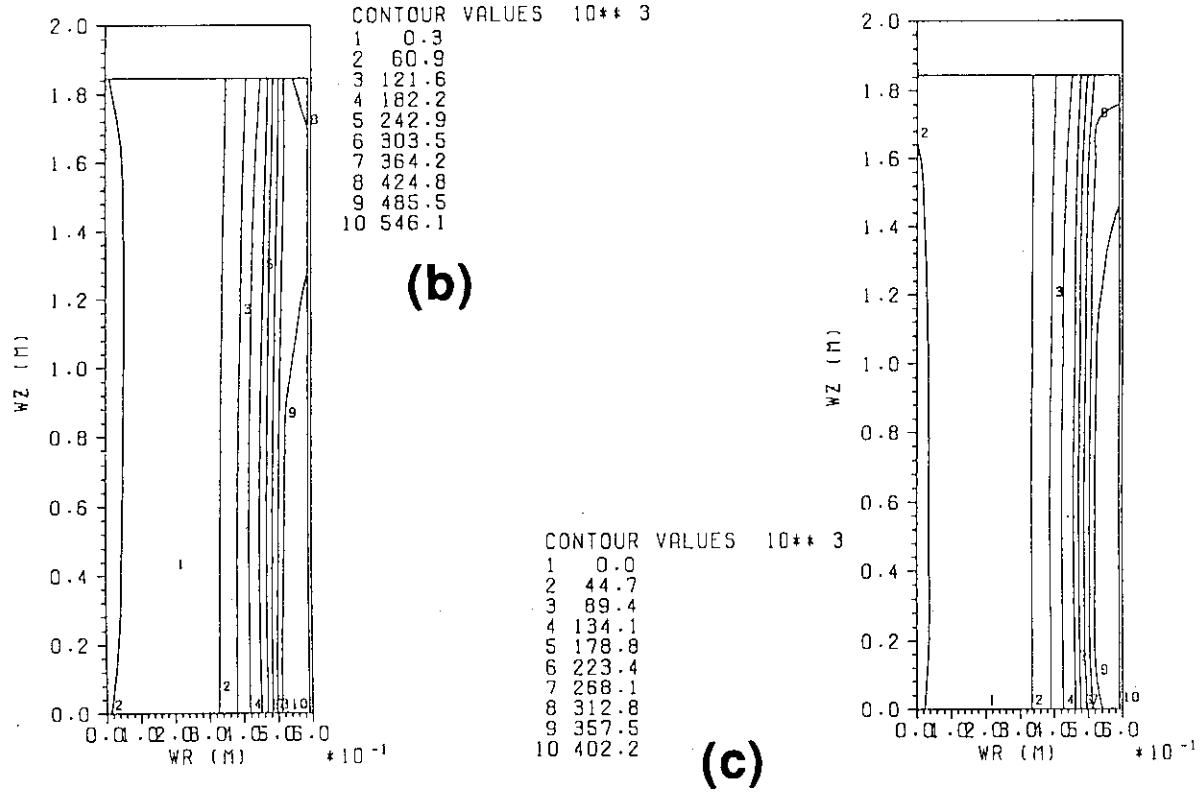

Fig.3.15 PF-1 coil AC loss.(during Disruption)
(a) Time dependencies of each component.(1 coil) (unit:W)
(b),(c) Spatial distribution of the power per unit volume on the cross-section at t= (b)15 ms, (c)35 ms. (unit : W/m^3)

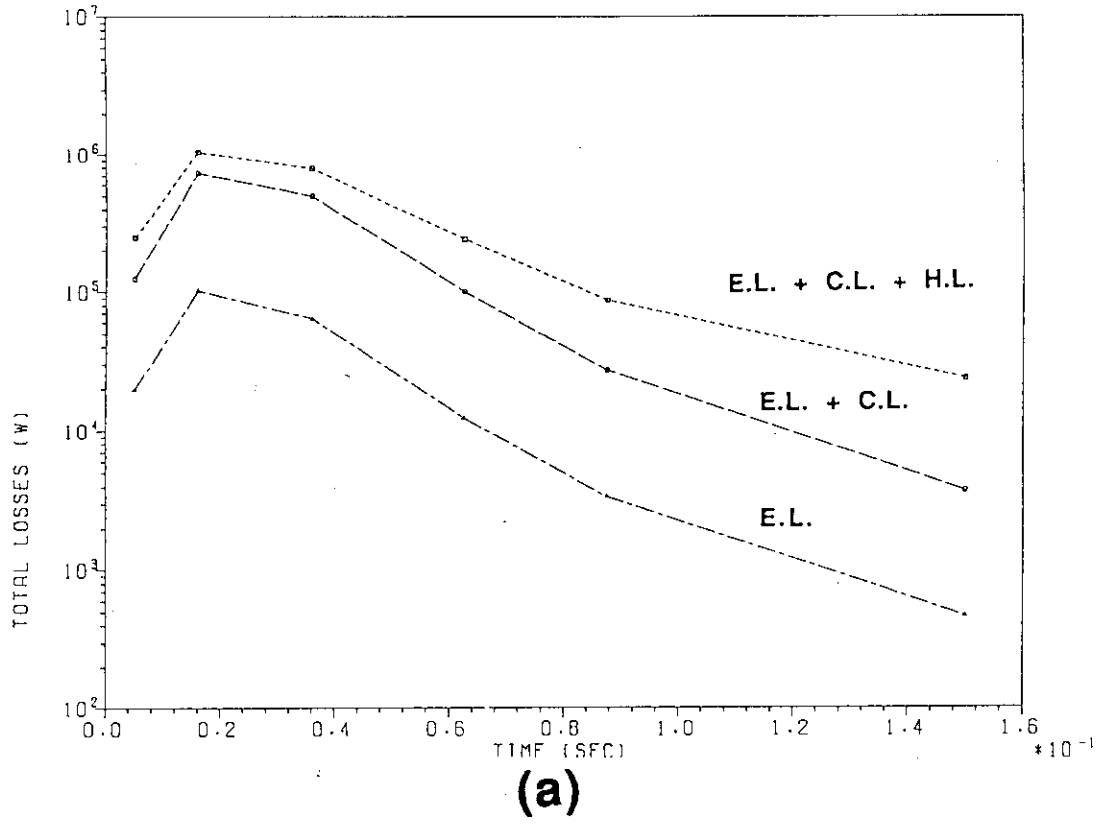

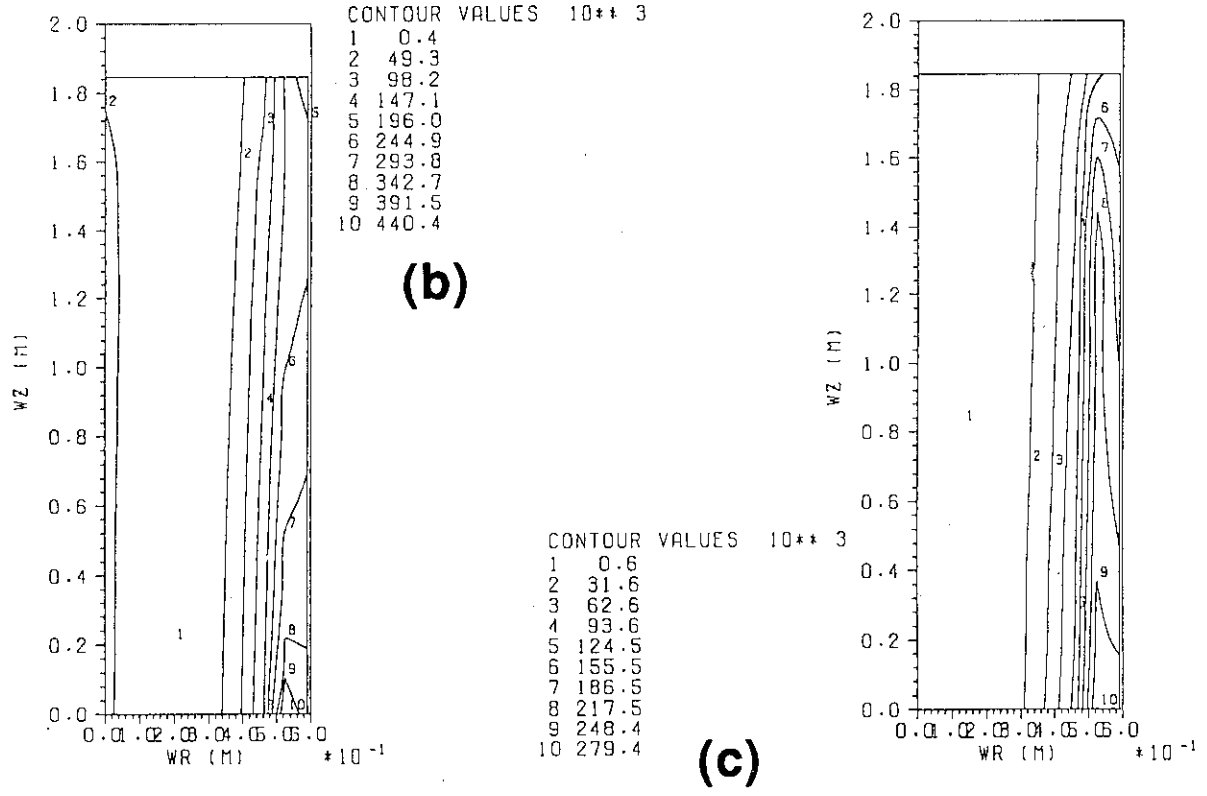

Fig.3.16 PF-2 coil AC loss.(during Disruption)
(a) Time dependencies of each component. (1 coil) (unit:W)
(b),(c) Spatial distribution of the power per unit volume on the cross-section at t= (b)15 ms, (c)35 ms. (unit : W/m^3)

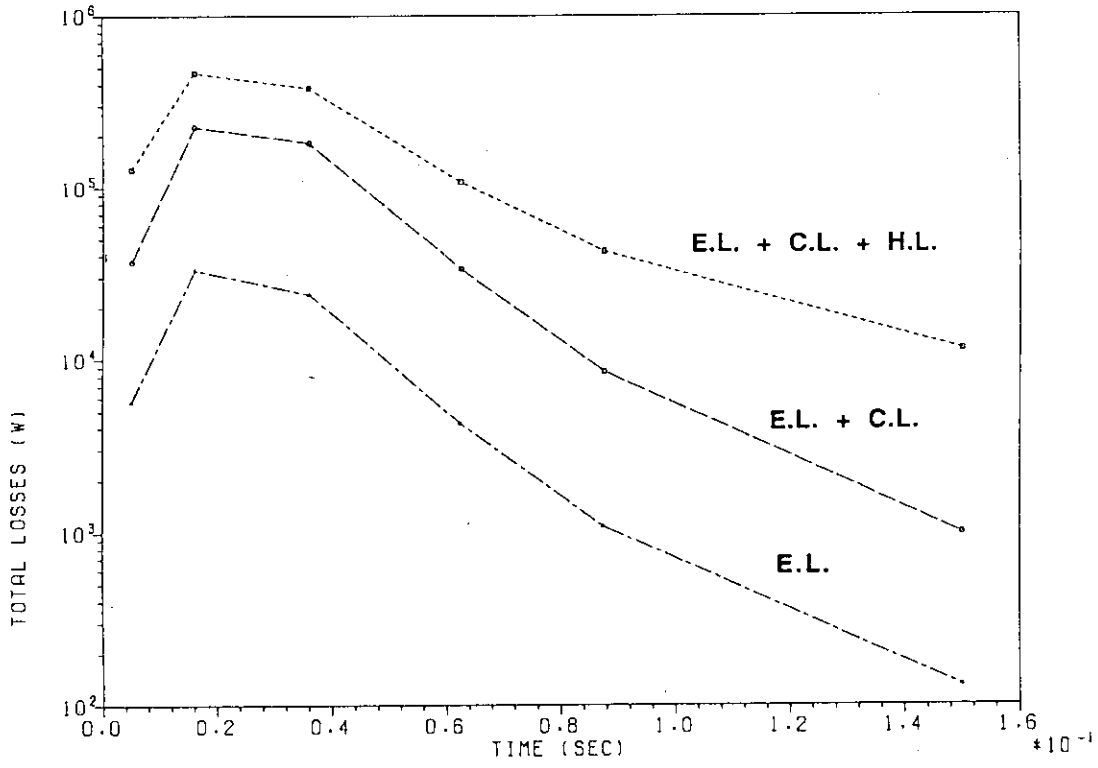

(a)

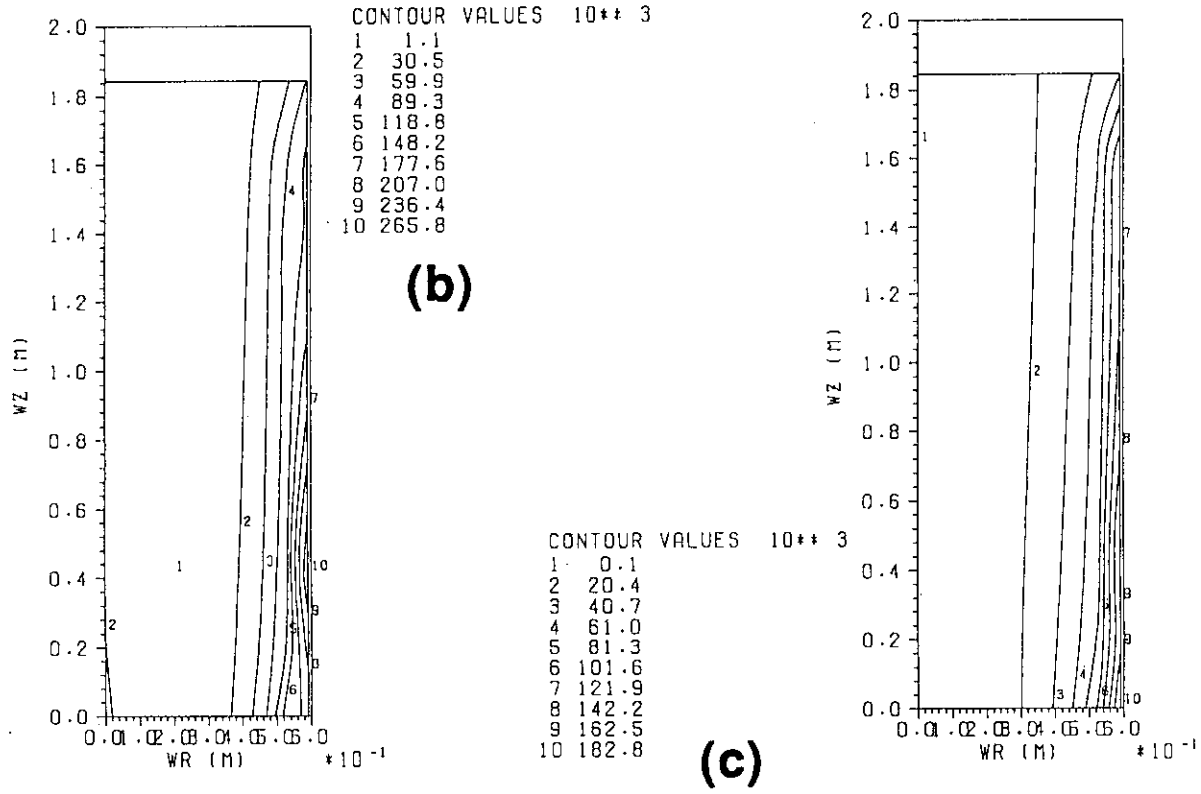

Fig.3.17 PF-3 coil AC loss.(during Disruption)
(a) Time dependencies of each component. (1 coil) (unit:W)
(b),(c) Spatial distribution of the power per unit volume on the cross-section at t= (b)15 ms, (c)35 ms. (unit : W/m^3)

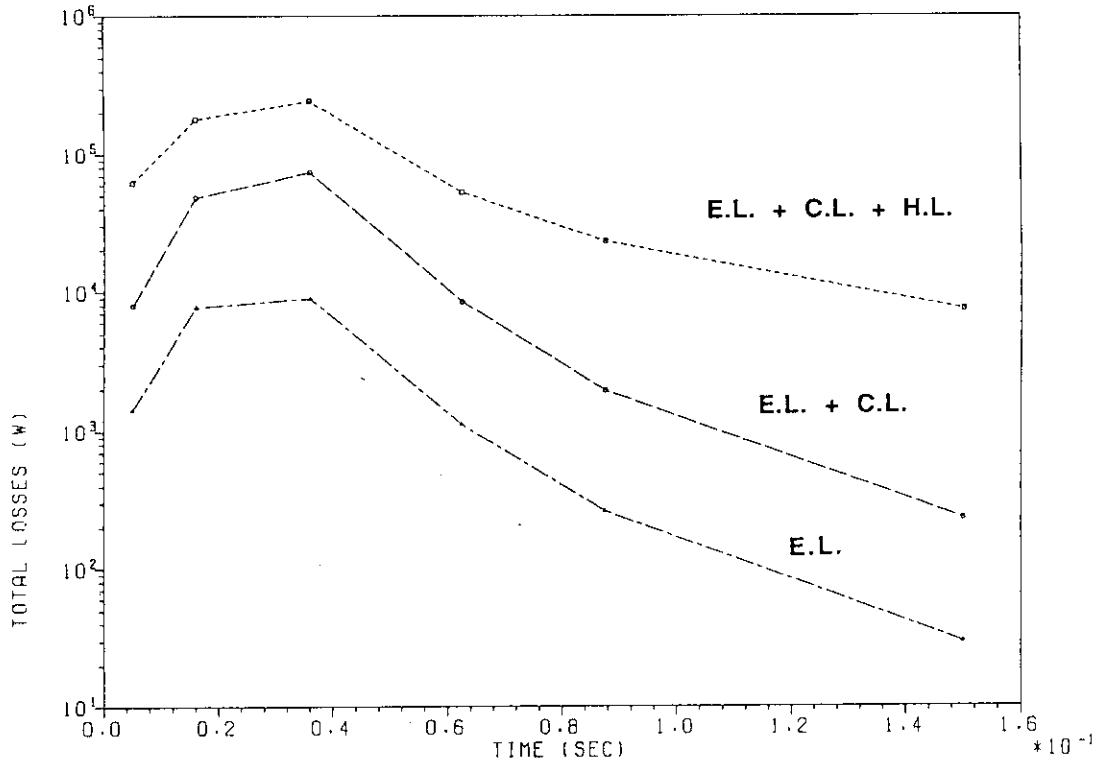

(a)

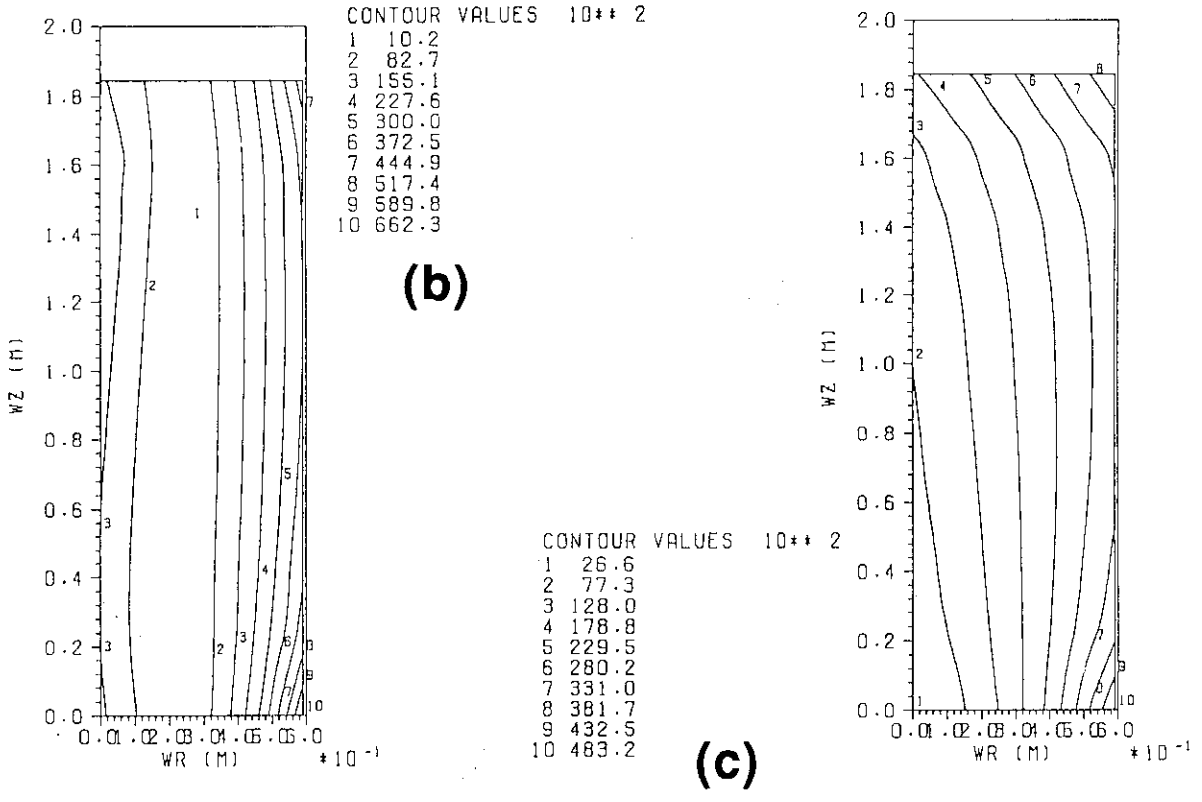

(b)

(c)

Fig.3.18 PF-4 coil AC loss.(during Disruption)
(a) Time dependencies of each component. (1 coil) (unit:W)
(b),(c) Spatial distribution of the power per unit volume on the cross-section at t= (b)15 ms, (c)35 ms. (unit : W/m^3)

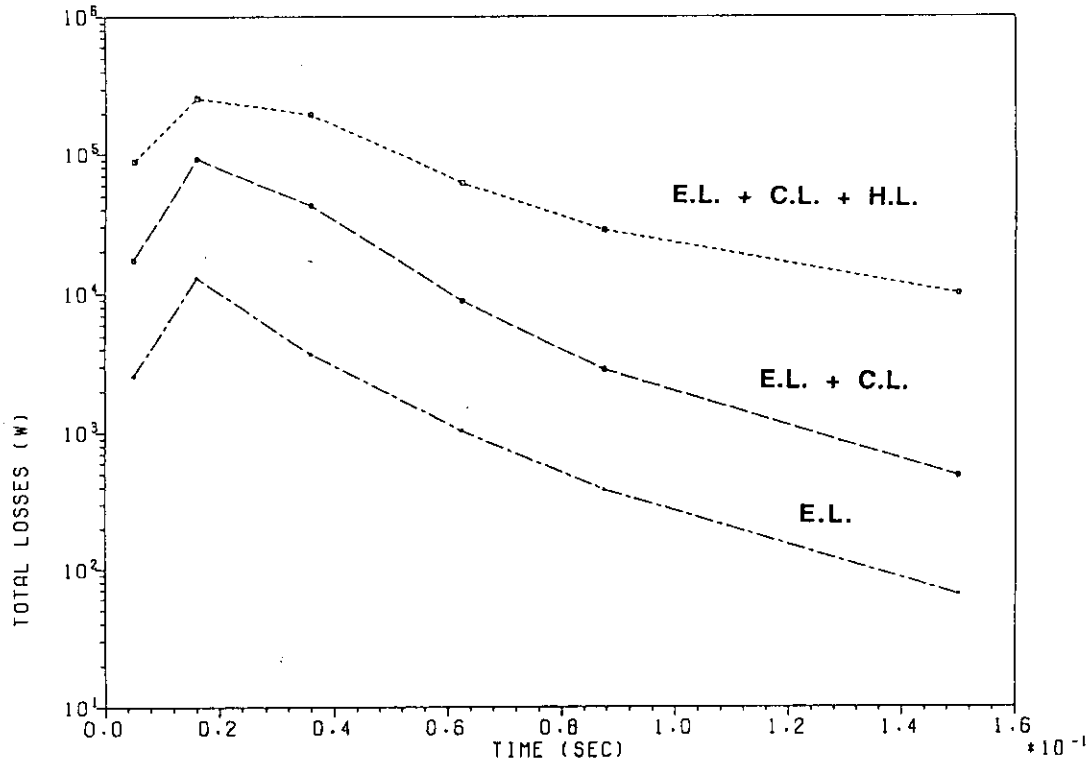

(a)

Fig.3.19 PF-5 coil AC loss.(during Disruption)
(a) Time dependencies of each component. (1 coil) (unit:W)

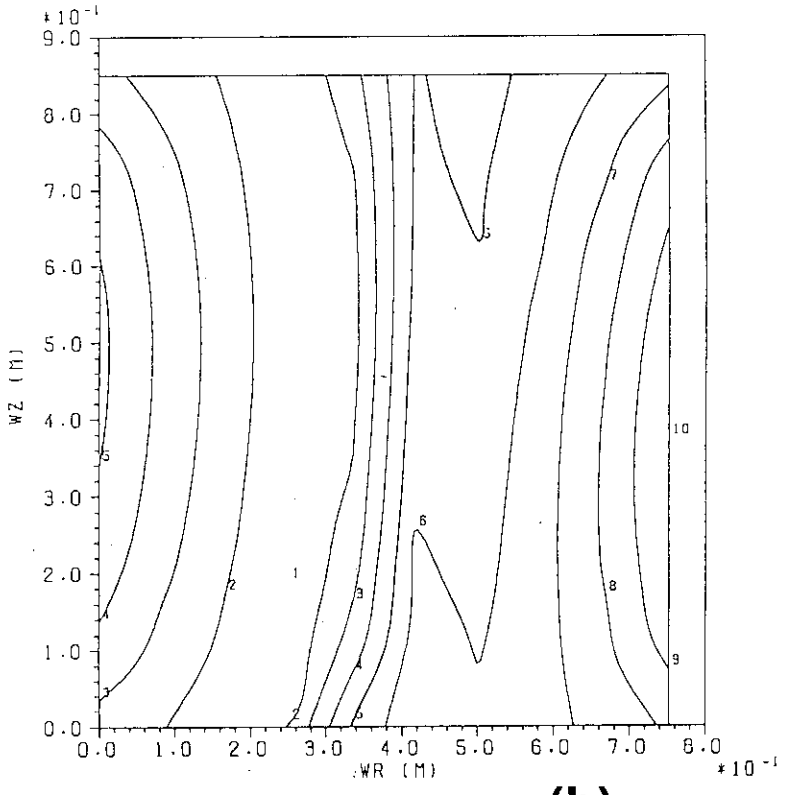

(b)

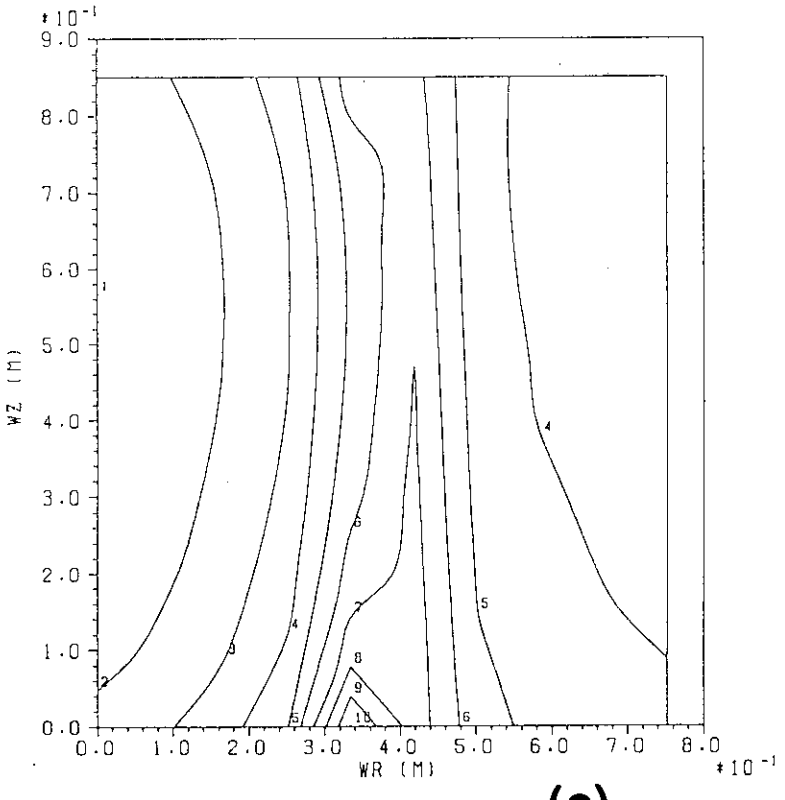

(c)

Fig.3.19 PF-5 coil AC loss.(during Disruption)
(b),(c) Spatial distribution of the power per unit volume on the cross-section at t= (b)15 ms, (c)35 ms. (unit : W/m^3)

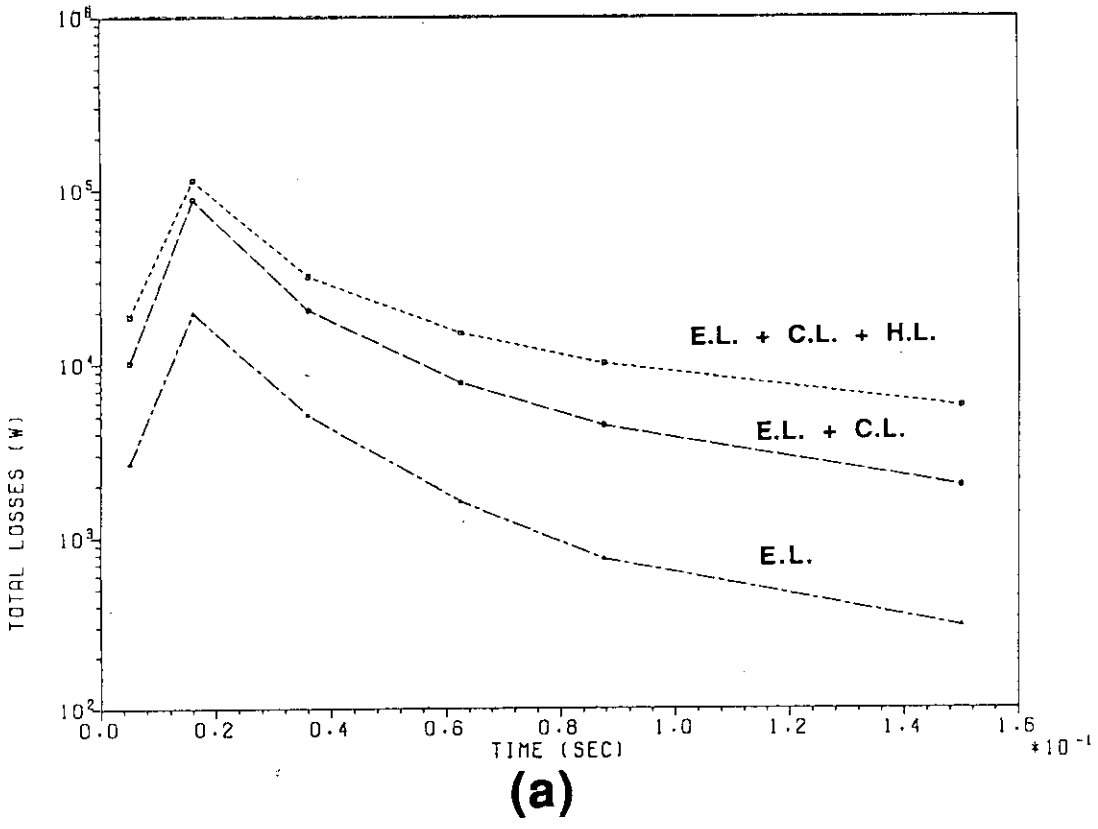

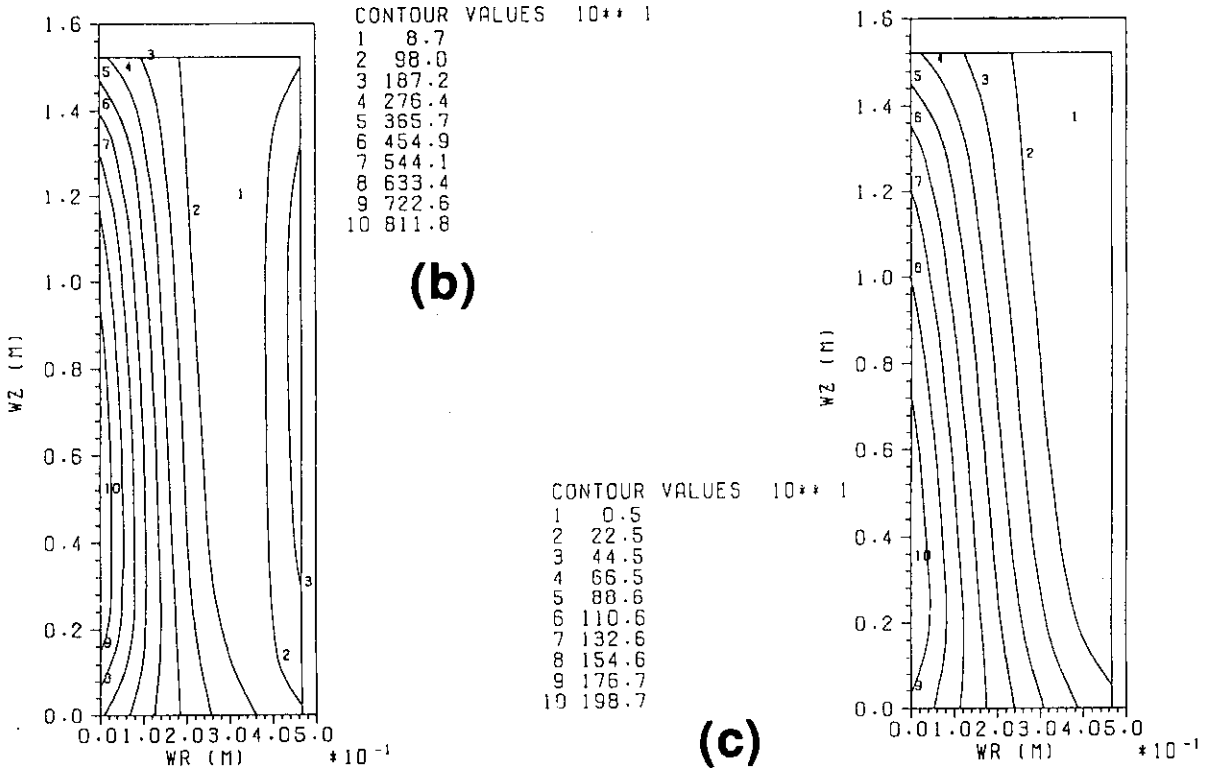

Fig.3.20 PF-6 coil AC loss.(during Disruption)
(a) Time dependencies of each component. (1 coil) (unit:W)
(b),(c) Spatial distribution of the power per unit volume on the cross-section at t= (b)15 ms, (c)35 ms. (unit : W/m^3)

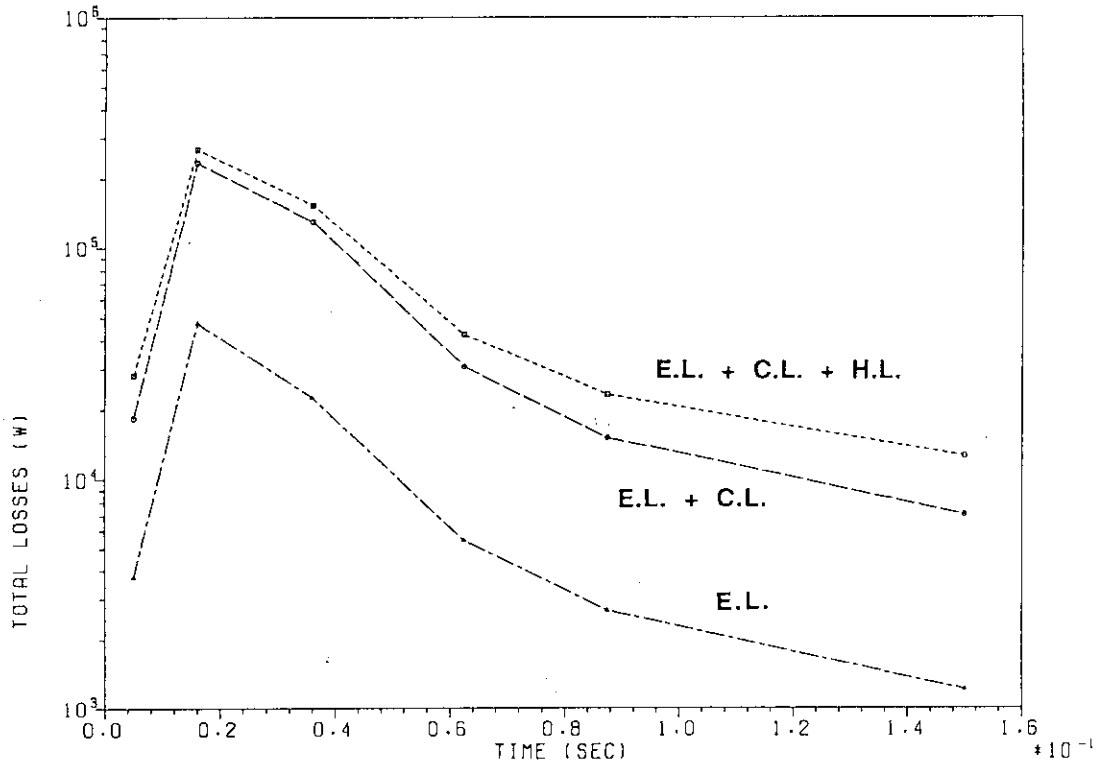

Fig.3.21 PF-7 coil AC loss.(during Disruption)
(a) Time dependencies of each component. (1 coil) (unit:W)

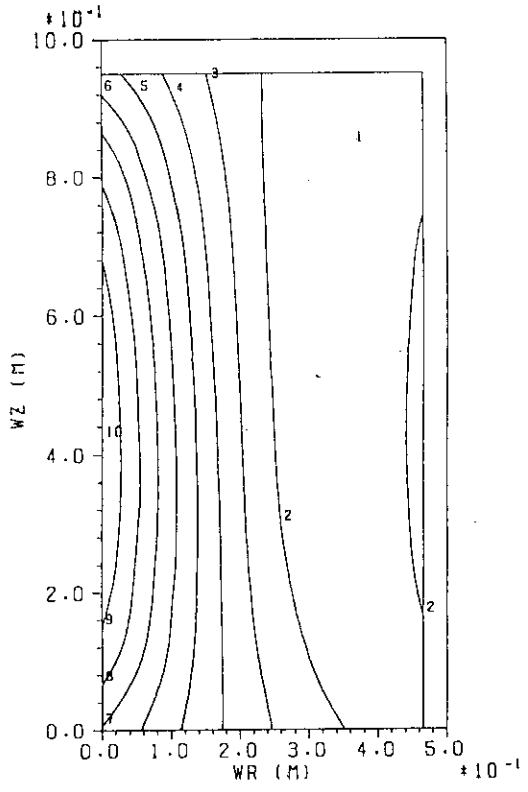

CONTOUR VALUES 10** 2

1	1.9
2	35.9
3	70.0
4	104.0
5	138.1
6	172.1
7	206.2
8	240.2
9	274.3
10	308.3

(b)

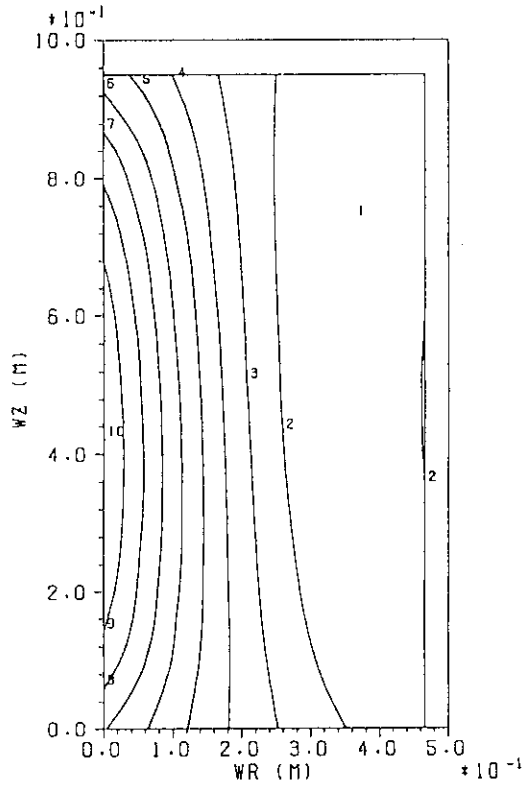

CONTOUR VALUES 10** 2

1	0.7
2	19.8
3	39.0
4	58.2
5	77.4
6	96.5
7	115.7
8	134.9
9	154.1
10	173.2

(c)

Fig.3.21 PF-7 coil AC loss.(during Disruption)
(b),(c) Spatial distribution of the power per unit volume on the cross-section at t= (b)15 ms, (c)35 ms. (unit : W/m^3)

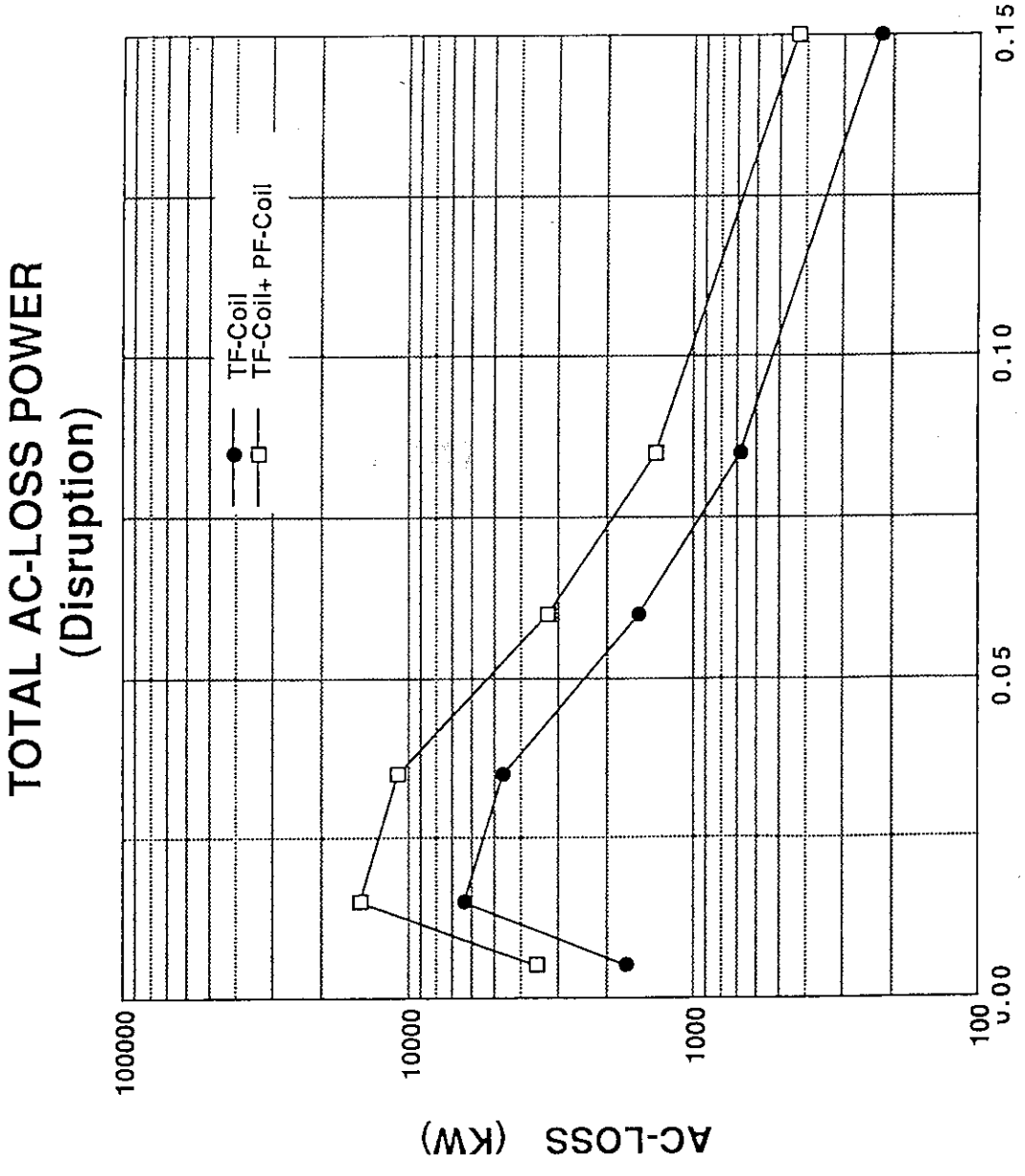

Fig.3.22 Total power of AC loss of all TF and PF coils.(unit :kW)
(During Disruption)

4. AC Loss in supporting structure

4.1 Introduction

It is indispensable to evaluate AC losses in cryogenic structures for making a decision of a capacity of a refrigerator. The cryogenic structure includes a TF coil case, a TF inter coil structure and a center solenoid coil support structure. Three kinds of transient electromagnetic phenomena are considered. These are plasma disruption, one cycle operation and a separatrix sweep, whose time histories are listed in Table 4.1, 4.2 and 4.3, respectively.

4.2 Calculation Method

The finite element descritized equations, which can be derived from the principle of minimum potential energy using the current vector potential, are used for analyses. The detail is shown in Ref. [1].

4.3 TF coil case and TF inter coil structure

Effects of induced currents on vacuum vessel are considered. Figure 4.1 shows the vacuum vessel calculation model. Figure 4.2 shows a TF coil case calculation model. A TF inter coil structure, TF coil case and vacuum vessel are all together shown in Fig.4.3. Figure 4.4 shows five candidates of insulated TF coil case. TF AC (joule) losses in only TF coil case are shown in Fig.4.5 for the plasma disruption, Fig.4.6 for the one cycle operation and Fig.4.7 for the separatrix sweep operation, respectively. It should be noted that the values of graphs are those of the half sector and 32 multiplication is required to obtain total AC losses. The AC (joule) losses in both the TF inter coil structure and the TF coil case are also calculated based on the type E insulated TF coil case. (The type E

insulation was adopted in the real design.) These are shown in Fig.4.8 for the plasma disruption, Fig.4.9 for the one cycle operation and Fig.4.10 for the separatrix sweep, respectively. In these figures E' corresponds to the TF coil case with insulated inter coil structure and E" corresponds to the TF coil case with non-insulated inter coil structure. All the calculated results are listed in Table 4.4.

4.4 Center solenoid coil support structure

As same as evaluating the joule losses in the TF coil related cryogenic structure, effects of induced currents on vacuum vessel are considered for calculating the joule loss in the center solenoid coil support structure. Two kinds of structure models are considered. One is the plate model as shown in Fig.4.11. The other is the box model as shown in Fig.4.12. Figure 4.13 shows that both for the plasma disruption and the one cycle operation, a dependence of joule loss on No. of insulation cut.

References

[1] S. Nishio, T. Horie, "A Computer Program System for Transient Electromagnetic Analysis on a Tokamak Device", IEEE Trans. MAG-26, 865, (1990).

Table 4.1 Plasma disruption scenario

Time	I_p(MA)	a_p(m)	Z_p(m)	R_p(m)	κ	δ
0.0	22.0	2.20	0.0	6.0	2.0	0.4
0.1	22.0	2.2	-0.05	6.0	2.0	0.4
5.0	17.0	1.93	-0.08	5.73	1.8	0.3
11.0	11.0	1.5	-0.15	5.3	1.5	0.2
18.0	4.0	0.9	-0.3	4.7	1.3	0.0
20.0	2.0	0.66	-0.37	4.46	1.0	0.0
22.0	0.0	0.0	-0.45	3.8	1.0	0.0

Table 4.2 One cycle operation scenario of PF coil system and plasma.

TIME (sec)	0.00	0.10	0.60	3.00	10.00	20.00	28.00	44.00	70.00	90.00	290	310	330	350	360	380	390	400	500
Plasma (MA)	0.00	0.00	0.50 LIM	2.00 LIM	5.00 LIM	10.00 LIM	10.00 DN	15.00 DN	22.00 SOFT	22.00 SOB	22.00 EOB	20.00 EOC	15.00 DN	10.00 DN	8.00 LIM	5.00 LIM	2.00 LIM	0.5 LIM	0
PF1 (MA)	20.411	20.09	19.32	17.31	13.53	5.24	4.56	-3.78	-16.79	-17.87	-22.30	-22.41	-21.94	-17.97	-17.50	-11.71	-10.25	-9.92	20.411
PF2 (MA)	20.411	20.09	19.32	17.31	13.53	5.24	4.56	-3.78	-16.79	-17.87	-22.30	-22.41	-21.94	-17.97	-17.50	-11.71	-10.25	-9.92	20.411
PF3 (MA)	20.411	20.09	18.15	14.56	10.87	12.25	13.69	8.86	2.85	-2.41	-9.14	-8.77	-12.70	-12.45	-5.57	-15.89	-11.98	-10.22	20.411
PF4 (MA)	20.411	20.09	18.15	14.56	5.91	8.00	13.69	10.06	0.00	0.00	0.00	0.37	-3.56	-4.87	-2.54	-15.89	-11.98	-10.22	20.411
PF5 (MA)	14.529	14.303	13.61	10.92	5.24	7.89	12.87	12.90	13.60	10.79	6.25	5.04	0.22	-2.16	-3.95	-11.92	-8.99	-7.67	14.529
PF6 (MA)	0.2507	0.2468	0.122	-0.16	-0.58	-1.96	-3.82	-5.80	-8.45	-7.14	-6.49	-7.25	-5.36	-3.52	-4.78	-0.97	-0.51	-0.23	0.2507
PF7 (MA)	0.2507	0.2468	0.122	-0.16	-0.58	-1.96	-0.99	-1.79	-2.72	-4.79	-5.25	-3.12	-2.51	-1.78	-0.91	-0.97	-0.51	-0.23	0.2507
R(M)	0	0	4.50	4.90	5.40	5.85	6.00	6.00	6.00	6.00	6.00	6.00	6.00	6.00	5.61	5.40	4.90	4.50	
a(M)	0	0	0.8	1.20	1.7	2.14	2.15	2.15	2.15	2.15	2.15	2.15	2.15	2.15	1.79	1.70	1.20	0.80	
b/a	0	0	1.00	1.00	1.00	1.41	2.22	2.22	2.22	2.22	2.22	2.22	2.22	2.22	1.68	1.00	1.00	1.00	
c/a	0	0	0.00	0.00	0.00	0.11	0.60	0.60	0.60	0.60	0.60	0.60	0.60	0.60	0.27	0.00	0.00	0.00	

Table 4.3 Separatrix sweep scenario
(0.3 Hz, ΔX = +/- 12 cm Separatrix Sweep Operation at SOB)

	+/-ΔI (kAT)	+I (MAT)	-I (MAT)
PF-1	84.0	-17.786	-17.954
PF-2	84.0	-17.786	-17.954
PF-3	-603.0	-3.013	-1.807
PF-4	-27.6	-0.0276	0.0276
PF-5	423.0	11.213	10.367
PF-6	13.2	-7.1268	-7.1532
PF-7	-31.2	-4.8212	-4.7588

Table 4.4 Summary of joule losses of TF coil related cryogenic structure.

(unit : MJ)

Structure Model	Disruption	One Cycle Operation (500 sec)	Separatrix Sweep (3.33 sec)
A	55.4	26.6	0.923
B	9.5	25.0	0.912
C	4.7	2.9	0.093
D	10.0	7.6	0.244
E	5.0	6.7	0.223
E'	7.6	12.0	0.242
E"	12.6	235.0	0.261

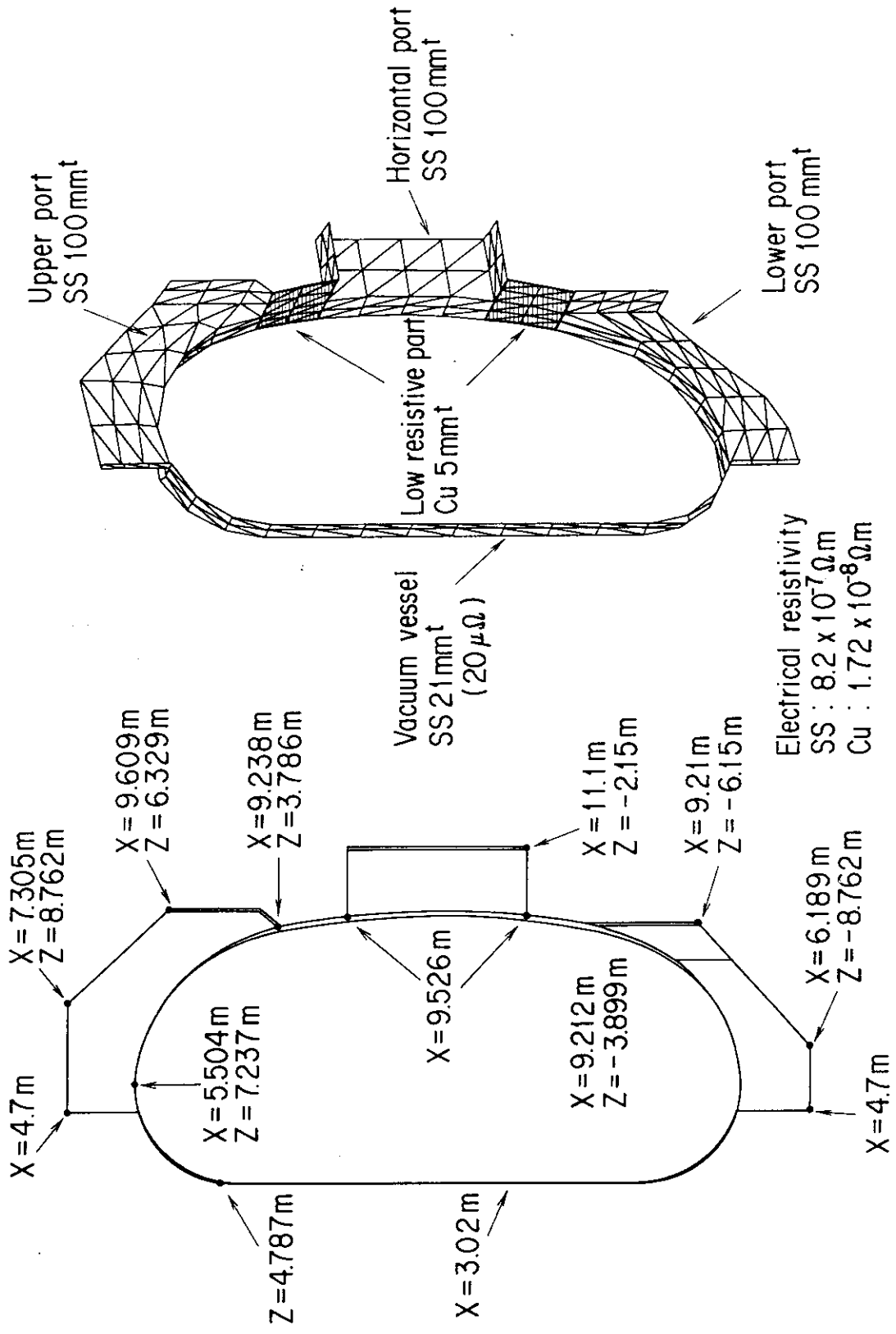

Fig.4.1 Vacuum vessel calculation model.

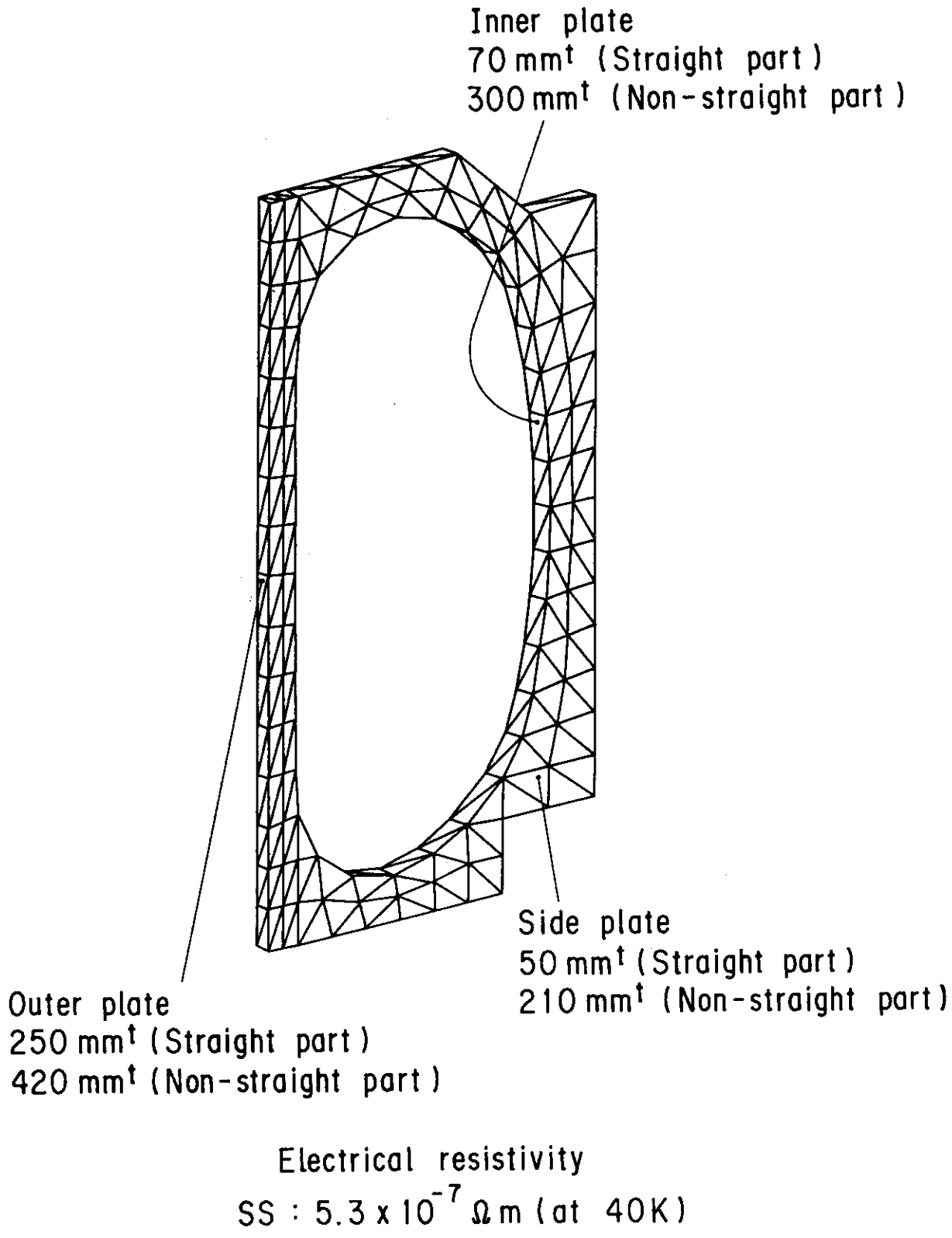

Fig.4.2 TF coil case calculation model.

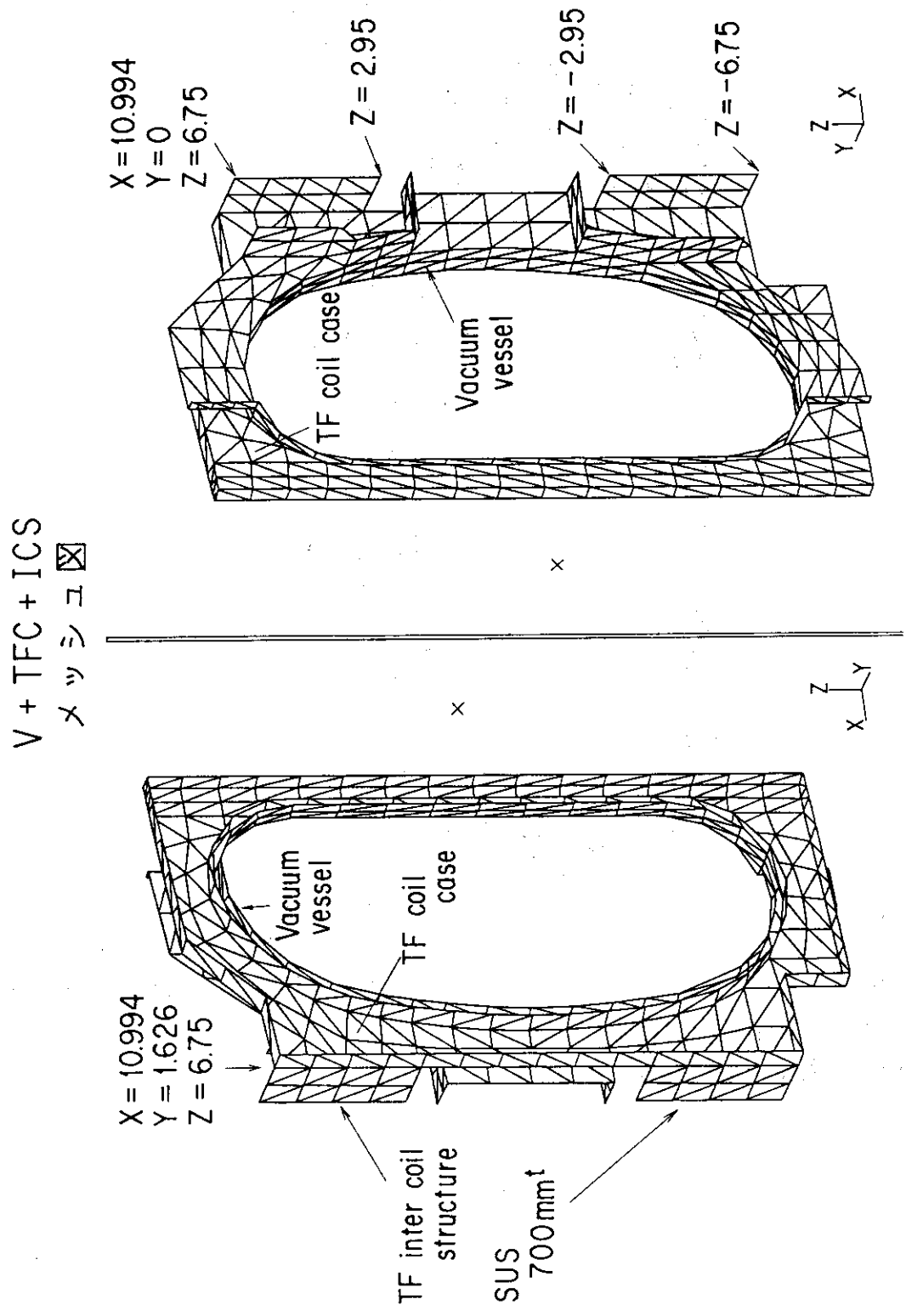

Fig.4.3 TF inter coil structure, TF coil case and vacuum vessel.

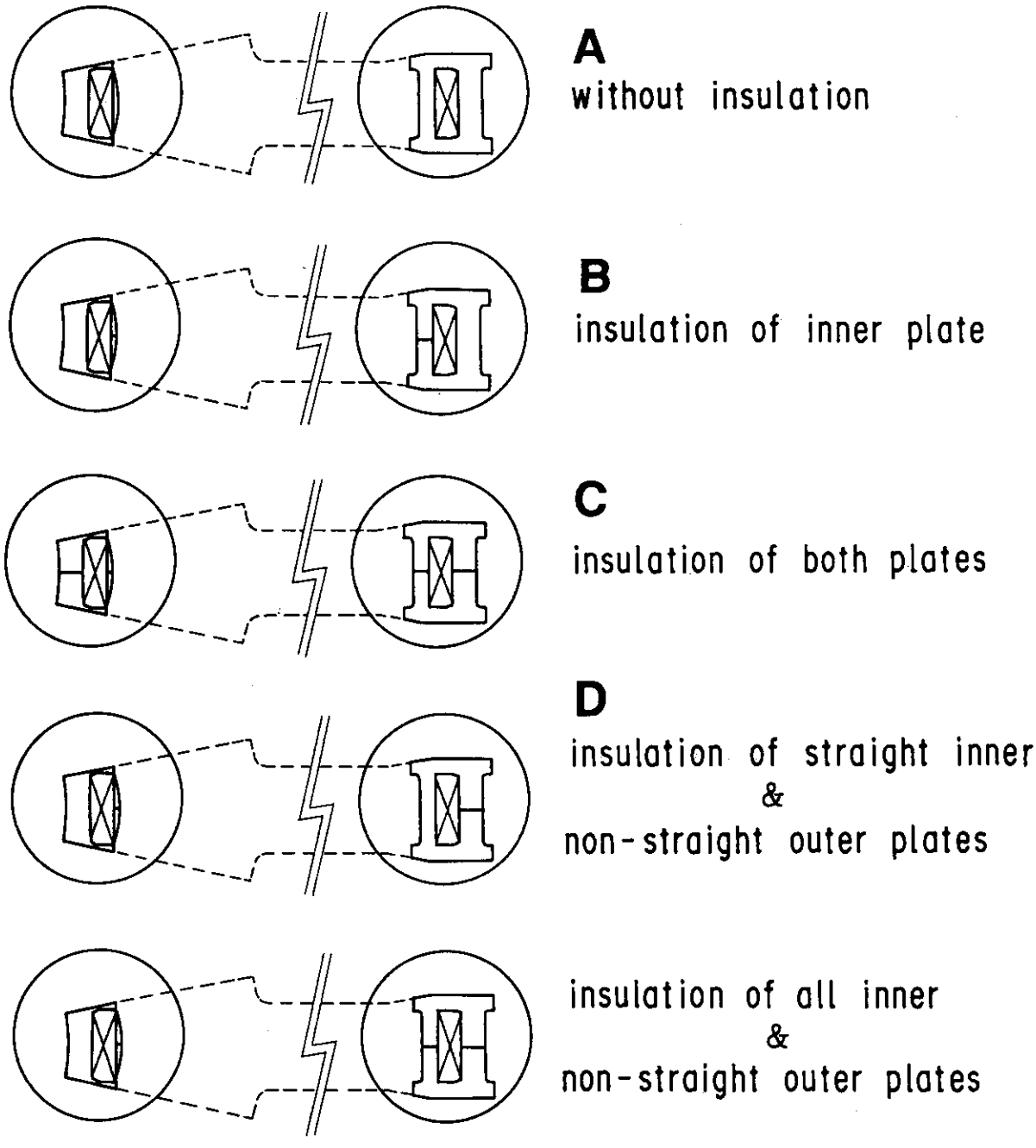

Fig.4.4 Five candidates of insulated TF coil case.

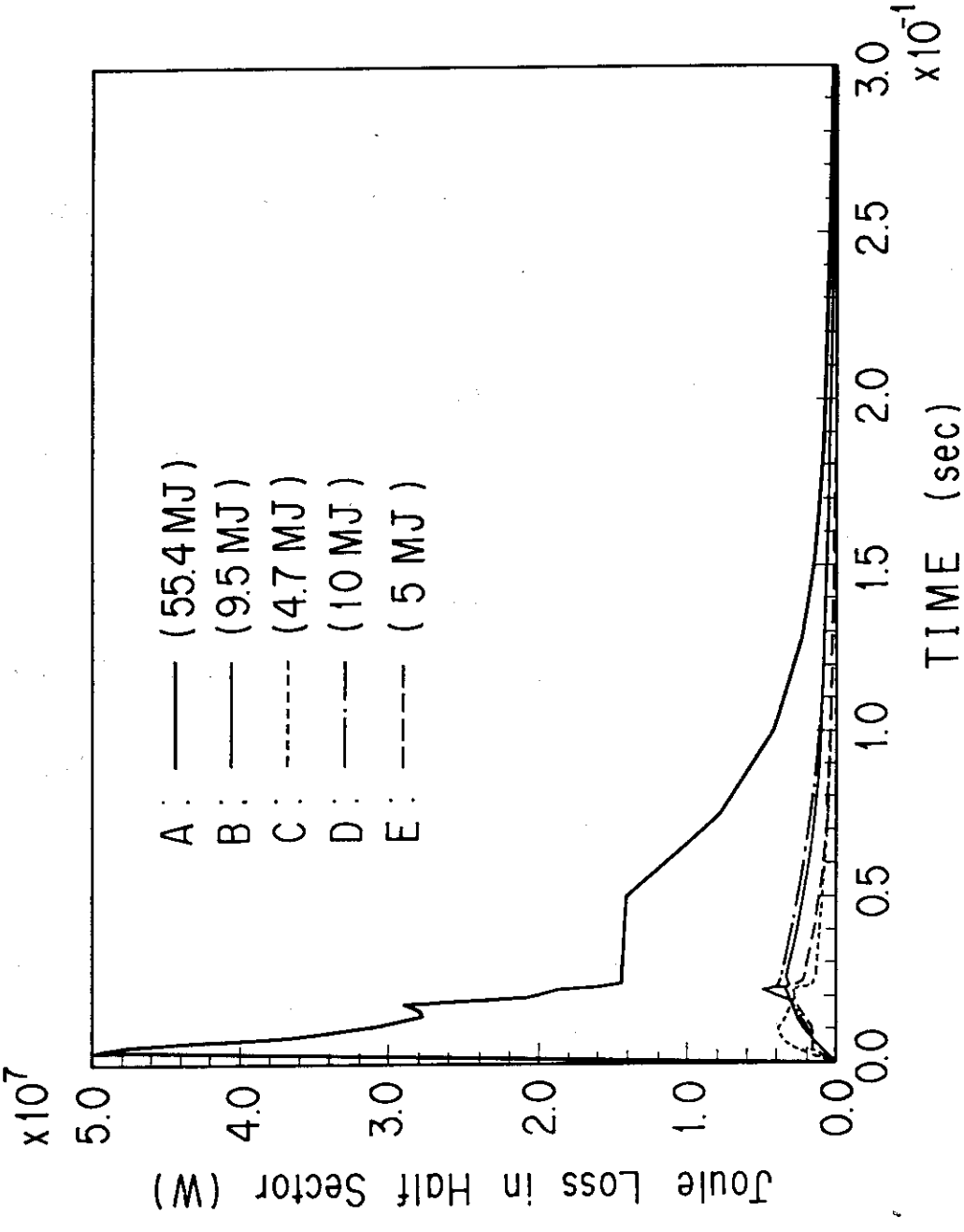

Fig.4.5 Joule loss in TF coil case for plasma disruption.

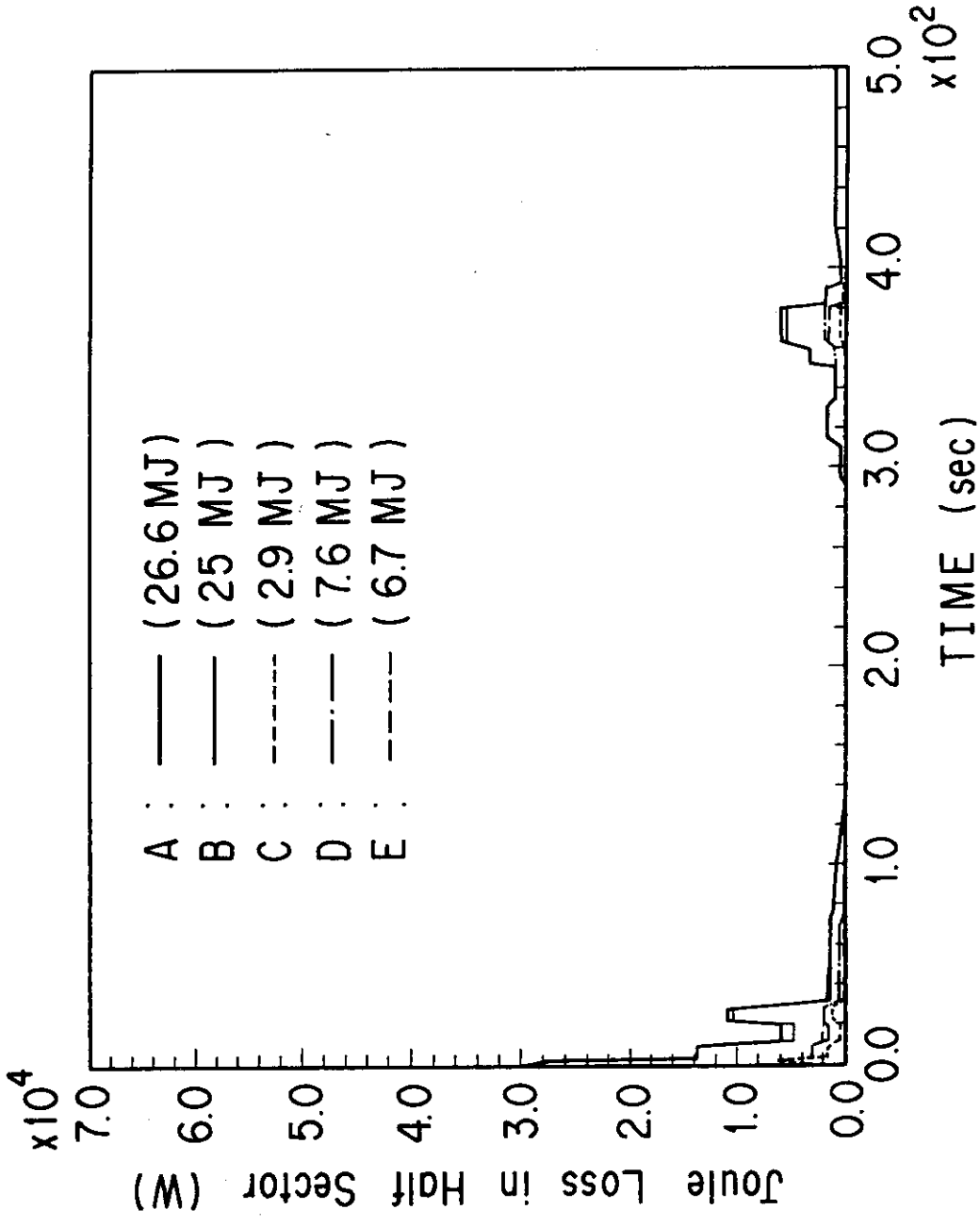

Fig.4.6 Joule loss in TF coil case for one cycle operation.

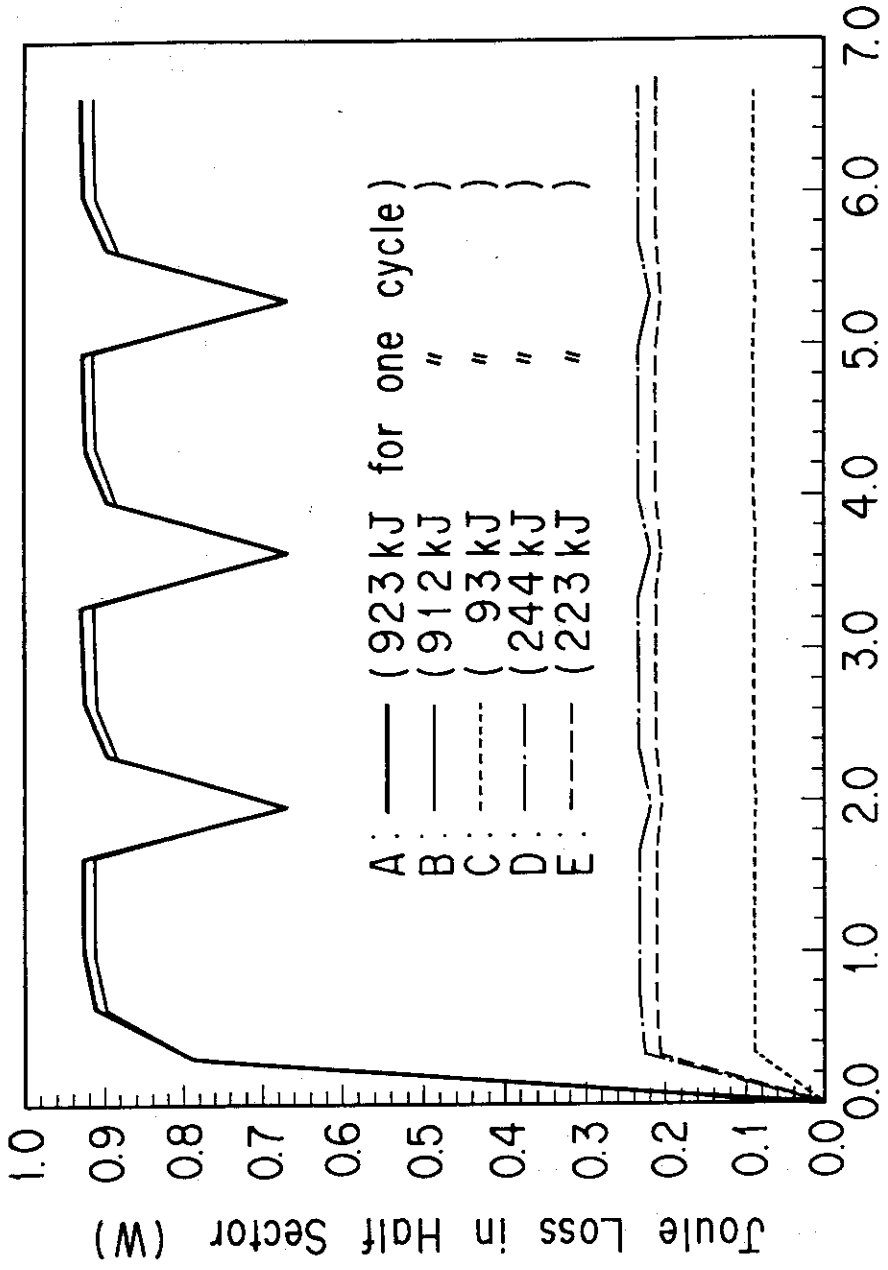

Fig.4.7 Joule loss in TF coil case for separatrix sweep operation.

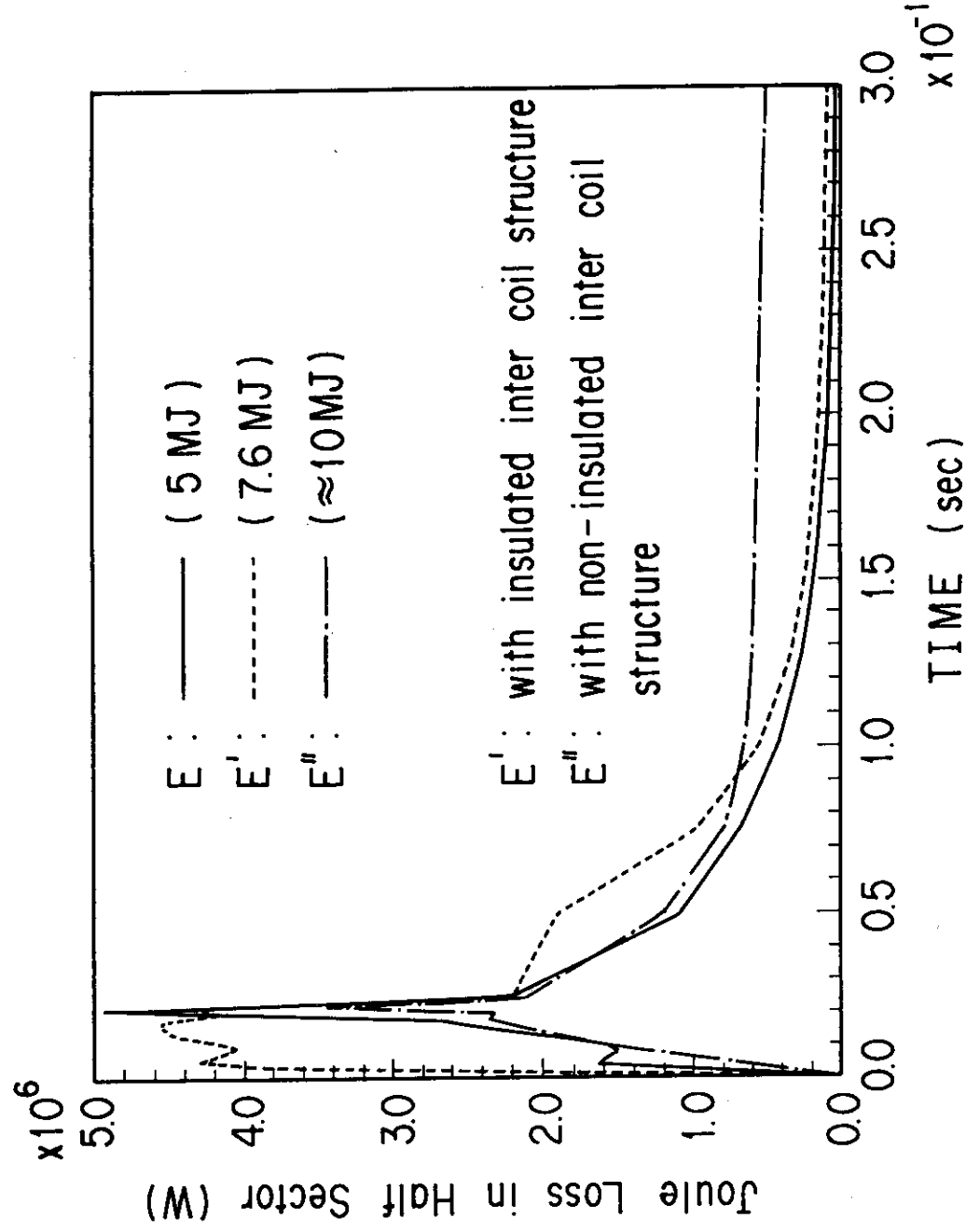

Fig.4.8 Joule loss in TF coil case and TF inter coil structure for plasma disruption.

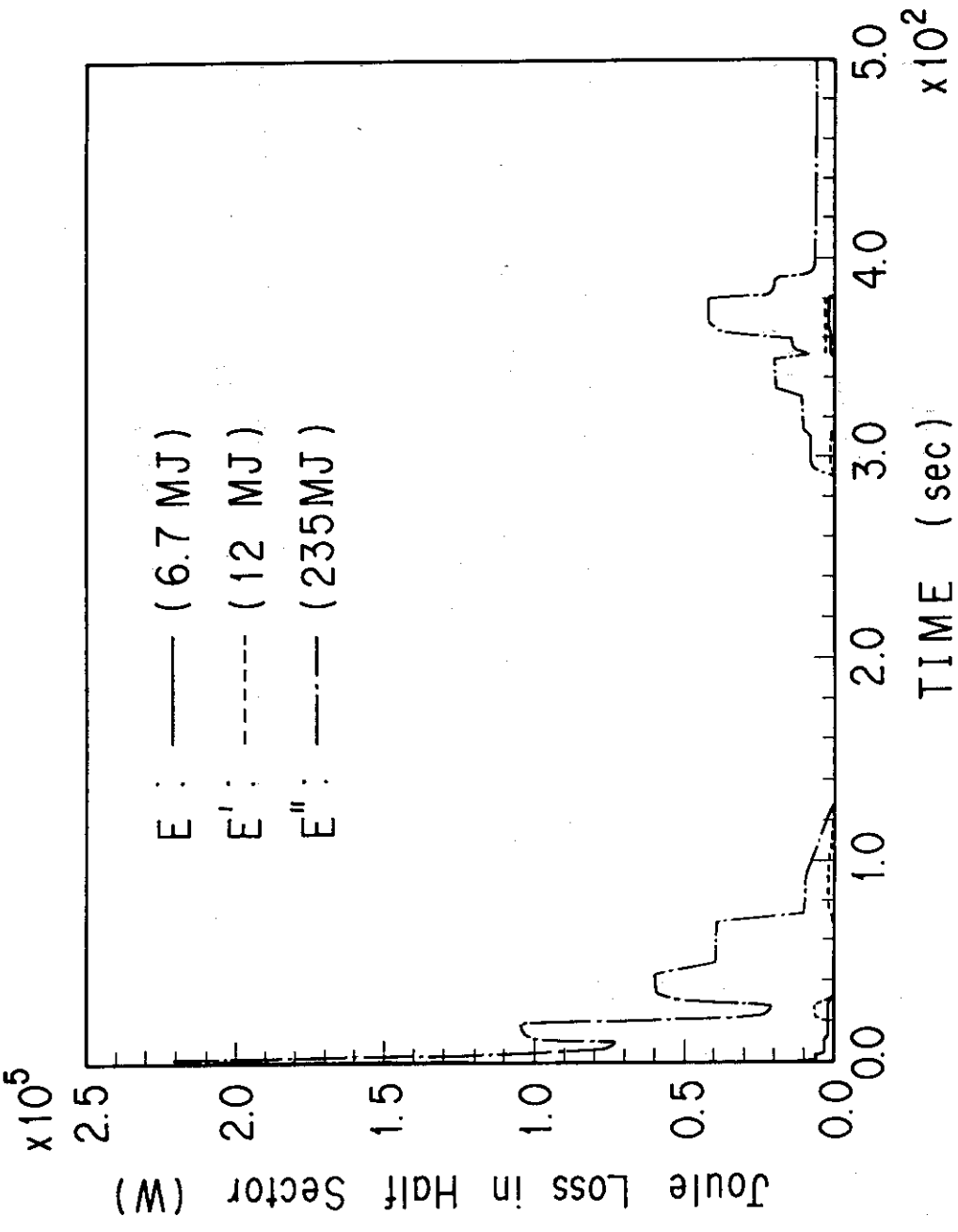

Fig.4.9 Joule loss in TF coil case and TF inter coil structure for one cycle operation.

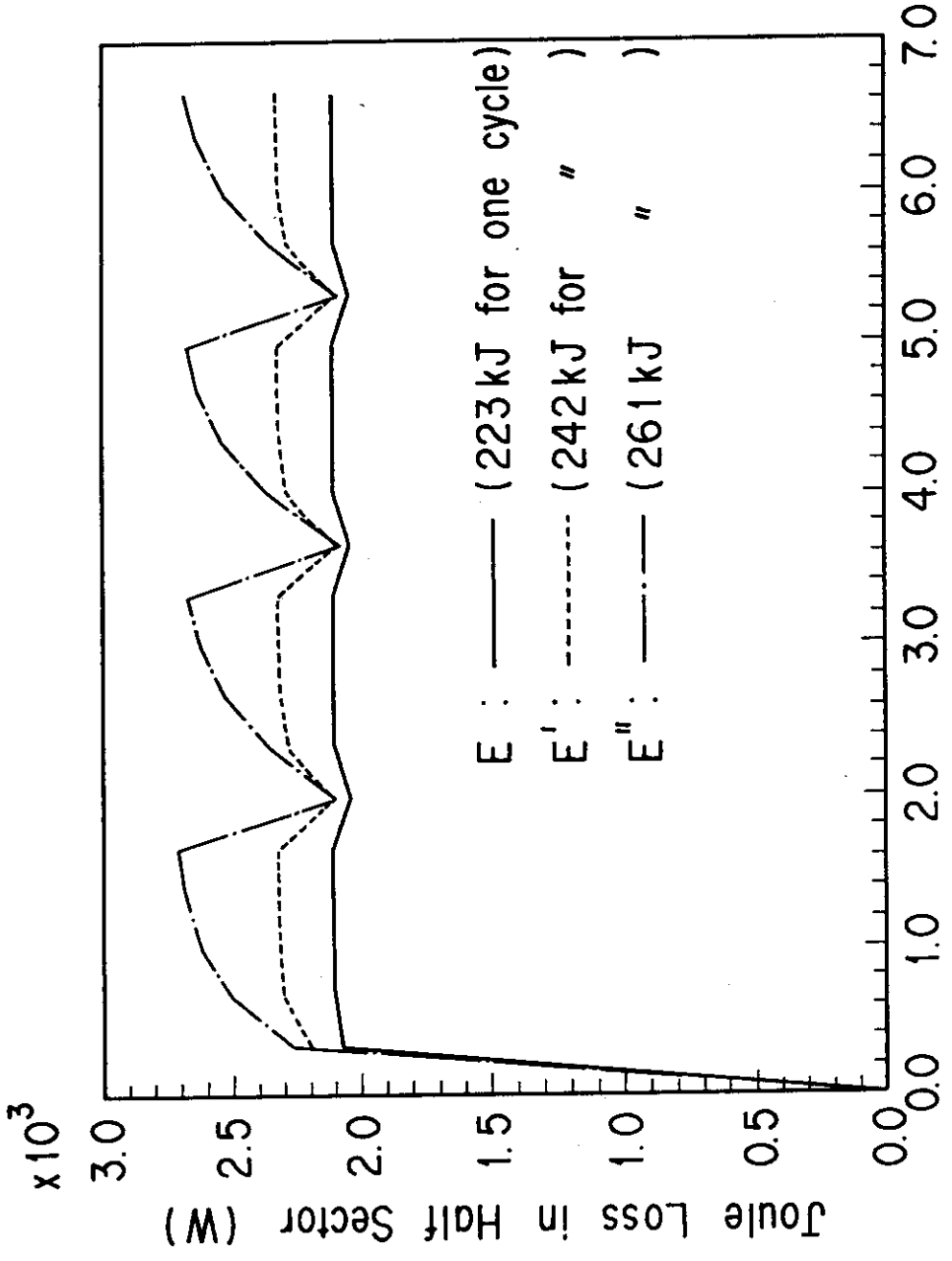

Fig.4.10 Joule loss in TF coil case and TF inter coil structure for separatrix sweep operation.

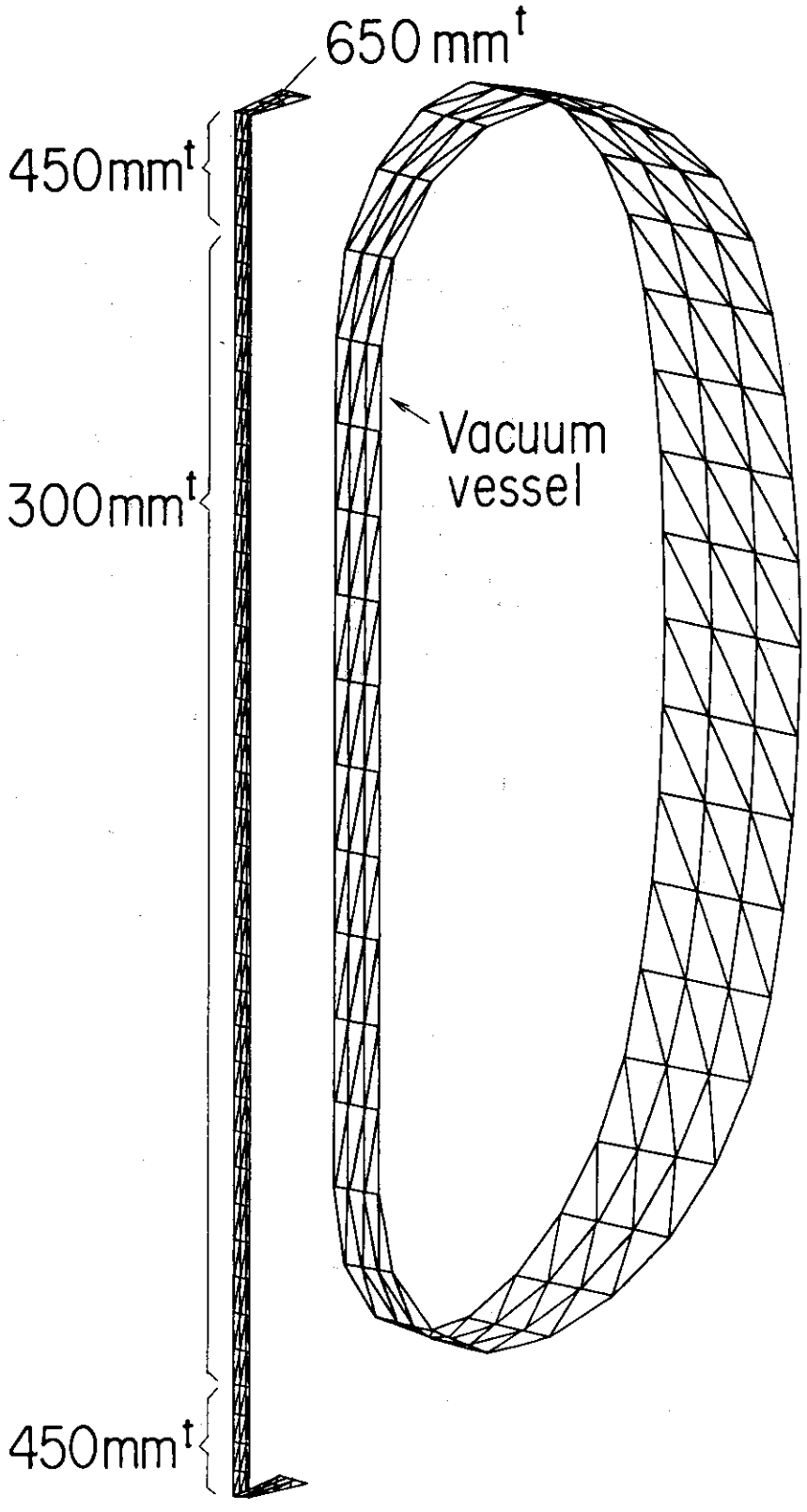

Fig.4.11 Plate model of center solenoid coil support structure.

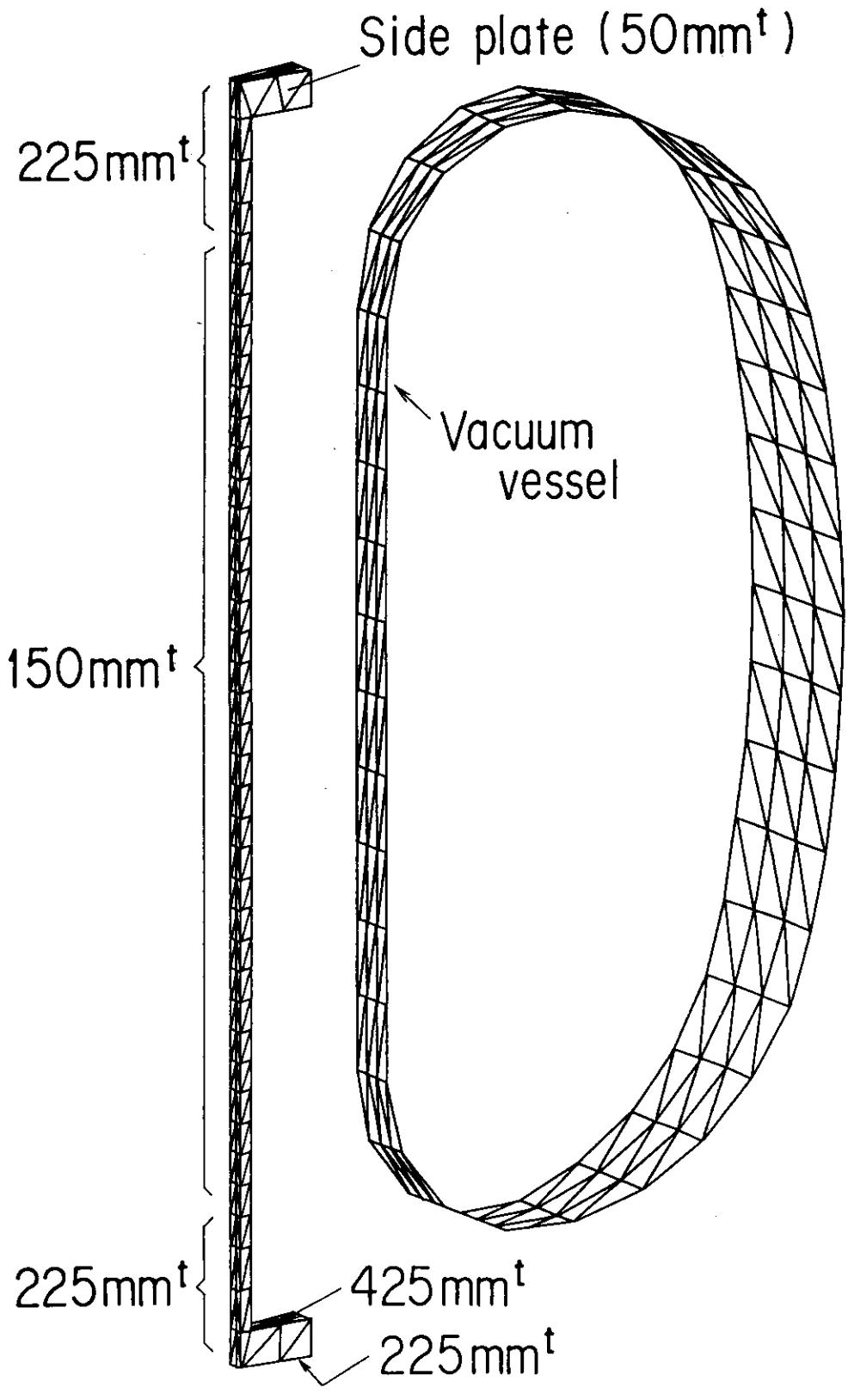

Fig.4.12 Box model of center solenoid coil support structure.

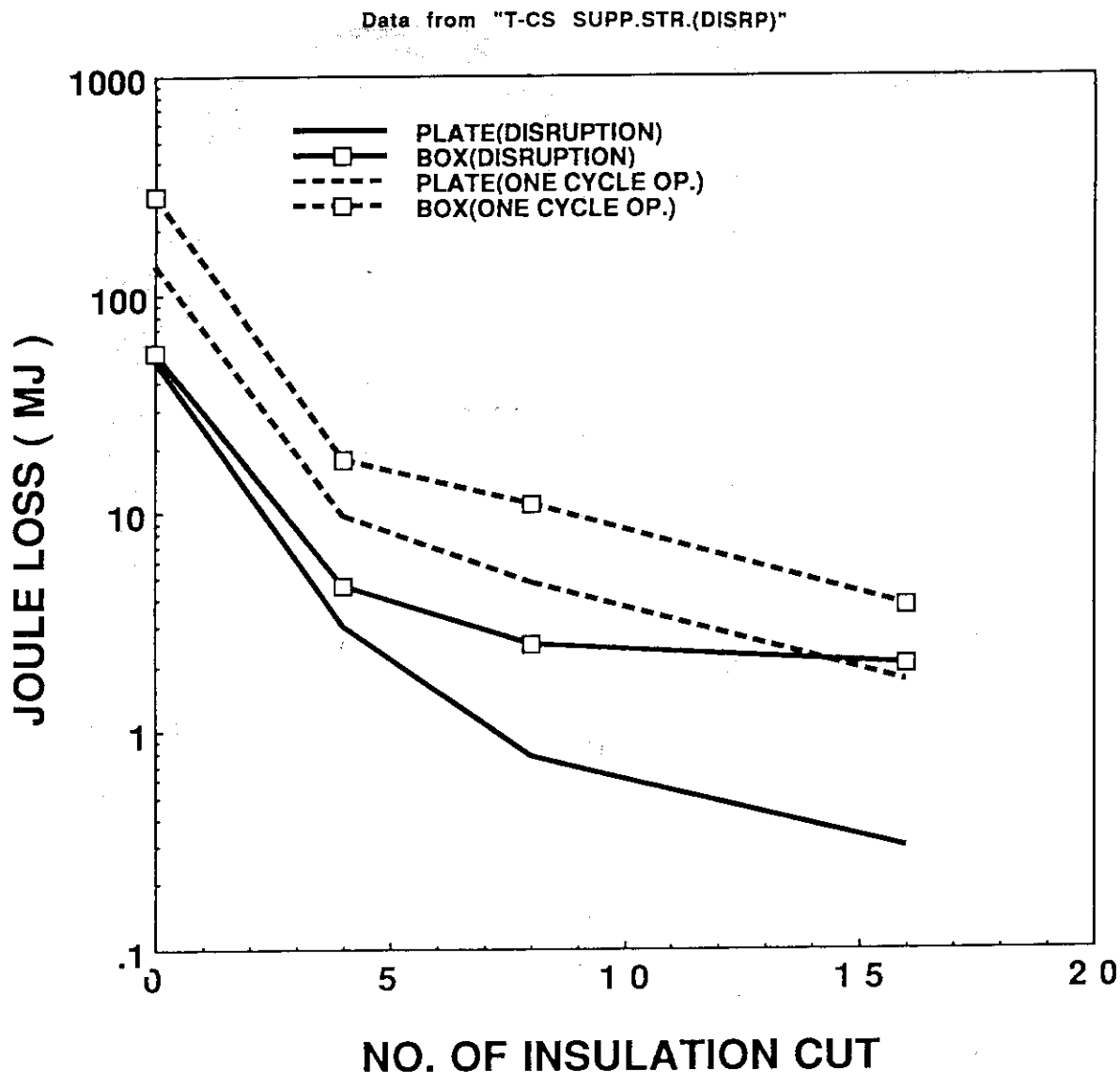

Fig.4.13 Dependence of joule losses on No. of insulation cut.

5. Summary

As the results of analyses, the AC losses occupy about 50 % of the total heat loads during the normal operation. The obtained AC losses are summarized in Table 5.1.

On the other hand, the AC losses during the plasma disruption is about 26.6 mJ/cc (130 mJ/cc for strand) in low field region (less than 5 T). In the high field region (greater than 13 T) the maximum value is about (12 mJ/cc in strand) and sufficiently smaller than the theoretically estimated critical value of 100 mJ/cc. Consequently, it can be considered that the coil quench will not occur on the condition that the stability margin is greater than 100 mJ/cc in 13 T.

As for the AC loss in the winding, the analyses and the measured results have a good agreement for the filament to filament coupling loss and the hysteresis loss of the NbTi coil in perpendicular magnetic field. For the estimation of strand to strand coupling loss, the experimental measurements of the strand to strand time constants are required. For the estimation of the hysteresis loss of the Nb_3Sn conductor, the careful measurements of the effective filament diameter is necessary. Hence, the measurements of AC losses should be performed at each level of the conductor, i.e., strand, sub-size and full size before the design work and the construction of the coils.

The AC losses of the supporting structure and TF coil case were also estimated. These losses are almost twice those of the winding packs. The AC losses greatly depend on the positions of insulation. These results were used for the design of the supporting structure and TF coil case.

Table 5.1 Loss power during normal operation (unit : kW)

		Average (500s)	
Winding Pack	PFC	3	
	TFC	12	
Cold Structure	PFC	8	(16 divided)
	TFC	24	
Total		47	

ACKNOWLEDGEMENTS

The authors would like to thank Dr. S. Shimamoto and Dr. S. Mastuda for their strong support and kind encouragement of our design activities during the past three years. Also, the authors wish to thank the staff of the Superconducting Laboratory and the Fusion Experimental Reactor Design Team for their consultation. And authors would also like to thank Mr. T. Shimizu, Mr. Y. Nakane, Mr. H. Shimane, Mr. T. Nishino, and Mr. E. Yaguti from Kanazawa Computer Service Co Ltd for their computer analysis. Also thanks to Miss Y. Iida, Miss Y. Hasegawa, Mr. K.Hirano, and Miss H.Nagahori for the CAD operations, and Miss A. Miwa of Gensiryoku Shiryo Service Co Ltd for the publishing.